AN INTRODUCTION TO PROTON-PROTON COLLISIONS AT HIGH ENERGIES

By N. Schmitz

Max-Planck-Institut für Physik und Astrophysik, München*

(Presented at the XIII Cracow School of Theoretical Physics, Zakopane, June 1–12, 1973)

The experimental data on topological cross sections, single particle distributions and correlations observed in proton-proton collisions at high energies are discussed in the framework of multiperipheral and fragmentation pictures.

CONTENTS

* Address: Max-Planck Institut für Physik und Astrophysik, Föhringer Ring 6, D-8000 München 23, Germany, Federal Republic.

A. INTRODUCTION

In these lectures on proton-proton-collisions at high energies the following subjects will be treated:

Topological cross sections and multiplicities
Inclusive single particle distributions
Correlations

The emphasis will be on experimental results. However, in order to have a framework for discussing these results, two phenomenological pictures, namely the multiperipheral picture and the diffractive fragmentation picture, will be briefly introduced at the beginning in a qualitative and descriptive way.

The paper is intended to be a general survey without getting too deeply involved into more specific questions and into all refinements and complications. In this sense it is considered as an introduction into the field and a preparation for more specific topics discussed in other papers of this issue.

If not stated otherwise, all experimental results presented in these lectures refer to pp-collisions.

B. TWO PICTURES FOR HIGH ENERGY REACTIONS

Numerous models have been developed to describe elementary particle reactions at high energies. Most models exist in several versions which have often emerged from the attempt to adjust them to the available experimental results. This flexibility generally

reduces the predictive power of such models and makes it difficult to distinguish between them on the basis of the experimental data.

Because of these limitations and since these lectures are mainly concerned with experimental results and with the knowledge we have about high energy reactions directly from experiment, we do not intend to give a detailed, quantitative and complete discussion of the many models available. Instead we will describe only qualitatively two extreme pictures in their simplest form in order to have a framework, in which the high energy multiparticle data can be interpreted. These two pictures are:

the multiperipheral picture (MPP).
the diffractive fragmentation picture (DFP).

We will mention, at the appropriate places in the presentation of the experimental results, the predictions which these pictures make, and confront them with the data. For more details (quantitative treatments, various versions and modifications, other models) we refer to the extensive literature, *e. g.* to the recent reviews [1–7].

1. Multiperipheral picture (MPP)

The multiperipheral model is a generalisation to many particles of the relatively successful one-particle-exchange model for quasi-two-body-reactions $a+b \to c+d$

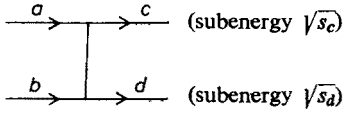

with small subenergies $\sqrt{s_c}$ and $\sqrt{s_d}$ of the systems c and d. The multiperipheral model was originally introduced by Amati, Fubini and Stanghellini [8], was revived in the framework of Regge theory by Chan and co-workers (multi-Regge-exchange model of Chan, Łoskiewicz and Allison [9]) and was formulated in several specific versions [2] (*e. g.* Chew-Pignotti-model [10]; De Tar model [11], in which transverse momenta are neglected).

The MPP starts from the following diagram for the reaction

$$a+b \to c_1+\ldots+c_n: \tag{1}$$

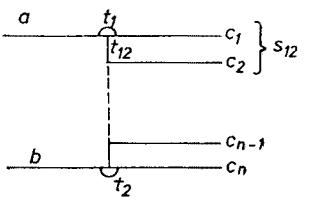

The secondary particles (or particle systems) come off a multiperipheral chain. In quantitative formulations the chain is resolved into a sequence of two-body processes with one-

particle exchange (factorisability) the exchanged particles usually being described by their Regge-trajectories. Some models assume dominance of multi-pion-exchange since the pion pole is close to the physical region, which leads to an enhancement of small momentum transfers $t_{i,i+1}$.

Instead of assuming individual particles coming off the multiperipheral chain, various models consider also clusters of particles (*e. g.* $\pi^+\pi^-$ pairs) coming off with small subenergies of the clusters. In this way, one hopes to extend the validity of the model to a larger part of the n-particle phase space.

In the MPP the cms longitudinal momenta of the secondary particles tend to be continuously distributed. The two particles c_1 and c_n at both ends of the chain have the tendency to keep the direction and a larger fraction of the energy of the two primary particles whereas particles towards the center of the chain populate predominantly the central region of the total longitudinal momentum distribution. This central region is often referred to as the pionisation region, where however several definitions for "pionisation" have been given in the literature.

2. *Diffractive fragmentation picture (DFP)*

In the fragmentation model the secondary particles are considered as fragments of the two incident particles a (beam) and b (target) so that they can be subdivided into two groups:

particles coming from the fragmentation of the beam particle a (a-fragments). They should have the tendency to go forward in the cm system (forward fragments), the forward tendency becoming stronger with increasing energy;
particles coming from the fragmentation of the target particle b (b-fragments). They should have the tendency, increasing with larger energy, to go backward in the cms (backward fragments).

Two hypotheses have been made concerning the behaviour of the fragments at high cms energies $\sqrt{s}$:

factorisation: The fragmentation of a, *i. e.* the behaviour of the forward fragments, should depend on particle a and not on particle b, *i. e.* not on the particle which causes particle a to fragment; and *vice versa.*
limiting fragmentation [12]: In the rest system of a (projectile system) the momentum $\boldsymbol{p}$ of an a-fragment should remain finite and the various momentum distributions in the projectile system should approach limiting functions of $\boldsymbol{p}$ independent of s. Analogously for a b-fragment: Its momentum should be finite and the momentum distributions should become independent of s in the rest system of b (lab system).

The hypothesis of limiting fragmentation (HLF) will be discussed in more detail in connection with the single particle distributions in Chapter D4.

A specific and important kind of fragmentation occurs if the system of a-fragments (b-fragments) has the same quantum numbers (apart from spin and parity) as a (b), *i. e.*

if in the fragmentation process no quantum numbers are exchanged. In elastic scattering such a process without exchange of quantum numbers is dominated at high energies by diffraction scattering (Pomeron $\mathcal{P}$-exchange) with energy independent cross section. Its generalisation to few- and many-body processes then leads to the diffractive fragmentation picture (DFP) in which the fragmentation of a and/or b comes about by inelastic diffraction scattering (diffraction dissociation) with the diagrams

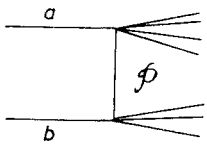

double diffraction dissociation

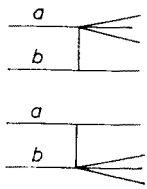

single diffraction dissociation

Both the MPP and the DFP are extreme pictures; none of them seems to be able alone to describe all the data. As a more realistic picture several authors [13–20] have therefore introduced various versions of a two-component-model, according to which both mechanisms MPP and the DFP (or similar mechanisms) contribute to particle production at high energy. The two-component picture will be discussed in more detail in Chapter C5 below.

C. TOPOLOGICAL CROSS SECTIONS AND MULTIPLICITIES

1. Introduction

This Chapter is concerned with the cross section $\sigma(n, s)$ for the production of n particles in pp-collisions as a function of the multiplicity n and the total cms energy $\sqrt{s}$. Various multiplicities may be of interest, *e. g.*:

n_t = number of all secondaries (total multiplicity);
$n = n_{ch}$ = number of charged secondaries (charged multiplicity, prong number);
$n_{\pm}$ = number of positive or negative secondaries, mainly pions (positive, negative multiplicity);
n_{π^0} = number of produced π^0's, *etc.*

Relatively little is known at high energies about the π^0 multiplicity, the main results being:

From data at NAL [21] and ISR [22] energies the average π^0 multiplicity $\bar{n}_{\pi^0}$ seems to grow roughly like $\log s$, *i. e.* proportionally to the average charged multiplicity (see below). This is seen in Fig. 1a. The straight line is

$$\bar{n}_{\pi^0} = 1.51 \log (0.512 \sqrt{s}). \tag{2}$$

Notice however the large errors of the ISR points.

At 205 GeV/c [21] the rates of π^0 and π^- production for each prong number are very similar (Fig. 1b). At ISR energies it was concluded [23] from the data of Ref. [22]

that in the average, at least for particular parts of the phase space, $\bar{n}_{\pi^0} \approx \bar{n}_{\pi^-} \approx \bar{n}_{\pi^+}$. It was found that the average π^0 multiplicity $\bar{n}_{\pi^0}$ increases, at fixed energy, proportionally to the charged multiplicity n of an event, see Fig. 1c (NAL 205 GeV/c) and Fig. 2 (ISR). This indicates strong positive correlations between neutral and charged pions (see Chapter E).

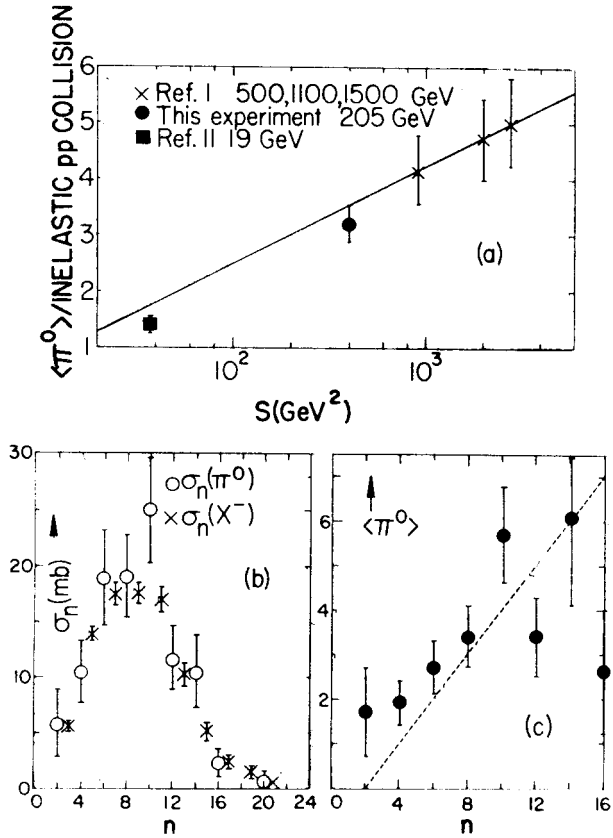

Fig. 1. (a) Average π^0 multiplicity $\bar{n}_{\pi^0}$ *vs* s. The curve corresponds to $\bar{n}_{\pi^0} = 1.51 \log (0.512 \sqrt{s})$. (b) Cross sections for π^0 and π^- production *vs* prong number n at 205 GeV/c. (c) $\bar{n}_{\pi^0}$ *vs* prong number n at 205 GeV/c. The dashed straight line is $\bar{n}_{\pi^0} = n_-$ (from Ref. [21])

At lower energies on the other hand $\bar{n}_{\pi^0}$ seems to be independent of n, see *e. g.* Fig. 3 of the Bonn-Hamburg-München (BHM) collaboration at 12 and 24 GeV/c.

In the following we concentrate on the multiplicities for charged particles. The following quantities are of interest:

a. topological cross sections $\pi(n, s)$ as functions of s for fixed prong number n.

b. Energy dependence of average multiplicity:

$$\bar{n}(s) = \frac{\sum_n n\sigma(n, s)}{\sum_n \sigma(n, s)} = \frac{1}{\sigma_T(s)} \sum_n n\sigma(n, s), \tag{3}$$

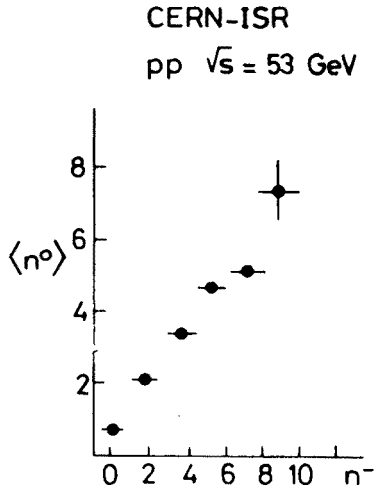

Fig. 2. $\bar{n}_{\pi^0}$ *vs* number n_- of negative particles at $\sqrt{s} = 53$ GeV (CERN–Hamburg–Vienna collaboration, from Ref. [7])

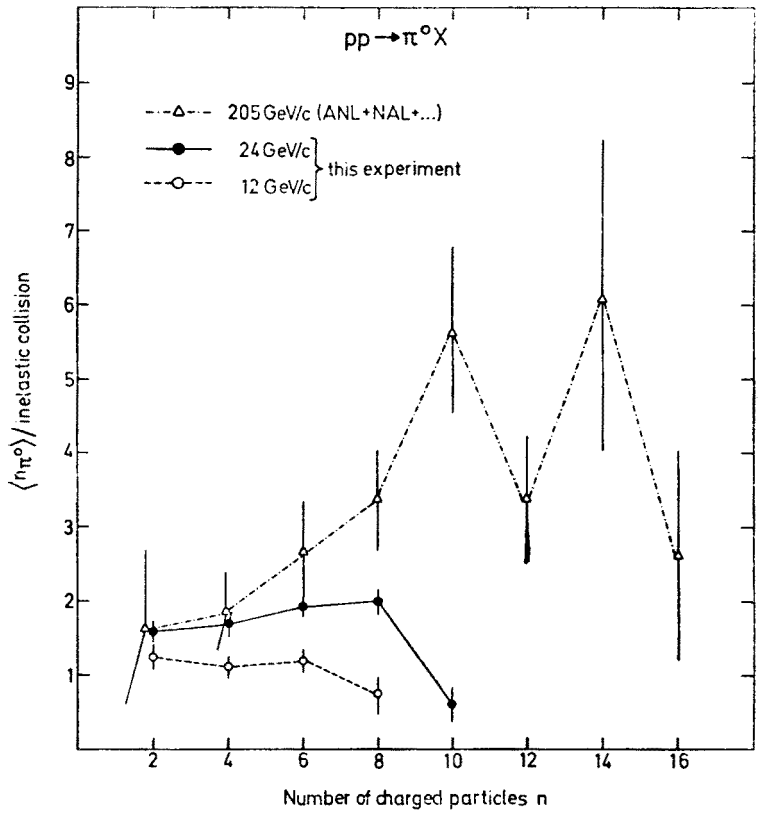

Fig. 3. $\bar{n}_{\pi^0}$ *vs* prong number n at 12, 24 and 205 GeV/c (Bonn–Hamburg–München collaboration [57] and Ref. [21])

where $\sigma_T(s)$ = total or total inelastic pp cross section, depending on whether elastic pp scattering is included or not (usually, elastic scattering is excluded).

c. Multiplicity distributions: $W(n, s) \propto \sigma(n, s)$ as a function of n for fixed s. Quantities to be deduced from a multiplicity distribution are:
average multiplicity $\bar{n}$ (see (3));
dispersion (width) D of the multiplicity distribution

$$D^2 = \overline{(n-\bar{n})^2} = \overline{n^2} - \bar{n}^2; \tag{4}$$

correlation parameter f_2 (= integral of two particle correlation function over momenta, see Chapter E)

$$f_2 = \overline{n(n-1)} - \bar{n}^2 = D^2 - \bar{n}. \tag{5}$$

For a Poisson distribution

$$P(n) = \frac{\bar{n}^n e^{-\bar{n}}}{n!}, \tag{6}$$

$$D^2 = \bar{n}, f_2 = 0 \tag{7}$$

i. e. the n particles or particle clusters are emitted uncorrelated;

higher multiplicity moments $\overline{n^2}$ and higher correlation parameters (integrals of higher correlation functions).

Assume that between two multiplicities n_1 and n_2 the following relation exists:

$$n_2 = \alpha n_1 + \beta. \tag{8}$$

Examples for pp collisions: $n = n_{ch} = 2n_- + 2 = 2n_+ - 2$, $n_+ = n_- + 2$.
It is then easy to show that the following relations hold for the average multiplicities, the dispersions and the correlation parameters:

$$\bar{n}_2 = \alpha_1 \bar{n} + \beta, \tag{9}$$

$$D_2 = \alpha D_1 \Rightarrow D \gtrless D_1 \text{ for } \alpha \gtrless 1, \tag{10}$$

$$f_{22} = \alpha^2 f_{21} + \alpha(a-1)\,\bar{n}_1 - \beta = \alpha^2 f_{21} + (\alpha - 1)\,\bar{n}_2 - \alpha\beta. \tag{11}$$

From (11) it follows: If n_1 follows a Poisson distribution ($f_{21} = 0$), n_2 does not follow a Poisson distribution ($f_{22} \neq 0$). In fact, neglecting $\alpha\beta$ for large $\bar{n}_2$:

$$f_{22} \approx (\alpha - 1)\,\bar{n}_2 \begin{cases} > 0 \text{ (broader than Poisson) if } \alpha > 1, \\ < 0 \text{ (narrower than Poisson) if } \alpha < 1. \end{cases} \tag{12}$$

2. Predictions of MPP and DFP

Before we come to the experimental results, we summarize the predictions which the two pictures MPP and DFP in their simplest forms make for $\sigma(n, s)$ and the related quantities introduced above (see *e. g.* Table 4.1 of Ref. [2]).

a. Predictions of MPP

multiplicity distribution (see *e. g.* Ref. [24])

If the secondary particles come off the multiperipheral chain in uncorrelated clusters, *i. e.* in groups of particles with possible correlations within, but not amongst the clusters, then one expects a Poisson distribution for the number of clusters. Flexibility exists in that one can make various assumptions as to the nature of the clusters, *e. g.*:

* Poisson distribution for the number of all produced particles (mainly pions, Chew-Pignotti model). The multiplicity distribution $W(n)$ for the charged particles, *i. e.* the topological cross sections can then be derived only with assumptions for the ratio of charged to neutral pions.[1]

* Poisson distribution for the number n of charged particles (independent emission of charged particles):

$$W_1(n) = \frac{\bar{n}^n e^{-\bar{n}}}{n!}. \tag{13}$$

* Poisson distribution for the number n_- of $\pi^+\pi^-$ pairs (independent emission of pion pairs. This case one would get for multipion exchange, it would mean local charge conservation):

$$W(n_-) = \frac{\bar{n}_-^{n_-} e^{-\bar{n}_-}}{n_-!}, \quad f_{2-} = D_-^2 - \bar{n}_- = 0. \tag{14}$$

With (8) to (11) one would then get for the charged multiplicity $n = 2n^- + 2$

$$W_2(n) = \frac{[\frac{1}{2}(\bar{n}-2)]^{\frac{1}{2}(n-2)} e^{-\frac{1}{2}(\bar{n}-2)}}{[\frac{1}{2}(n-2)]!}, \quad D = 2D_-, \quad f_2 = \bar{n} - 4. \tag{15}$$

Thus, n is not distributed Poisson-like; for large $\bar{n}$ f_2 is positive, *i. e.* the distribution is broader than a Poisson distribution.

* Further possibilities can be thought of. In general however it has to be emphasized that in a realistic picture there is no sharp separation between correlated and uncorrelated particles. Instead, short range correlations are expected to go down smoothly with increasing distance of the particles in momentum space, *e. g.* exponentially with the difference in rapidity. Thus, any Poisson distribution is expected to be only a rough approximation, as will indeed be seen from the data below.

average multiplicity and topological cross sections as functions of s

A typical feature of the MPP, already pointed out in the original version of Amati, Fubini and Stanghellini, is the prediction that at high energies $\bar{n}$ should increase as $\log s$:

$$\bar{n}(s) = A + B \log s \text{ with } B > 0. \tag{16}$$

[1] *E. g.* alternating $I = 0$ and $I = 1$ exchange along the multiperipheral chain.

Combining this with a Poisson distribution (13) assumed for n, one obtains for the topological cross section:

$$\sigma(n, s) = \sigma_T \frac{(A+B \log s)^n e^{-(A+B \log s)}}{n!} \xrightarrow[s\to\infty]{} \propto \frac{B^n}{n!} (\log s)^n s^{-B} \xrightarrow[s\to\infty]{} 0, \tag{17}$$

$$i.\,e.\ \sigma(n, s) \xrightarrow[r\to\infty]{} 0 \text{ for fixed } n. \tag{18}$$

σ_T is the total (inelastic) pp cross section, which is roughly energy independent at high energies (notice however the increase from $\sim$ 39 to $\sim$ 43 mb recently observed [25] for the pp total cross section in the range of ISR energies). With a Poisson like distribution and with $\bar{n} \propto \log s$ the MPP thus predicts that each topological cross section $\sigma(n, s)$ should go asymptotically to zero such that $\sigma_T = \sum_n \sigma(n, s)$ remains roughly constant. This rough constancy of the sum is then due to the inset, with increasing energy, of new channels with higher and higher multiplicities, *i. e.* the decrease of each $\sigma(n, s)$ is roughly compensated by the increasing number of channels.

correlation parameter f_2 and dispersion D

Consider as an example the correlation parameter f_{2-} for negative particles, experimental data on which will be discussed below. Three cases may be thought of:

* If n_- satisfies a Poisson distribution, then $f_{2-} = 0$ according to (7).

* If the number n of charged particles satisfies a Poisson distribution, the distribution for $n_- = \frac{1}{2}(n-2)$ is narrower than Poisson according to (11) and (12) ($\alpha = \frac{1}{2}$) and $f_{2-} = -\frac{1}{2}\bar{n}_- + \frac{1}{2}$. With $\bar{n}_- \propto \log s$ according to (16) one obtains for f_{2-} the energy dependence $f_{2-} \propto -\log s$.

* On the other hand short range correlations between the negative particles lead to an energy dependence $f_{2-} \propto +\log s$. In a Poisson description this case would correspond to a Poisson distribution for clusters containing several negative particles ($\alpha > 1$ in (11) and (12)), so that the n_- distribution is broader than Poisson leading to positive f_{2-}.

One thus sees, that the MPP predicts for f_{2-} the energy dependence

$$f_2^-(s) = k \log s \tag{19}$$

with vanishing, negative or positive k. The prediction for the dispersion D is

$$D_-^2(s) \propto \log s \tag{20}$$

since $D_-^2 = f_{2-} + \bar{n}_-$ according to (5).

b. Predictions of DFP

topological cross sections, average multiplicity and multiplicity distributions

A main feature of DFP is the prediction that each topological cross section $\sigma(n, s)$ goes with increasing energy towards a finite, energy independent diffractive rest σ_n:

$$\sigma(n, s) \xrightarrow[s\to\infty]{} \sigma_n. \tag{21}$$

No prediction is made in the DFP about the energy dependence of the average multiplicity. Hwa [26] has pointed out that the logarithmic law (16) $\bar{n}(s) \propto \log s$ can be obtained with (21) and a constant total cross section σ_T, if one assumes for the asymptotic topological cross sections σ_n, the following n-dependence for large n:

$$\sigma_n = \frac{c}{n^2}. \tag{22}$$

Proof:

$$\bar{n}(s) = \frac{1}{\sigma_T} \sum_n n\sigma_n \propto \int^{N(s)} dn \frac{n}{n^2} \propto \log N(s) + b = A + B \log s, \tag{23}$$

since the maximum number $N(s)$ of particles which can be produced is proportional to the total cms energy $\sqrt{s}$.

dispersion D and correlation parameter f_2

With (21) and (22) one obtains at high energies

$$\overline{n^2} = \frac{1}{\sigma_T} \sum n^2 \sigma_n \propto \int^{N(s)} n^2 \frac{1}{n^2} dn \propto N(s) + c' \propto \sqrt{s} + c.$$

Therefore

$$D^2 = \overline{n^2} - \bar{n}^2 \propto +\sqrt{s} \text{ for large } s, \tag{24}$$

$$f_2 = D^2 - \bar{n} \propto +\sqrt{s}. \tag{25}$$

So the DFP predicts a positive correlation parameter which varies with energy stronger ($\propto \sqrt{s}$) than in the MPP ($\propto \log s$). This means that in the DFP the multiplicity distribution is broader than Poisson.

TABLE I

Summary of predictions of MPP and DFP

Quantity	MPP	DFP
$\bar{n}(s)$	$A + B \log s$	no prediction
s-dependence of $\sigma(n, s)$	$\xrightarrow[s\to\infty]{} 0$	$\xrightarrow[s\to\infty]{} \sigma_n = \text{const}$
n-dependence of $\sigma(n, s)$	Poisson like	const. $\frac{1}{n^2}$ if $\bar{n} \propto \log s$ assumed
$D^2(s)$	$\propto \log s$	$\propto \sqrt{s}$
$f_2(s)$	$\propto \log s$	$\propto \sqrt{s}$

3. Experimental results

a. Topological cross section $\sigma(n, s)$ as functions of s for fixed n

Fig. 4 (see also Fig. 14) shows a recent compilation [7] of topological pp cross sections up to large multiplicities ($n = 26$) as functions of energy. The points at the highest energies are from three NAL bubble chamber experiments [28, 29, 30] at $p_L = 102$, 205 and 303 GeV/c respectively. Values at ISR energies do not yet exist, but will become available soon.

For each n, $\sigma(n, s)$ rises from threshold, reaches a maximum and then seems to drop off with increasing energy. The energy of the maximum increases with increasing n, so that

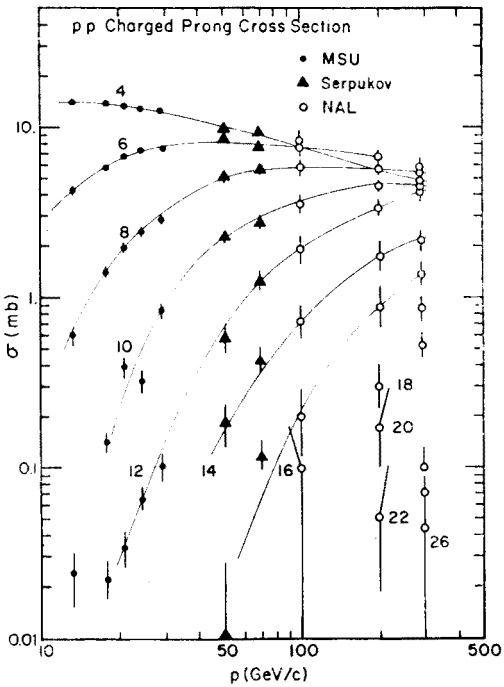

Fig. 4. Topological cross sections $\sigma(n, s)$ *vs* p_{Lab} for $n = 4$ to 26 (from Ref. [7])

in the energy range explored so far only for $\sigma(2)$ and $\sigma(4)$ a clear drop off can be noticed: $\sigma(2)$ decreases by a factor of ~ 6 and $\sigma(4)$ by a factor of ~ 3 between 13 and 300 GeV/c [16] and both cross sections seem to continue to decrease. From these experimental results it thus can be concluded that below 300 GeV/c $\sigma(2)$ and $\sigma(4)$ have not yet reached diffractive constant limits and that a purely diffractive model for low multiplicities does not yet work at NAL energies. The question, if the topological cross sections go to zero (MPP) or to finite constant values (DFM) cannot yet be answered and a decision between MPP and DFM on the basis of the energy dependence of $\sigma(n, s)$ is not yet possible.

A further discussion of $\sigma(n, s)$ will be given below in connection with the two-component model (Section C5).

b. Average charged multiplicity $\bar{n}(s)$ as a function of energy

Since the last year new results for the average charged multiplicity have been obtained at Serpukhov [31] (50 and 69 GeV/c), at NAL [28, 29, 30] (102, 205, 303 GeV/c) and at the ISR [7, 23, 32, 33]. Two recent compilations are shown in Figs 5 and 6. Fig. 6 contains also the average multiplicities for various kinds of produced particles. The new results have

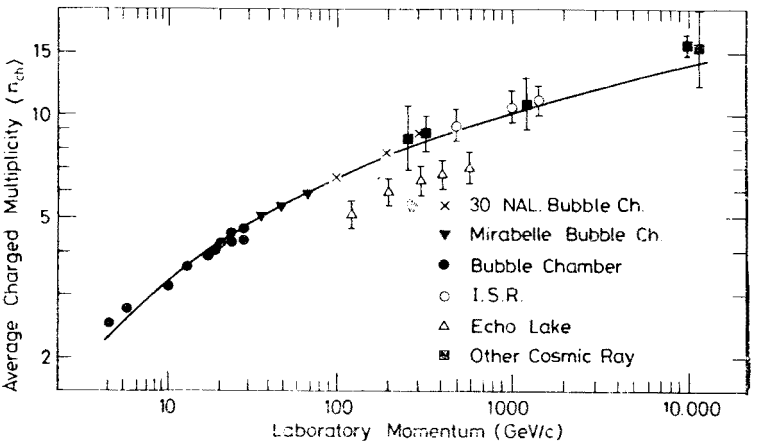

Fig. 5. Average charged multiplicity *vs* p_{Lab} (from Ref. [33])

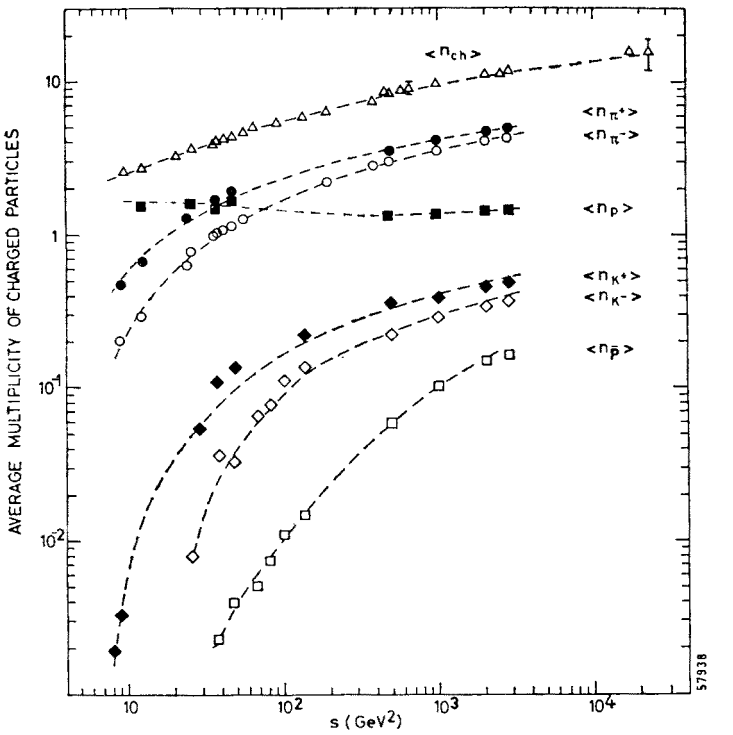

Fig. 6. Average multiplicity for various and all charged particles *vs* s (from Ref. [32])

shown that earlier results, obtained in a cosmic ray experiment at Echo Lake [34] between 100 and 1000 GeV/c, are too low (see Fig. 5).

Many authors have fitted a variety of energy dependent expressions to the experimental values for $\bar{n}(s)$. The most recent one is given in Ref. [32] (see curve in Fig. 6)

$$\bar{n}(s) = (-3.8 \pm 0.4) + (1.88 \pm 0.07) \log s + (6.4 \pm 0.7)\, s^{-\frac{1}{2}} \ (s \text{ in } \mathrm{GeV}^2) \tag{26}$$

and is shown by the curve in Fig. 6. The fit reflects the observation, that up to NAL energies $\bar{n}(s)$ rises steeper than $\propto \log s$, *i. e.* has a positive curvature. It seems that at lower energy $\bar{n}(s)$ increases with a power of s, whereas at higher energies the logarithmic s-dependence takes over (at $s = 3000\ \mathrm{GeV}^2$ the $s^{-\frac{1}{2}}$ term in (26) contributes only 0.1 to $\bar{n}(s)$, whereas the log s term contributes 15).

As will be discussed in Section D5, a central plateau has been observed at ISR energies in the rapidity distribution $d\sigma/dy$ (integrated over transverse momenta) for pions in inclusive pp-reactions, so that the cms rapidity distribution has roughly the following shape:

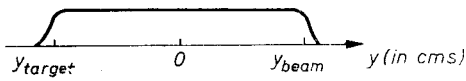

From the relation (see equation (114) below)

$$\bar{n} = \frac{1}{\sigma_T} \int \frac{d\sigma}{dy}\, dy$$

one then obtains the following relation between the average π^--multiplicity and the height $d\sigma/dy|_{y=0}$ of the π^- plateau:

$$\bar{n}_-(s) = \frac{1}{\sigma_T} \int \frac{d\sigma}{dy}\, dy \approx \frac{1}{\sigma_T} \frac{d\sigma}{dy}(s)\bigg|_{y=0} \quad \text{range of } y.$$

Since the range of $y \approx \log s/m_p^2$ (see (80)),

$$\bar{n}_-(s) = A_- + B_- \cdot \log s \text{ with } B_- = \frac{1}{\sigma_T} \frac{d\sigma}{dy}\bigg|_{y=0}. \tag{27}$$

A more rigorous derivation of the relation between average multiplicity and the differential cross section at $y = 0$ can be found *e. g.* in Ref. [3].

Ferbel [35] has studied the energy dependence of $d\sigma/dy|_{y=0}$ for pions in various inclusive reactions. He finds, within the relatively large errors, a good description by the expression

$$B(s) \equiv \frac{1}{\sigma_T} \frac{d\sigma}{dy}(s)\bigg|_{y=0} = c + \frac{d}{p_L^{\frac{1}{2}}}, \tag{28}$$

where p_L is the lab momentum in GeV/c ($\propto s$ at large energy), see Fig. 7. d depends on the particular reaction (πp, γp, pp, Kp) whereas the scaling limit c could be independent of the initial particles as expected from factorisation in the double Regge limit of Mueller. Scaling

(see Section D4) would imply energy independence of $d\sigma/dy$, but is perhaps not yet fulfilled rigorously at present energies for all parts of the phase space.

For π^- in pp-collisions Ferbel finds

$$B_-(s) = 0.75\left(1 - \frac{1.24}{p_L^{\frac{1}{2}}}\right). \tag{29}$$

Inserting this into (27) and remembering that $n = 2n_- + 2$, he then obtains for the average charged multiplicity $\bar{n}(s)$ the energy dependence ($\log s = \log p_L +$ const):

$$\bar{n}(s) = \alpha + \beta\left(1 - \frac{1.24}{p_L^{\frac{1}{2}}}\right)\log p_L, \tag{30}$$

where β should be $2 \cdot 0.75 = 1.5$. Fig. 8 shows the experimental $\bar{n}$ values together with expression (30) (solid curve) with $\alpha = 2.2$ and $\beta = 1.5$. One sees that the extra energy

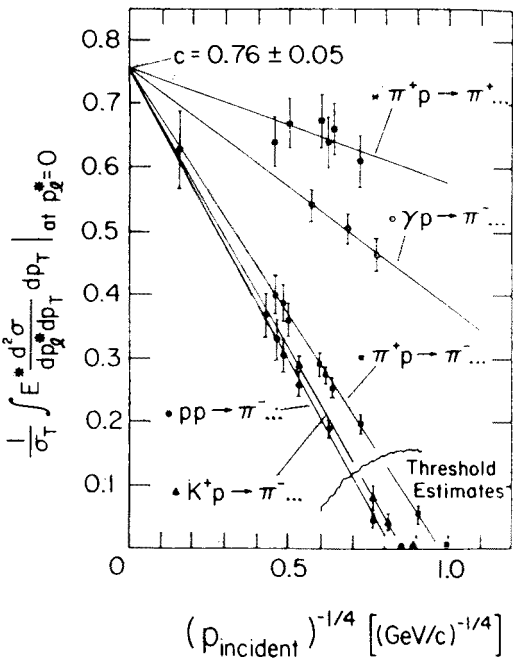

Fig. 7. Normalised invariant single particle inclusive cross section at $x = 0$ *vs* $p_{\text{Lab}}^{-1/4}$ (from Ref. [35])

dependence (29) of $B(s)$, as deduced from the height of the central plateau, describes the deviation of the experimental points from a simple $A + B \log s$ fit with constant B (dashed curve) rather well. On the other hand, the errors in Fig. 7 are large. Furthermore, more recent ISR data seem to indicate a $p_L^{-\frac{1}{2}}$ rather than a $p_L^{-\frac{1}{4}}$-dependence of $d\sigma/dy(s)|_{y=0}$. Finally, the latest data show that the $d\sigma/dy$ distribution in the central region is not completely independent of y (see Section D5). The analysis of Ferbel should therefore be considered with caution.

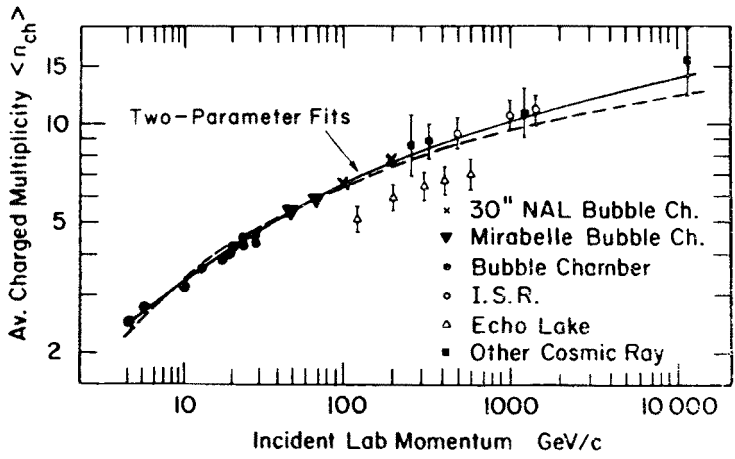

Fig. 8. Average charged multiplicity $\bar{n}$ *vs* p_{Lab}. For curves see text (from Ref. [35])

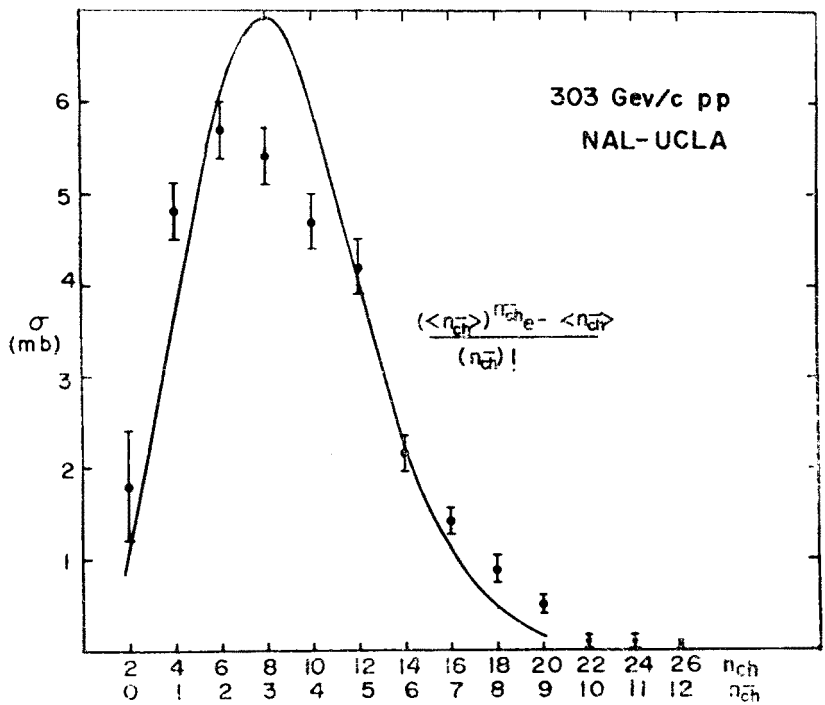

Fig. 9. Charged multiplicity distribution at 303 GeV/*c*. The curve is a Poisson distribution for n_- (NAL--UCLA collaboration, from Ref. [6])

c. Multiplicity distributions. It was pointed out already in 1970 by Wróblewski [24] at the Kiev Conference that the experimental multiplicity distributions are not described well by any of the various Poisson distributions (see *e. g.* (13), (15)). This result has been substantiated by the new NAL data [28, 29, 30, 36], as can be seen *e. g.* from

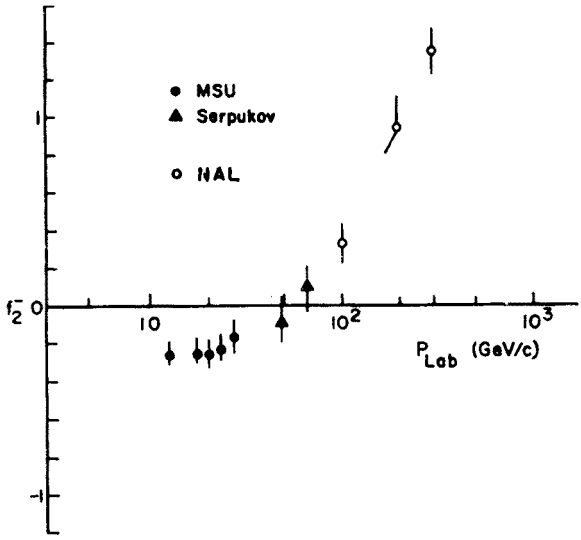

Fig. 10. Correlation parameter f_{2-} for negative particles *vs* p_{Lab} (from Ref. [6, 7])

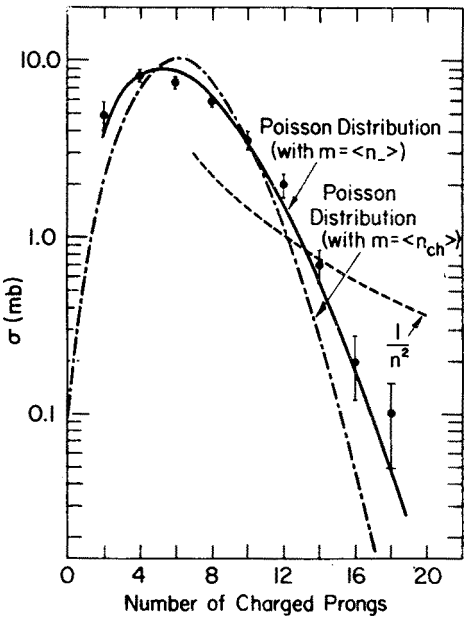

Fig. 11. Charged multiplicity distribution at 102 GeV/*c* (from Ref. [28])

Fig. 9 at 303 GeV/*c*, where the curve is a Poisson distribution for n^-. At the various energies the result is as follows [36]:

below Serpukhov energies ($\sim$ 70 GeV/*c*) the n_- distribution is narrower than Poisson ($D_-^2 < \bar{n}_-$);

at Serpukhov energies the n_- distribution is well described by Poisson ($D^2 \approx n^-$);

at NAL energies the n_- distribution is broader than Poisson; there is an excess of events with large n_- ($D^2_- > \bar{n}_-$).

According to (5) this result is reflected in the energy variation of the correlation parameter f_{2-} for negative particles, shown in Fig. 10: f_{2-} is negative below $\sim$ 70 GeV/c, vanishes at $\sim$ 70 GeV/c, and becomes positive above with rising tendency, indicating strong positive correlations between the negative particles at high energies. This rise

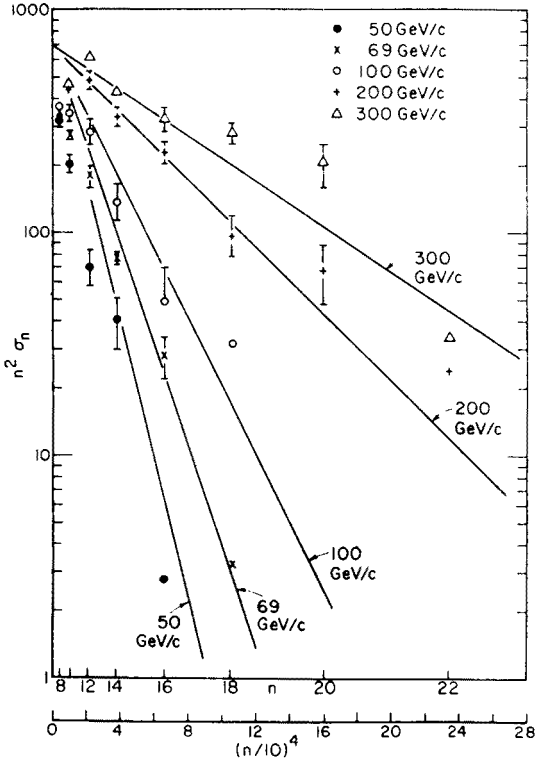

Fig. 12. $n^2\sigma_n$ *vs* n^4 for five momenta between 50 and 300 GeV/c. The lines are given by formula (35) in the text (from Ref. [37])

is faster than log s predicted by MPP. Similar evidence against MPP was reached by Berger [36] from a comparison of the energy dependence of $\overline{n(n-1)}$ and $\bar{n}^2$ for charged particles.

The $1/n^2$ law of DFP falls off for large n less steeply than a Poisson distribution and has therefore the right tendency at large energies. However a quantitative comparison with the data shows that $1/n^2$ falls off too slowly, see *e. g.* dashed curve in Fig. 11 at 102 GeV/c (where a Poisson for n_- (full curve) fits still rather well, $f_2 = 0.39 \pm 0.10$, *i. e.* still rather small).

In order to remove this discrepancy, Abarbanel and Kane [37] have modified the $1/n^2$ dependence using the following argument: With a $1/n^2$ law of DFP, $\sigma_n n^2$ *vs* n should be constant. As just mentioned this is not the case, as can also be seen from Fig. 12 where

$n^2\sigma_n$ is plotted *vs* n^4 for various energies. Large n values are suppressed. In a fireball model for the diffractive process large n originate from large masses M of the fireballs. For large M however the minimum momentum transfer $|t|_{\min}$ between incident proton and fireball is not zero, but larger than zero (boundary of Chew-Low plot $|t|$*vs* M^2). Thus the momentum transfer distribution

$$\frac{d\sigma}{dt} \propto e^{-b|t|} \tag{31}$$

starts at $|t|_{\min}$; the small-t part of the distribution is not allowed kinematically, which leads to a suppression of large M, *i. e.* of large n values. Therefore, integrating (31) from $|t|_{\min} > 0$, $n^2\sigma_n$ should not be constant, but proportional to $\exp(-b|t|_{\min})$:

$$n^2\sigma_n \propto e^{-b|t|_{\min}}, \tag{32}$$

where at large energies s

$$|t|_{\min} \approx M^4 m_p^2/s^2 \text{ for one fireball (single diffraction dissociation DD)}, \tag{33}$$

$$|t|_{\min} \approx M^2 M'^2/s \text{ for two fireballs (double diffraction dissociation DD)}.$$

M, M' are the masses of the fireballs, m_p is the proton mass. Notice the different s-dependence. With M and $M' \propto n$ and inserting (33) into (32) one obtains the result:

$$n^2\sigma_n \propto \exp\left(-\alpha \frac{n^4}{s^2}\right) \quad \text{for single DD},$$

$$n^2\sigma_n \propto \exp\left(-\beta \frac{n^4}{s}\right) \quad \text{for double DD}. \tag{34}$$

The lines in Fig. 12 show curves of the form

$$n^2\sigma_n = 700 \exp\left(-0.007 \frac{n^4}{s} \text{GeV}^2\right) \text{mb}. \tag{35}$$

They describe the experimental points not too badly in the whole energy region from 50 to 300 GeV/c, which means that in the exponent s^{-1} (*i. e.* double DD) and not s^{-2} (single DD) should be taken. This however is in contradiction with other results, according to which the contribution of double DD is small. Furthermore, it has been pointed out [38] that a t-cut leads to a depopulation in the rapidity distribution around $y^* \approx 0$ in the cms, which is not observed experimentally. Thus one has to conclude, that the attempt to save the $1/n^2$ law does not seem to be very satisfactory.

4. Summary of comparison of MPP and DFP with the data

Comparing the predictions of Table I with the experimental results just discussed, one can summarize the following weaknesses of MPP and DFP at present energies:

Weaknesses of MPP: At high energies the multiplicity distributions are broader than a Poisson distribution.

The correlation parameter f_2– rises with energy faster than log s. The average multiplicity rises somewhat faster than log s (although the log s behaviour is predicted only for very high energies).

Weaknesses of DFM: The $1/n^2$ law of DFM has too large a tail towards high n when compared with the experimental multiplicity distribution. The model of Abarbanel and Kane, which suppresses high n-values, is not in agreement with other experimental results.

At NAL energies the topological cross sections continue to fall with energy and have not yet reached a diffractive limit predicted by DFM.

5. *The two component picture (TCP)*

These failures of each of the two extreme pictures MPP and DFP have led several authors [13–20] to propose a two component picture (TCP), according to which both mechanisms MPP and DFP (or similar mechanisms) contribute to particle production at high energy. In this picture the contributions of the two mechanisms depend on the multiplicity n and on the energy s.

The quantitative formulation of the two component model goes as follows: Each topological cross section $\sigma_n(s)$ consists of a diffractive (fragmentation) and a nondiffractive (multiperipheral) part, $\sigma_n^{\mathrm{f}}(s)$ and $\sigma_n^{\mathrm{m}}(s)$:

$$\sigma_n(s) = \sigma_n^{\mathrm{f}}(s)+\sigma_n^{\mathrm{m}}(s). \tag{36}$$

(The energy dependence (s) will not be written explicitly in the following). The total (inelastic) cross section σ_{T} can then be written as:

$$\left.\begin{aligned} \sigma_{\mathrm{T}} &= \sum_n \sigma_n = F\sigma_{\mathrm{T}}+M\sigma_{\mathrm{T}} \text{ with} \\ F &= \frac{\sigma_{\mathrm{T}}^F}{\sigma_{\mathrm{T}}} = \frac{1}{\sigma_{\mathrm{T}}}\sum_n \sigma_n^{\mathrm{f}} \\ M &= \frac{\sigma_{\mathrm{T}}^M}{\sigma_{\mathrm{T}}} = \frac{1}{\sigma_{\mathrm{T}}}\sum_n \sigma_n^{\mathrm{m}} \end{aligned}\right\} F+M = 1. \tag{37}$$

For the lowest multiplicity moments $\bar{n}$ and $\overline{n^2}$, the dispersion D and the correlation parameter f_2 one then obtains:

$$\bar{n} = F\bar{n}^{\mathrm{f}}+M\bar{n}^{\mathrm{m}}, \tag{38}$$

$$\overline{n^2} = F\overline{n^{2\mathrm{f}}}+M\overline{n^{2\mathrm{m}}}, \tag{39}$$

with

$$\bar{n}^{\mathrm{f}} = \frac{\sum n\sigma_n^{\mathrm{f}}}{F\sigma_{\mathrm{T}}}, \quad \bar{n}^{\mathrm{m}} = \frac{\sum n\sigma_n^{\mathrm{m}}}{M\sigma_{\mathrm{T}}},$$

$$\overline{n^{2\mathrm{f}}} = \frac{\sum n^2\sigma_n^{\mathrm{f}}}{F\sigma_{\mathrm{T}}}, \quad \overline{n^{2\mathrm{m}}} = \frac{\sum n^2\sigma_n^{\mathrm{m}}}{M\sigma_{\mathrm{T}}}.$$

$$D^2 \equiv \overline{n^2} - \bar{n}^2 = FD_f^2 + MD_m^2 + FM(\bar{n}^f - \bar{n}^m)^2 \tag{40}$$

with $$D_f^2 = \overline{n^{2f}} - (\bar{n}^f)^2, \quad D_m^2 = \overline{n^{2m}} - (\bar{n}^m)^2.$$

$$f_2 \equiv D^2 - \bar{n} = Ff_{2f} + Mf_{2m} + FM(\bar{n}^f - \bar{n}^m)^2 \tag{41}$$

with $$f_{2f} = D_f^2 - \bar{n}^f = \overline{n(n-1)}^f - (\bar{n}^f)^2,$$

$$f_{2m} = D_m^2 - \bar{n}^m = \overline{n(n-1)}^m - (\bar{n}^m)^2.$$

These relations have been applied by Van Hove [19] with the following general assumptions (independent of any particular mechanism):

F and therefore M are energy independent;
the widths D_f and D_m are small compared to $\bar{n}_f$ and $\bar{n}_m$;
the average multiplicity for one mechanism is large compared to the average multiplicity for the other mechanism, *e. g.* $\bar{n}_f \ll \bar{n}_m$.

Expanding equation (40) according to these assumptions one then obtains:

$$D \approx a\bar{n} - b \text{ with } a = \sqrt{\frac{F}{M}},$$

$$b = a\bar{n}_f - \frac{MD_m^2 + FD_f^2}{2a\bar{n}}. \tag{42}$$

As will be discussed below, a linear relation of the form (42) has been observed by Wróblewski [39] with constant a and b, the empirical values being $a = b = 0.585$. Using this value for a one obtains [19] $F = 0.255$, $M = 0.745$ and from (37) $\sigma_T^F \approx 7.7$ mb, $\sigma_T^M = 22.5$ mb.

Analyses with more specific assumptions and therefore more detailed predictions have been carried out by several authors [15–18]. As an example we discuss the analysis of Harari and Rabinovici [16] in more detail. Since only the production of charged particles is considered (topological cross sections), n indicates in the following the number of negative particles ($n \equiv n_- = \frac{1}{2}(n_{ch} - 2)$). Thus $\sigma_0, \sigma_1, \ldots$ are the cross sections of inelastic two prongs, four prongs *etc.*

In order to fit the TCP to the experimental results, the following assumptions for the diffractive and nondiffractive parts are made:

a. The diffractive cross sections σ_n^f are energy independent, as predicted by DFM, and only σ_0^f, σ_1^f and σ_2^f are different from zero:

$$\sigma_0^f, \sigma_1^f, \sigma_2^f = \text{constant parameters},$$

$$\sigma_n^f = 0 \text{ for } n \geqslant 3 \text{ (}i.\ e.\text{ for } \geqslant 8 \text{ prongs)}.$$

This assumption is supported by a fit, in which σ_3^f was left free and turned out to be compatible with zero. It means that DFP contributes only to the lower multiplicities and that the DFP part of the multiplicity distribution does not follow the $1/n^2$ law as in a pure

diffractive model with $\bar{n} \propto \log s$. The assumption may however be questioned, since with increasing energy also higher n are expected to contribute to diffractive scattering.

One obtains:

$$\sigma_T^F = \sigma_0^f + \sigma_1^f + \sigma_2^f = \text{const},$$

$$F = 1 - M = \frac{\sigma_T^F}{\sigma_T} \text{ is energy independent, assuming energy independent } \sigma_T, \quad (43)$$

$$\bar{n}^f = \frac{\sigma_1^f + 2\sigma_2^f}{F\sigma_T}, \quad \overline{n^{2f}} = \frac{\sigma_1^f + 4\sigma_2^f}{F\sigma_T} \Rightarrow D_f^2, f_{2m} \text{ from (40) and (41).}$$

b. As for the nondiffractive part, $\bar{n}^m$ and f_{2m} are assumed to increase like $\log s$, as predicted by MPP (see Table I):

$$\bar{n}^m(s) = c_1 \log \frac{s}{s_1}, \quad f_{2m}(s) = c_2 \log \frac{s}{s_2}. \quad (44)$$

Assuming furthermore that all higher multiplicity moments $\overline{n^\alpha}^m$ with $\alpha \geqslant 3$ vanish, all $\sigma_n^m(s)$ are then determined by $\bar{n}^m$ and f_{2m}. Indeed it is easy to show that

$$\sigma_n^m(s) = \frac{1}{n!} \frac{d^n Q(z, s)}{dz^n}\bigg|_{z=0}, \quad (45)$$

where the generating function $Q(z, s) = \sum_{n=0}^{\infty} z^n \sigma_n(s)$ is determined by $\bar{n}^m$ and f_{2m}:

$$Q(z, s) = M\sigma_T \exp\{\bar{n}^m(s)(z-1) + \tfrac{1}{2} f_{2m}(s)(z-1)^2\}. \quad (46)$$

With the seven free parameters $\sigma_0^f, \sigma_1^f, \sigma_2^f, c_1, s_1, c_2, s_2$ and taking σ_T from experiment, all topological cross sections (36) and all quantities (37) to (41) deduced from them are then given, *e.g.*:

$$\sigma_n(s) = \sigma_n^m(s) + (\sigma_0^f + \sigma_1^f + \sigma_2^f), \quad (47)$$

where $\sigma_n^m(s)$ is determined by c_1, s_1, c_2, s_2 *via* (44), (45), (46).

$$F = \frac{\sigma_0^f + \sigma_1^f + \sigma_2^f}{\sigma_T}, \quad M = 1 - F, \quad (48)$$

$$\bar{n}(s) = Mc_1 \log \frac{s}{s_1} + \frac{\sigma_1^f + 2\sigma_2^f}{\sigma_T}, \quad \textit{i.e. } \bar{n}(s) = A + B \log s, \quad (49)$$

$$f_2 = MFc_1^2 \log^2 \frac{s}{s_1} + O(\log s), \quad \textit{i.e. } f_2 = C + D \log s + E(\log s)^2. \quad (50)$$

The experimental data between 50 and 300 GeV/c and the results of the fit (curves) are shown in Figs 13, 14, 15.

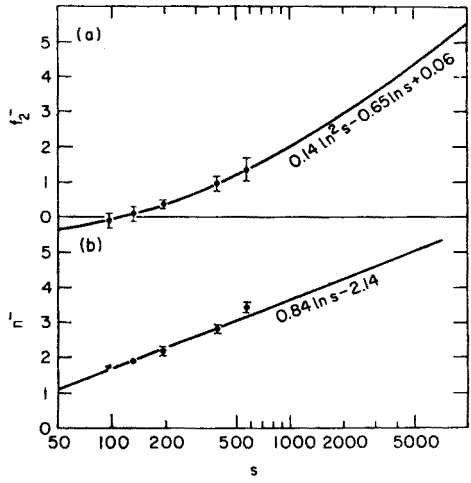

Fig. 13. (a) Correlation parameter f_{2-} and (b) average multiplicity $\bar{n}_-$ for negative particles *vs* s. The curves show the result of a fit described in the text (from Ref. [16])

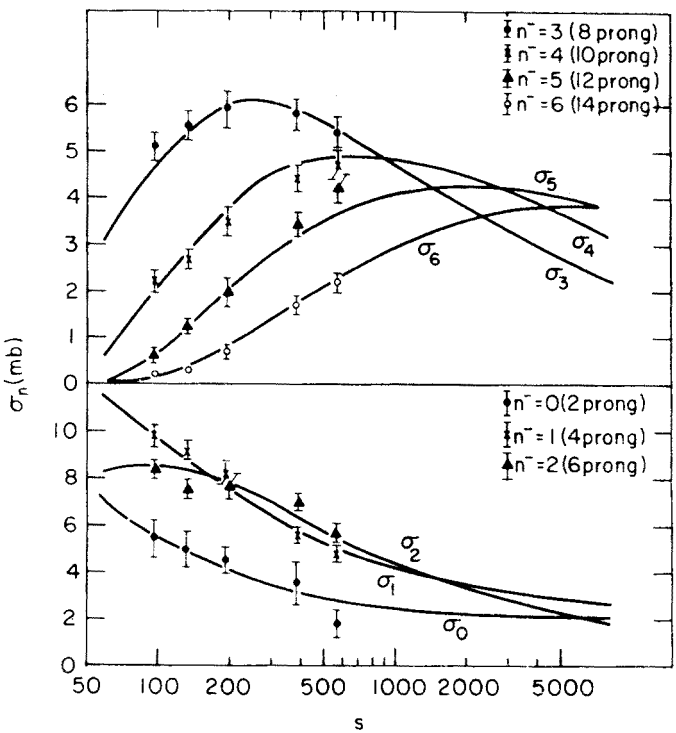

Fig. 14. Topological cross sections σ_n for 2–14 prongs *vs* s. The curves show the results of a fit described in the text (from Ref. [16])

One sees that the model fits the data very well. The parameters came out to be:

$$\sigma_0^f = 2.0 \text{ mb}, \ \sigma_1^f = 2.2 \text{ mb}, \ \sigma_2^f = 0.9 \text{ mb},$$

$$c_1 = 1.0, \ s_1 = 15 \text{ GeV}^2, \ c_2 = 0.35, \ s_2 = 200 \text{ GeV}^2,$$

leading to the following results:

$$F = 0.16, \quad M = 0.84, \quad \frac{F}{M} = 0.19,$$

$$\bar{n}_- = 0.84 \log s - 2.14,$$

$$f_{2-} = 0.14 \log^2 s - 0.65 \log s + 0.06.$$

Discussion:

The nondiffractive part M gives the main contribution (84%) whereas the fragmentation contributes only 16% to σ_T, *i. e.* $\sigma_T^F \sim 5$ mb and $\sigma_T^M \sim 26$ mb ($\sigma_T \sim 31$ mb). Fragmentation contributes to the low multiplicities, whereas the high multiplicities come

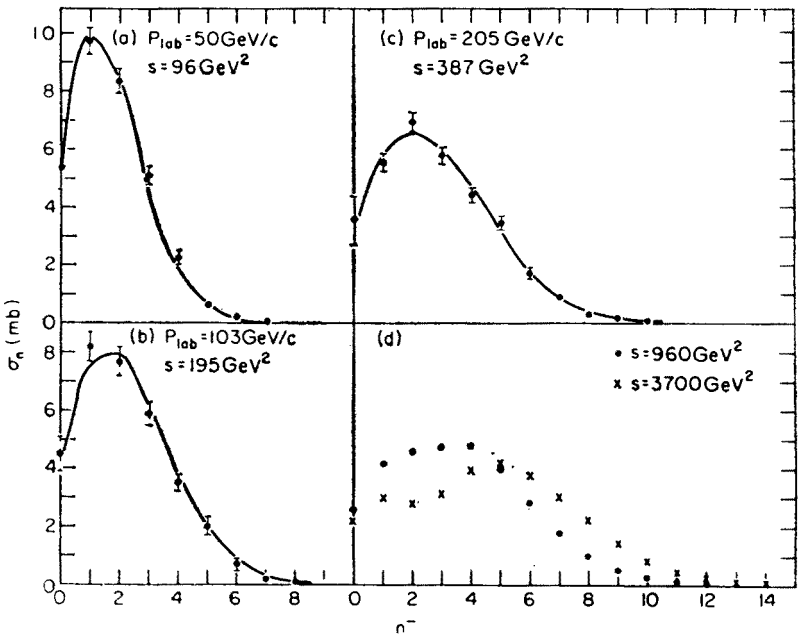

Fig. 15. Charged multiplicity distributions at $p_{Lab} = 50$ (a), 103 (b), 205 (c) GeV/c. The curves show the results of a fit described in the text. (d) Predictions of the fit at $s = 960$ and 3700 GeV² (from Ref. [16])

from the nondiffractive mechanism. For the topological cross sections the model makes predictions at higher energies (see Fig. 14) and it will be interesting to see how they agree with forthcoming ISR results. A very interesting prediction is made for the multiplicity distribution at the highest ISR energies (see Fig. 15d for $s = 3700$ GeV²). At these energies the diffractive and nondiffractive contributions begin to separate leading to a two bump

structure in the multiplicity distribution. It will be exciting to see, if such a structure will occur in future ISR data.

Analyses similar to the one of Ref. [16] have been performed by other authors, *e. g.* Ref. [15], [17] and [18]. They will not be discussed here in detail. Fiałkowski and Miettinen [17, 18] find $\sim 22\,\%$ diffractive ($\sigma_T^F \sim 7$ mb) and $\sim 78\,\%$ nondiffractive ($\sigma_T^M \sim 25$ mb) production (in good agreement with Ref. [19]); also here the diffraction contributes mainly to the low multiplicities. Also from this analysis a separation of the two mechanisms in the multiplicity distribution at very high energies is predicted.

6. Further studies of multiplicities

Several authors have observed various regularities of multiplicity distributions, some of which will be described in the following.

Czyżewski and Rybicki [40, 24] observed several years ago that the charged multiplicity distribution $\sigma_n(s)/\sigma_T$ for πp and pp collisions at high energies obeys the following scaling law:

$$D(s)\frac{\sigma_n(s)}{\sigma_T} = \tilde{\psi}\left(\frac{n-\bar{n}(s)}{D(s)}\right), \tag{51}$$

where D is the dispersion and $\tilde{\psi}(x)$ is a universal function depending only on $x = (n-\bar{n})/D$ and not explicitly on the energy s nor on the kind of incident particles. For $\tilde{\psi}(x)$ the authors gave the expression

$$\tilde{\psi}(x) = 2de^{-d^2}\frac{d^{2(dx+d^2)}}{\Gamma(xd+d^2+1)}, \tag{52}$$

where d is a free parameter and $\Gamma(z)$ the Γ-function. With $d = 1.8$ formulae (51) and (52) describe the experimental values rather well for πp and pp reactions and at all energies, as is seen from the curves in Fig. 16.

The same authors [40, 41] also found that

$$\frac{\bar{n}(s)}{D(s)} \approx \text{const.}\ (\approx 2) \tag{53}$$

above $\sim$ 50 GeV/c as can be seen *e. g.* from Fig. 17 which shows $\bar{n}/D$ *vs* p_L. Notice that for a Poisson distribution one would expect $\bar{n}/D^2 = 1$ (see (7)). It has been pointed out that with (53) and $\bar{n}(s) \propto \log s$ one gets for the correlation parameter

$$f_2 \equiv D^2 - \bar{n} \propto \bar{n}^2 - a\bar{n} \propto (\log s)^2 \text{ for large } s \tag{54}$$

i. e. an energy dependence in agreement with the two-component picture, see (50). If one inserts the empirical result (53) into the empirical formula (51) one obtains:

$$\bar{n}(s)\frac{\sigma_n(s)}{\sigma_T} = \psi\left(\frac{n}{\bar{n}(s)}\right) \tag{55}$$

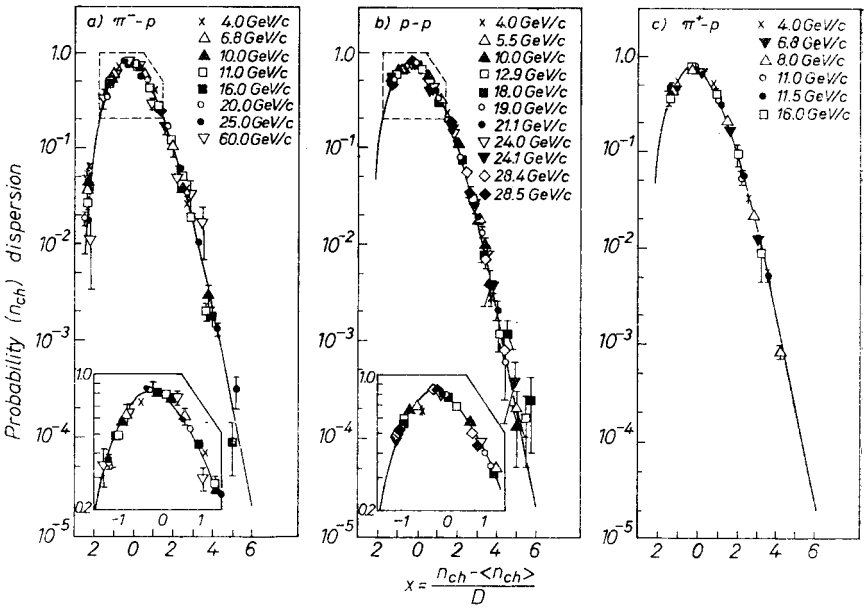

Fig. 16. $D \cdot \frac{\sigma_n}{\sigma_T}$ *vs* $\frac{n-\bar{n}}{D}$ for charged particles from (a) π^-p, (b) pp, (c) π^+p-collisions at various energies (see text for definition of variables) (from Ref. [24])

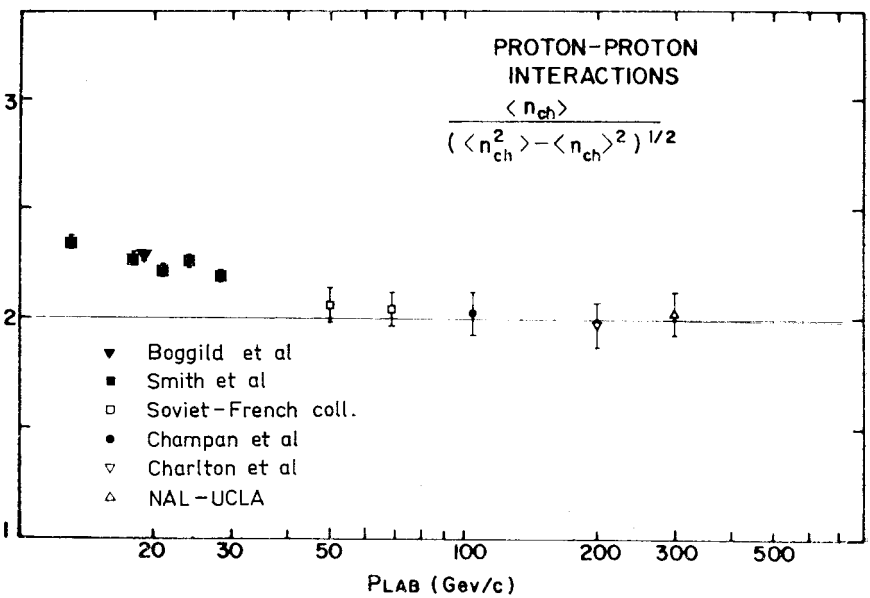

Fig. 17. $\frac{\bar{n}}{D}$ for charged particles *vs* p_{Lab} (from Ref. [30])

without explicit energy dependence. A derivation of this scaling formula has been given by Koba, Nielsen and Olesen [42] using the assumption that the semiinclusive invariant n-particle distribution (see Section D1) shows Feynman scaling for high energies (semi-inclusive scaling).

The Koba-Nielsen-Olesen formula (55) has been tested by Slattery [43] with pp data between 50 and 300 GeV/c, see Fig. 18. It is seen that in this energy range $\bar{n}\,\sigma_n/\sigma_T$

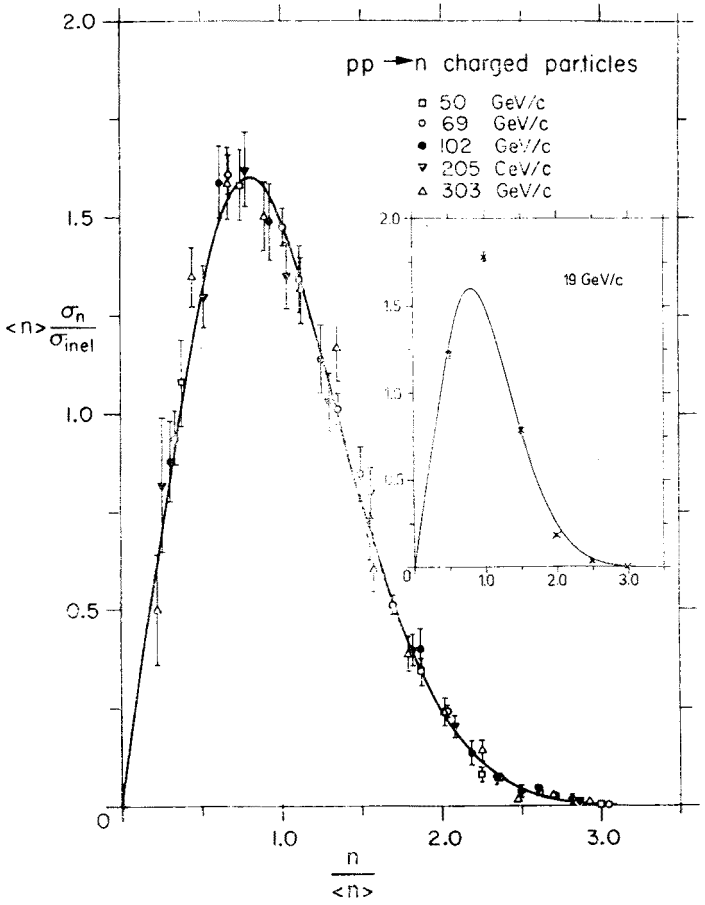

Fig. 18. $\bar{n}\cdot\frac{\sigma_n}{\sigma_T}$ *vs* $\frac{n}{\bar{n}}$ for charged particles at various lab momenta between 50 and 303 GeV/c. The curve is given by formula (56) in the text. Insert: The same at $p_{\mathrm{Lab}} = 19$ GeV/c (from Ref. [43])

indeed follows a universal curve when plotted against $n/\bar{n}$. Notice that in this plot a point for fixed n moves to the left with increasing energy, *i.e.* increasing $\bar{n}$. The curve in Fig. 18 is the function (determined from a fit):

$$\psi(z) = (3.79z + 33.7z^3 - 6.64z^5 + 0.332z^7)\exp(-3.04z) \quad \text{with} \quad z = \frac{n}{\bar{n}}. \tag{56}$$

The insert in Fig. 18 shows that the scaling function (56) does not describe the data at lower energies (19 GeV/c).

Two recent developments should be mentioned in connection with the Koba-Nielsen-Olesen (KNO) scaling. Instead of (53) Wróblewski [39] has observed the following regularity between $\bar{n}(s)$ and $D(s)$ in pp-collisions:

$$D(s) = 0.585\,(\bar{n}(s) - 1). \tag{57}$$

This relation is in good agreement with the data between 4 to 300 GeV/c, see Fig. 19. It thus includes in particular also the energies below 50 GeV/c and therefore covers a larger

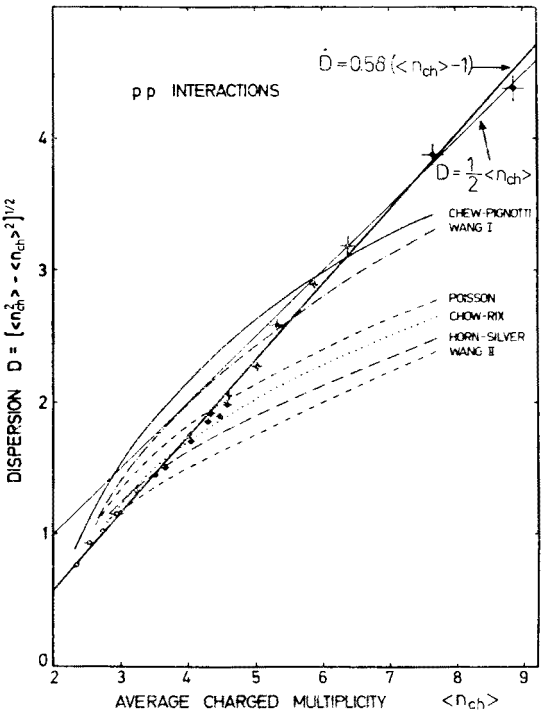

Fig. 19. Dispersion D *vs* $\bar{n}$ for charged particles. The straight line is $D = 0.585 \cdot (\bar{n} - 1)$ (from Ref. [39])

energy range than (53). Furthermore, instead of the KNO formula (55), Wróblewski proposes the following scaling relation, which is directly obtained by inserting (57) into (51):

$$(\bar{n}(s) - 1)\,\frac{\sigma_n(s)}{\sigma_T} = \psi\left(\frac{n-1}{\bar{n}(s)-1}\right) \tag{58}$$

i.e. n and $\bar{n}$ in (55) should be replaced by $n-1$ and $\bar{n}-1$ according to the replacement of (53) by (57). All the data, including also the ones below 50 GeV/c, follow the Wróblewski scaling-formula better than the original KNO scaling-formula, as is seen from Fig. 20.

Recently, Fiałkowski and Miettinen [44] have casted doubts on the validity of the conclusion that KNO scaling is reached already at present energies. They investigate

the KNO formula for two models, namely a Poisson distribution for n_- and a two-component model.
Their result is the following:

Within the limited range of present energies the predictions of the two models are in good agreement with the "universal" curve of Slattery shown in Fig. 18.
For much higher energies the predictions are however completely different. In fact they approach δ-functions for $s \to \infty$.

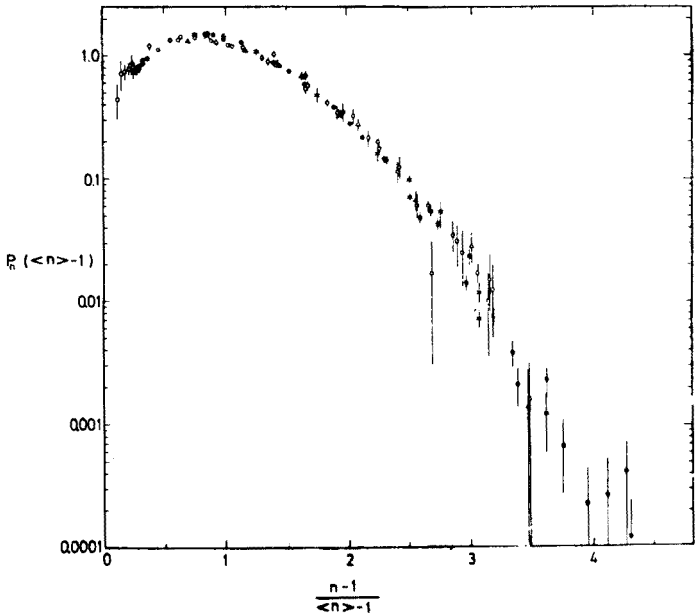

Fig. 20. $(\bar{n}-1)\cdot\frac{\sigma_n}{\sigma_T}$ *vs* $\frac{n-1}{\bar{n}-1}$ for charged particles (from Ref. [39])

The authors thus conclude, that the asymptotic KNO limit is approached extremely slowly so that within the limited energy interval explored so far and with present experimental errors early KNO scaling may be only simulated.

More recent and more refined studies of multiplicities are discussed by Wróblewski in his paper. Thus they will not be included here.

D. INCLUSIVE SINGLE PARTICLE DISTRIBUTIONS IN pp-COLLISIONS

1. Introduction

The notion of inclusive and exclusive reactions was introduced by Feynman [45]. Consider the reaction

$$a+b \to c_1+ \ldots +c_m, \tag{59}$$

where c_i are the outgoing particles with momenta $\boldsymbol{p}_i$ and energies $E_i = \sqrt{p_i^2 + m_i^2}$. If one studies a particular reaction of this type (*i.e.* with definite particles c_i) and measures all outgoing particles, one calls this an exclusive experiment for this m-body reaction (exclusive m-body reaction). The cross section for (59) in the cm system is given by

$$d\sigma = \frac{1}{p_{\mathrm{cm}}\sqrt{s}} |M|^2 \delta\left(\sum_1^m \boldsymbol{p}_i\right) \delta\left(\sum_1^m E_i - \sqrt{s}\right) \frac{d^3p_1}{E_1} \dots \frac{d^3p_m}{E_m}. \tag{60}$$

Consider now the following experiment:
one does not measure all m particles, but only n particles out of m, *i.e.* one integrates over the variables of the remaining ones. Furthermore:
one is not interested in what else besides the n particles comes out of the reaction, *i.e.* one sums over all possible reactions, in which the n measured particles occur.
This is called an inclusive n-body experiment (inclusive n-body reaction) written as

$$a + b \to c_1 + \dots + c_n + \text{anything}. \tag{61}$$

The cross section for such a reaction is given by (see *e.g.* [3])

$$d\sigma = g_n(\boldsymbol{p}_1, \dots, \boldsymbol{p}_n, s) \cdot \frac{d^3p_1}{E_1} \dots \frac{d^3p_n}{E_n}, \tag{62}$$

where $g_n(\boldsymbol{p}_1, \dots, \boldsymbol{p}_n, s)$ is the Lorentz invariant n-particle distribution given by (compare with (60)):

$$g_n(\boldsymbol{p}_1, \dots, \boldsymbol{p}_n, s) =$$

$$= \frac{1}{p_{\mathrm{cm}}\sqrt{s}} \sum_{m \geqslant n+2} \int |M|^2 \delta\left(\sum_1^m \boldsymbol{p}_i\right) \delta\left(\sum_1^m E_i - \sqrt{s}\right) \frac{d^3p_{n+1}}{E_{n+1}}, \dots, \frac{d^3p_m}{E_m}. \tag{63}$$

For simplicity the sum is started with $m = n+2$ and not with $n+1$, because then the momenta $\boldsymbol{p}_1, \dots, \boldsymbol{p}_n$ are independent, *i.e.* no constraint due to energy and momentum conservation exists between them.

The simplest case is $n = 1$, a single particle inclusive reaction

$$a + b \to c + \text{anything} \tag{64}$$

in which one studies the momentum distribution of a single particle c (inclusive single particle distribution). In our case of pp collisions this means inclusive reactions of the type

$$\mathrm{p} + \mathrm{p} \to c + \text{anything (short: pp} \to c), \tag{65}$$

where $c = \pi, K, \mathrm{N}, \Lambda, \Sigma, \bar{\mathrm{N}}$ *etc.* with definite charges. According to (62) the cross section for (65) is given by

$$d\sigma = f(\boldsymbol{p}, s) \frac{d^3p}{E} \Rightarrow \frac{d\sigma}{d^3\boldsymbol{p}} = \frac{1}{E} f(\boldsymbol{p}, s), \quad f(\boldsymbol{p}, s) = E \frac{d\sigma}{d^3\boldsymbol{p}}, \tag{66}$$

where $\boldsymbol{p}, E, d\sigma/d^3\boldsymbol{p}, f(\boldsymbol{p}, s)$[2] are momentum, energy, momentum distribution, invariant distribution (invariant differential cross section) of particle c.

Before we come to the experimental results on single particle distributions in pp-collisions, we will summarize the variables, hypotheses and some predictions for inclusive reactions. Although these topics can be found in many places in the literature (see *e.g.* Ref. [2–7], [46–52]), it is perhaps justifiable and useful to collect them here for completeness.

2. *Variables*

To study momentum distributions, the following variables may be used:

a. Momentum $\boldsymbol{p}$ and angles $(\Theta, \varphi) = \Omega$:

$$d^3p = p^2 dp d\Omega. \tag{67}$$

b. Longitudinal momentum $p_{\|} = q$ and transverse momentum $p_T = r$:

$$d^3p = \pi dr^2 dq \text{ after integration over } \Phi; \tag{68}$$

q depends on the frame of reference; r is the same in the cm system, the lab (target) system and antilab (projectile) system.

For the study of the high energy behaviour of longitudinal momentum distributions two other useful variables are used instead of q, namely the Feynman variable x and the rapidity y:

c. Feynman variable (scaling variable) x:

x is defined in the cms by (the star here indicates the cms)

$$x = \frac{q^*}{|q^*_{\max}|} \approx \frac{q^*}{\sqrt{s}/2} \quad \text{for large } s, \tag{69}$$

where $|q^*_{\max}|$ is the maximum longitudinal momentum which particle c can have in the cms, with $|q^*_{\max}| \to \frac{1}{2}\sqrt{s}$ for $s \to \infty$. Thus, x is the longitudinal cms momentum scaled down, at any energy, into the interval

$$-1 \leqslant x \leqslant 1. \tag{70}$$

Furthermore:

$$\left.\begin{array}{l} x > 0, \text{ if } c \text{ goes forward (beam direction)} \\ x < 0, \text{ if } c \text{ goes backward (target direction)} \end{array}\right\} \text{ in the cms.} \tag{71}$$

In the cms:

$$d^3p = \frac{\pi\sqrt{s}}{2} dr^2 dx. \tag{72}$$

---

[2] Following the literature we use the notation $f(\boldsymbol{p}, s)$ instead of $g_1(\boldsymbol{p}, s)$ (see (62)) for the single particle distribution.

d. Rapidity y:

The longitudinal rapidity y is defined in any system moving along the line of collision by

$$y = \tanh^{-1}\frac{q}{E} = \sinh^{-1}\frac{q}{\sqrt{m^2+r^2}} = \frac{1}{2}\log\frac{E+q}{E-q} = \frac{1}{2}\log\frac{1+\beta_{||}}{1-\beta_{||}} =$$

$$= -\log\frac{E-q}{\sqrt{m^2+r^2}} = \log\frac{E+q}{\sqrt{m^2+r^2}}, \tag{73}$$

where E and $\beta_{||}$ are the energy and longitudinal velocity of the particle. y has the following properties:

$$y < 0 \text{ for } q < 0,\ y > 0 \text{ for } q > 0,\ y(-q) = -y(q). \tag{74}$$

Notice that y is not a purely longitudinal variable like q and x, since it contains also the transverse momentum r. Since however r is small in the average, the longitudinal behaviour at high energies can be expressed almost purely by y. In the non-relativistic limit $\beta_{||} \ll 1$

$$y \approx \beta_{||}, \textit{ i.e. } \text{rapidity} \approx \text{longitudinal velocity}. \tag{75}$$

For $E \gg m$ (*i.e.* $E \approx p \Rightarrow q = p\cos\Theta \approx E\cos\Theta$) and $\Theta \neq 0$

$$y \approx \frac{1}{2}\log\frac{1+\cos\Theta}{1-\cos\Theta} = -\log\left(\tan\frac{\Theta}{2}\right). \tag{76}$$

This approximation is often used in experiments, which measure only the angles, but not the momenta. y has the following simple additivity property under longitudinal transformations (= Lorentz transformations along the line of collision):

$$y = y' + \frac{1}{2}\log\frac{1+\bar{\beta}}{1-\bar{\beta}}, \tag{77}$$

where $\bar{\beta}$ is the relative velocity of the two systems. In the non-relativistic limit (75), relation (77) reduces to the addition of velocities. (77) means that under a longitudinal transformation all rapidities are shifted by a constant amount; differences of rapidities are invariant, $dy = dy'$, *i.e.* a rapidity distribution is invariant and only shifted horizontally.

According to (77) the following relation holds between lab rapidity y and cms rapidity y^*:

$$y = y^* + y_{\text{cms}} \quad \text{with} \quad y_{\text{cms}} = \frac{1}{2}\log\frac{1+\beta_{\text{cms}}}{1-\beta_{\text{cms}}}, \tag{78}$$

where y_{cms} and β_{cms} are the rapidity and velocity of the cm system in the lab system.

Rapidity of incident particles a (beam) and b (target) ($r_a = r_b = 0_0$):
In the cms $p_a^* = -p_b^* = p^* \approx \frac{1}{2}\sqrt{s}$ for large s and

$$y_a^* = \sinh^{-1}\frac{p^*}{m_a} \approx \sinh^{-1}\frac{\sqrt{s}}{2m_a},$$

$$y_b^* = -\sinh^{-1}\frac{p^*}{m_b} \approx -\sinh^{-1}\frac{\sqrt{s}}{2m_b}. \tag{79}$$

For the invariant difference of the two incident particles in rapidity one obtains

$$y_a^* - y_b^* = \log\frac{(E_a^*+p^*)(E_b^*+p^*)}{m_a m_b} \approx \log\frac{s}{m_a m_b} \quad \text{for large s.} \tag{80}$$

Since the rapidities of the secondary particles lie in this interval or can exceed it only by a small amount (*e.g.* a particle going backward in the lab has $y^* < y_b^*$), it follows from (80), that the y-range of a rapidity distribution grows like log s (see sketch).

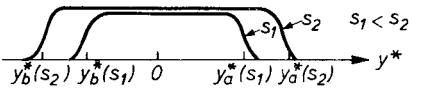

In the lab

$$y_b = 0, \quad y_a = y_a^* - y_b^* \approx \log\frac{s}{m_a m_b}. \tag{81}$$

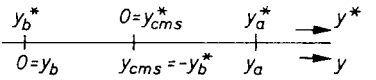

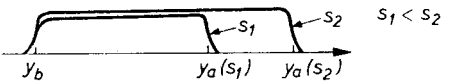

From (69) and (73) one obtains the relation between x and y in cms (the star is dropped in the following)

$$y = \log\frac{\sqrt{x^2+\frac{4m_l^2}{s}}+x}{\frac{2m_l}{\sqrt{s}}} = -\log\frac{\sqrt{x^2+\frac{4m_l^2}{s}}-x}{\frac{2m_l}{\sqrt{s}}} \tag{82}$$

with

$$m_l = \sqrt{m^2+r^2} = \text{longitudinal mass}, \tag{83}$$

$$\frac{dy}{dx} = \frac{1}{\sqrt{x^2+\frac{4m_l^2}{s}}}. \tag{84}$$

For $x = 0$: $y = 0$, $dy/dx = \sqrt{s}/2m_l$. Thus the slope of y *vs* x at $x = 0$ increases with increasing primary energy and decreasing transverse momentum. For $|x| \gg 2m_l/\sqrt{s}$ (*i. e.* $|q| \gg m$ and r) (notice that for limited r this condition is fulfilled for smaller and smaller $|x|$, when s increases; at infinite energy for all $x \neq 0$):

$$y \approx \log \frac{|x| + x + \dfrac{2m_l^2}{s|x|}}{\dfrac{2m_l}{\sqrt{s}}} \approx \pm \log \frac{|x|\sqrt{s}}{m_l} \quad \text{for } x \gtrless 0, \tag{85}$$

$$\frac{dy}{dx} \approx \frac{1}{|x|}. \tag{86}$$

Guided by these relations we draw qualitatively in the sketch below the curves of y *vs* x and notice the following property, which is also seen from Fig. 21, showing in a r *vs* q-plot

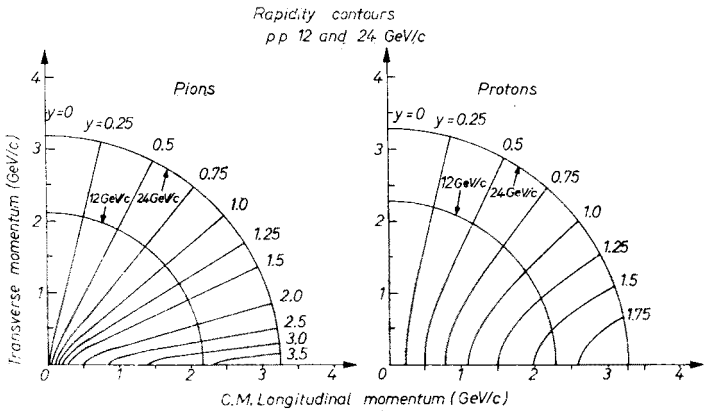

Fig 21. Lines of constant cms rapidity in the plane of transverse *vs* cms longitudinal momentum (Peyrou-plot) for pions and protons. The circles give the boundaries for 12 and 24 GeV/c

(Peyrou-plot) lines of constant y (The circles are the kinematical boundaries for 12 and 24 GeV/c pp collisions): The curve y *vs* x becomes steeper with increasing energy, decreasing transverse momentum and decreasing $|x|$.

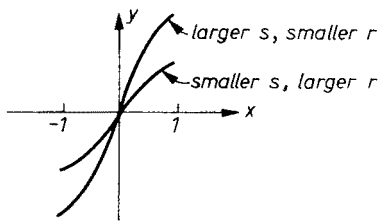

From the relations and the sketch one notices:
The central region appears shrunk in x around $x = 0$ and expanded in y. So y is the more sensitive variable to study the central region.

The fragmentation regions appear expanded in x and shrunk to a smaller fraction of the total y range around $y = y_a$ and y_b. So x is the more sensitive variable to study the fragmentation region.

At infinite energy the slope is infinite at $x = 0$; finite y (central region) correspond to $x = 0$, finite $x \neq 0$ correspond to $y = \pm\infty$.

$$d^3p = E\pi dr^2 dy, \quad \text{since} \quad \frac{dy}{dq} = \frac{1}{E}. \tag{87}$$

e. Momentum transfer t and missing mass M

Instead of the variables (p, Ω), (q, r^2), (x, r^2) or (y, r^2) one can also use the momentum transfer t between c and b (target) and the missing mass squared M^2, defined by

$$t = (p_b - p_c)^2, \quad M^2 = (p_a + p_b - p_c)^2, \tag{88}$$

to describe the inclusive reaction $a+b \to c+$anything (p_a, p_b, p_c are the four-momenta of a, b, c respectively).

$$dtdM^2 = \frac{2p_b^* \sqrt{s}}{E_c^*} dq_c^* dr_c^2 \approx \frac{s}{E_c^*} dq_c^* dr_c^2. \tag{89}$$

f. Summary

From (67), (68), (72), (87) and (89) one obtains for the momentum distribution and the invariant distribution (66), expressed in the various variables, the following relations in the cms:

$$\frac{d\sigma}{d^3p} = \frac{1}{p^2}\frac{d\sigma}{dpd\Omega} = \frac{1}{\pi}\frac{d\sigma}{dr^2dq} = \frac{2}{\pi\sqrt{s}}\frac{d\sigma}{dr^2dx} = \frac{1}{E\pi}\frac{d\sigma}{dr^2dy} = \frac{s}{E\pi}\frac{d\sigma}{dtdM^2}, \tag{90}$$

$$f(p, s) \equiv E\frac{d\sigma}{d^3p} = \frac{E}{p^2}\frac{d\sigma}{dpd\Omega} = \frac{E}{\pi}\frac{d\sigma}{dr^2dq} = \frac{2E}{\pi\sqrt{s}}\frac{d\sigma}{dr^2dx} = \frac{1}{\pi}\frac{d\sigma}{dr^2dy} = \frac{s}{\pi}\frac{d\sigma}{dtdM^2}. \tag{91}$$

3. Various regions

In the cm system the total x or y interval can be subdivided into the following regions, *e.g.* for y:

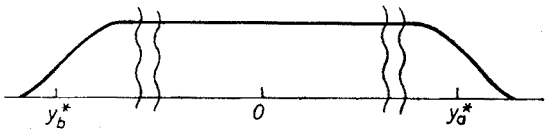

region α of target (b) fragments | central region γ („pionisation" region) | region β of beam (a) fragments

α) region of target fragments, around $y_b^* = y_{\text{target}}^*$

β) region of beam fragments, around $y_a^* = y_{\text{projectile}}^*$

γ) central region (region of intermediate particles), where particles emitted *e.g.* from a multiperipheral chain (mainly pions) can be found. This region is also called "pionisation" region.

Due to the relation between x and y at high energies, discussed above, the three regions are given in x by:

$$\text{region } \alpha : x < 0 \left(x \ll -\frac{2m_l}{\sqrt{s}} \right),$$

$$\text{region } \beta : x > 0 \left(x \gg \frac{2m_l}{\sqrt{s}} \right),$$

$$\text{region } \gamma : x \approx 0.$$

The boundaries of the three regions are not well defined quantitatively; in particular at low energies there is considerable overlap.

4. Hypotheses and predictions

Various hypotheses and predictions have been made for the high energy behaviour of inclusive particle distributions.

a. Feynman's scaling hypothesis

Feynman scaling [45] means that at high energies the invariant cross section (66) depends only on the scaling variable x and the transverse momentum r and not explicitly on the energy s:

$$E \frac{d\sigma}{d^3p} \equiv f(q, r^2, s) \xrightarrow[s\to\infty]{} \tilde{f}(x, r^2). \tag{92}$$

The generalisation of the scaling hypothesis to the inclusive n-particle distribution $g_n(\boldsymbol{p}_1, \ldots, \boldsymbol{p}_n, s)$ (see (62)) is analogous.

b. Hypothesis of limiting fragmentation (HLF)

The hypothesis of limiting fragmentation, introduced by Benecke *et al.* [12], predicts that at high energies the momentum distribution of a target (beam) fragment c approaches a limiting function in the target (beam) rest system, independent of energy:

$$f_b(\boldsymbol{p}_c^{(b)}, s) \to \varrho_b(\boldsymbol{p}_c^{(b)}) \text{ for a target } (b) \text{ fragment } c,$$

$$f_a(\boldsymbol{p}_c^{(a)}, s) \to \varrho_a(\boldsymbol{p}_c^{(a)}) \text{ for a beam } (a) \text{ fragment } c, \tag{93}$$

where $\boldsymbol{p}_c^{(b)}(\boldsymbol{p}_c^{(a)})$ is the momentum of c in the target (beam) rest system. Since the rapidity $y_c^{(b)}(y_c^{(a)})$ in the target (beam) system depends on $\boldsymbol{p}_c^{(b)}$ $(\boldsymbol{p}_c^{(a)})$ and not on s, HFL implies scaling (*i.e.* energy independence) of the y distribution in the target (beam) fragmentation region.

c. Relation between Feynman scaling and HLF at high energies

It is easy to show that for $|x| \gg 2m_l/\sqrt{s}$, *i.e.* for x in the fragmentation regions, the following relations hold between x (defined in cms!) and the longitudinal momentum $q^{(b)}$ ($q^{(a)}$) in the target (beam) system:

$$\text{For } x \ll -\frac{2m_l}{\sqrt{s}} \text{ (target fragment)} \quad q^{(b)} \to \frac{1}{2}\left[m_b x - \frac{m_l^2}{x m_b}\right],$$

$$\text{For } x \gg \frac{2m_l}{\sqrt{s}} \text{ (beam fragment)} \quad q^{(a)} \to \frac{1}{2}\left[m_a x - \frac{m_l^2}{x m_a}\right]. \tag{94}$$

These relations do not contain s, *i.e.* fixed (x, r^2) corresponds to fixed $\boldsymbol{p}^{(b)}(\boldsymbol{p}^{(a)})$ in the target (beam) system. Thus, HLF implies Feynman scaling in the fragmentation regions. Feynman scaling however makes also a prediction about the central region $x \approx 0$, where HLF does not apply.

d. Mueller's Regge analysis for inclusive reactions

The following questions arise:
How can the hypotheses for limiting behaviour of particle distributions be justified theoretically?
At what energies is the limiting behaviour expected to start?
With what energy dependence is this asymptotic behaviour approached from lower energies?
The hypotheses of Feynman scaling and limiting fragmentation do not give answers to such quantitative questions. Answers however can be provided in the framework of Mueller's Regge analysis [53], which has been reviewed in many places in the literature (see *e.g.* Ref. [2], [5], [6], [46–49], [54–56]). In this analysis the single particle invariant distribution $Ed\sigma/d^3p$ $(s, \boldsymbol{p})$ for $a+b \to c+$anything is related to a discontinuity in the amplitude for the elastic three body process $a+b+\bar{c} \to a+b+\bar{c}$. Applying then Regge theory to this amplitude in various kinematical regions, one is led to predictions for the invariant distributions (energy dependence, scaling, factorisation *etc.*). Here we will however not go into further details but rather refer to the literature given above.

e. Predictions of MPP and DFP (see *e.g.* Ref. [11])

In the MPP the particles are emitted along the multiperipheral chain and should thus be distributed in momentum space rather continuously. In rapidity the particles would have predominantly roughly equal spacing leading to a rather flat rapidity distribution with a central plateau (see sketch).

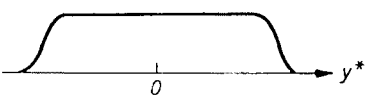

In the DFP the secondary particles are the fragments of the two incident particles and can thus be divided into two groups. At high energies and for low multiplicities the two groups should be separated in phase space, one group of particles going forward and

the other group backward in the cms. This would lead to a two bump structure in the rapidity distribution (see sketch) with the two bumps moving away from each other (like log s) and the valley between them becoming deeper with increasing energy. It has been

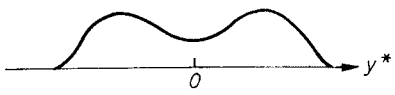

pointed out however (see *e.g.* Ref. [7]) that also the DFP can yield a smooth (flat) rapidity distribution. This is because with increasing energy fragmentation into higher and higher multiplicities is allowed. Particles from high multiplicity clusters tend to have small cms momentum thus filling the central part of the rapidity distribution, whereas particles from low multiplicity clusters have larger $|y^*|$ in the cms.

5. Experimental results on single particle distributions

a. Introduction

The following two prominent features are common to all high energy reactions: the transverse momenta p_T are predominantly confined to small values, with $\langle p_T \rangle \sim$ $\sim$ 400 MeV/c;
the longitudinal momenta vary over the whole kinematically allowed region.
Because of these two features particles prefer the forward and backward directions in the cm system (peripheralism); the events tend to lie in a cylindrical phase space.

Introductory remarks: It is of course impossible to discuss all experimental data on the inclusive reactions of the type pp $\rightarrow c +$ anything. Therefore we will choose only a few examples to show the general and most important properties. These examples will be taken mainly from a pp-experiment of the Bonn–Hamburg–München (BHM) collaboration at 12 and 24 GeV/c [57], but in order to study the variation with energy also some ISR-results will be included. More detailed and more recent ISR-data will be discussed by Lillethun in his paper (see also Ref. [27], [58]).

We start with the longitudinal distributions (x and y-distributions) and then discuss the distributions of transverse momenta.

b. x and y-distributions

Because of the symmetry of pp-collisions in the cm system, the events are folded onto one half of the full x- and y-range in the following.

pp $\rightarrow \pi^{\pm}$

Figs 22 and 23 show the lab rapidity distributions $\frac{1}{\pi}\frac{d\sigma}{dp_T^2 dy}$ of π^+ and π^- for fixed transverse momenta $p_T =$ 0.2, 0.4, 0.6, 0.8 and 1 GeV/c. The dashed and full curves connect the data points at 12 and 24 GeV/c of the BHM collaboration [57], the black points are ISR values [59] at equivalent lab momenta of 225, 500, 1100 and 1500 GeV/c. The distribu-

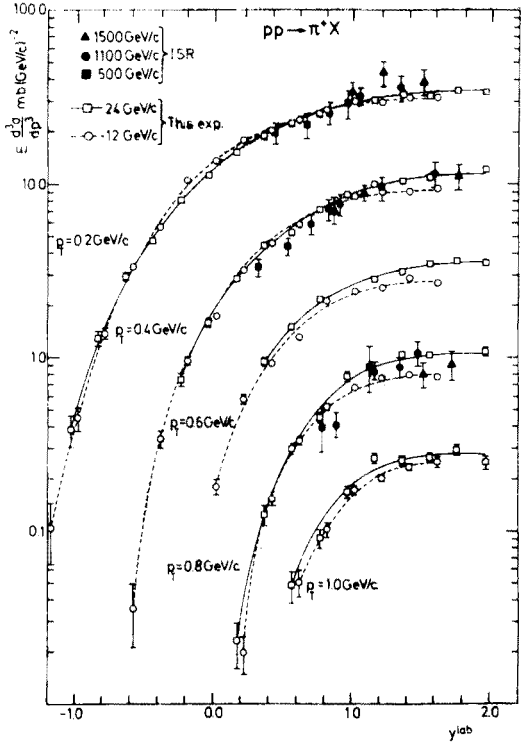

Fig. 22

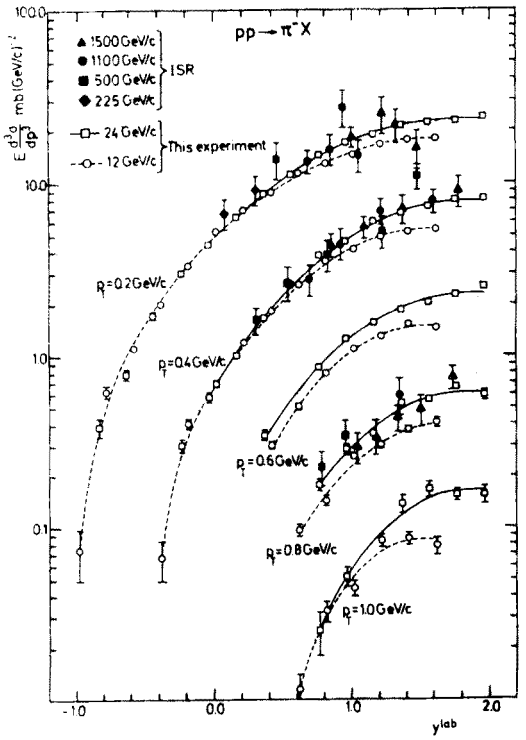

Fig. 23

Fig. 22. Lab rapidity-distributions of π^+ for various transverse momenta at 12 and 24 GeV/c and at ISR energies [59] (from Ref. [57c])
Fig. 23. Lab rapidity-distributions of π^- for various transverse momenta at 12 and 24 GeV/c and at ISR energies [59] (from Ref. [57c])

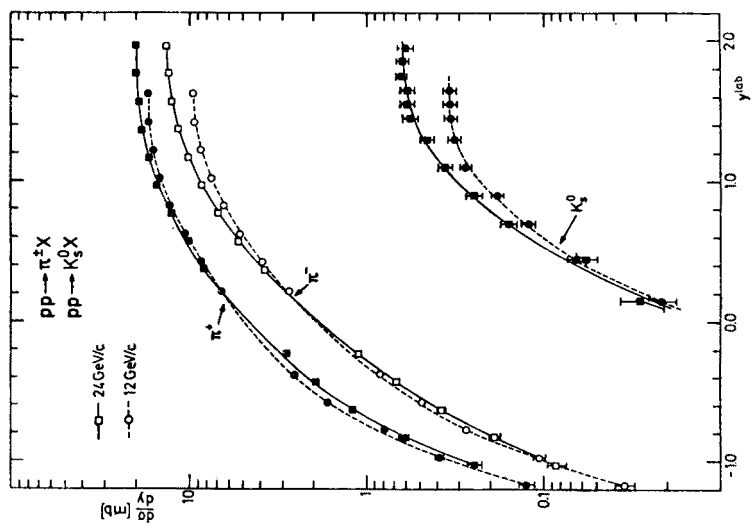

Fig. 24

Fig. 24. Lab rapidity-distributions of π^+, π^- and K_s^0, integrated over p_T, at 12 and 24 GeV/c (from Ref. [57c])

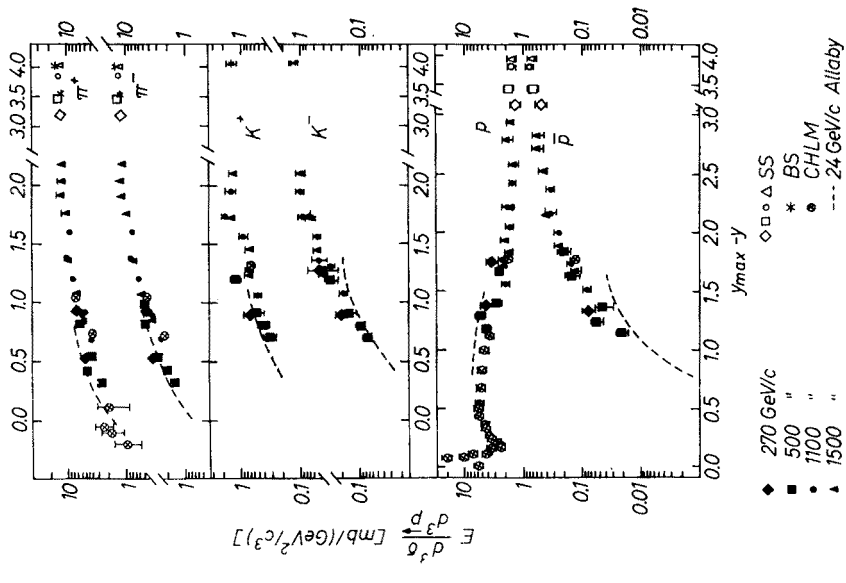

Fig. 25

Fig. 25. Rapidity-distributions of π^+, π^-, K^+, K^-, p, $\bar{p}$ at $p_T = 0.4$ GeV/c at ISR energies. The curves show the results at 24 GeV/c (from Ref. [32, 33])

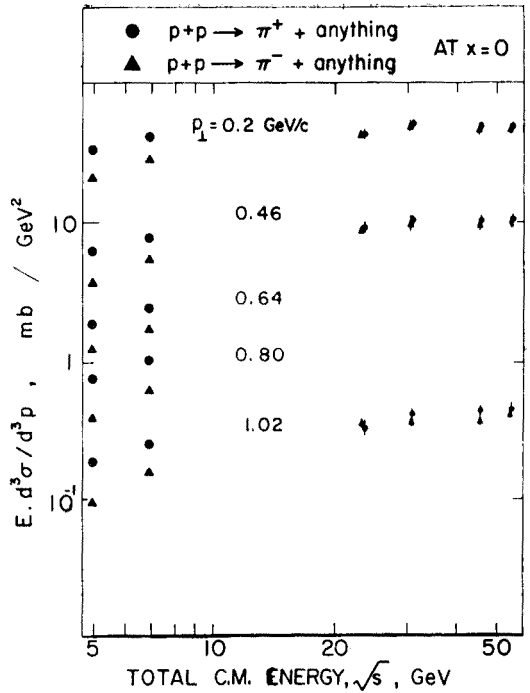

Fig. 26

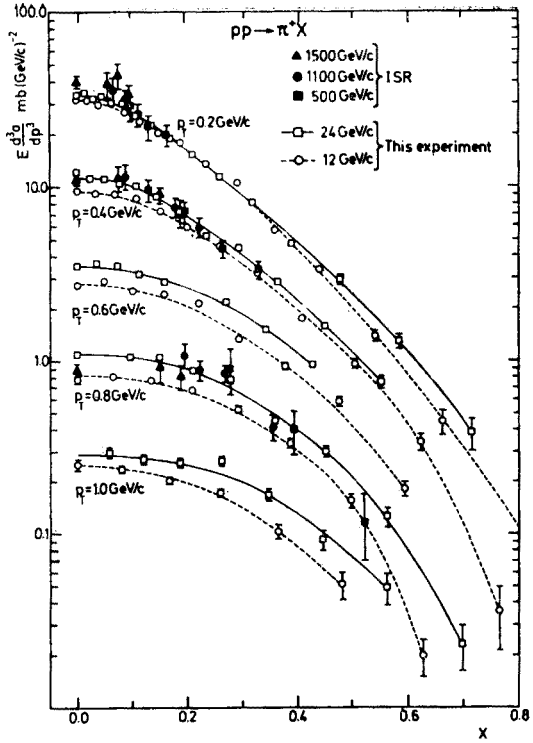

Fig. 27

Fig. 26. Invariant cross section of π^+ and π^- at $x = 0$ for various transverse momenta *vs* cms energy (BHM collaboration and Saclay–Strasbourg collaboration, from Ref. [62])

Fig. 27. x-distributions of π^+ for various transverse momenta at 12 and 24 GeV/c and at ISR energies [59] (from Ref. [57c])

tions end at the rapidities of the cm system ($y_{cms} = 1.62$ at 12 GeV/c and $y_{cms} = 1.97$ at 24 GeV/c), *i.e.* at the points where $y^* = x = 0$ ($\Theta^* = 90°$). Fig. 24 shows the $\pi^{\pm}$ lab rapidity distributions $d\sigma/dy$ at 12 and 24 GeV/c integrated over all transverse momenta.

The following observations can be made from the figures:

In the fragmentation region (y_{lab} between ~ -1.0 and ~ 1.0, notice that $y_{lab} < 0$ corresponds to pions going backward in the lab) the distributions for π^+ and π^- show little energy dependence from 12 GeV/c to ISR energies at least for small p_T. Thus scaling (limiting fragmentation) is reached rather early for $\pi^{\pm}$ from proton fragmentation. For large p_T there seems to be a rise of the distributions from 12 to 24 GeV/c.

Going from the fragmentation region towards the central region, which of course is still very limited and not well separated from fragmentation at 12 and 24 GeV/c, one still notices an increase from 12 to 24 GeV/c, which is larger for π^- than for π^+. However at ISR energies also in the central region the scaling limit seems to be reached.

This scaling at ISR energies in the fragmentation and central region for π^+ and π^- is seen more clearly from a recent compilation of ISR data at $p_T = 0.4$ GeV/c by Giacomelli [33] shown in Fig. 25: The total y-range has now increased from ~ 4 at 24 GeV/c to ~ 8 at ISR energies, the central region is well developed and extends from $y_{lab} \sim 1$ to ~ 7. In the figure the points do not show an appreciable energy dependence within the ISR energies. This is also seen from Fig. 26 in which the $\pi^{\pm}$ invariant cross section at 90° ($x = 0$) is plotted as a function of energy for various transverse momenta. From 24 GeV/c to ISR energies the cross section still rises considerably but stays rather constant within the ISR energies.

Fig. 25 shows that in the central region the cross section for $\pi^{\pm}$ is rather independent of y leading to a central plateau. An indication of the development of a central plateau can already be observed at 24 GeV/c, see Figs 22 and 23. A more careful look at Fig. 25 however shows that the plateau is not completely flat, but seems to rise slightly towards $y^* = 0$ in the cms.

Figs 22, 23, 25 and in particular Fig. 24 show that in the fragmentation region the cross section is larger for π^+ than for π^-, which means that a proton fragments more often into a π^+ than into a π^-. Going towards the central region and towards higher energies the two cross sections become nearly equal (see *e.g.* Figs. 24 and 25) indicating that in the central region pions are produced in $\pi^+\pi^-$ pairs.

Figs 27 and 28 show the x-distributions for π^+ and π^-, corresponding to the y-distributions of Figs. 22 and 23 respectively. According to the relationship between x and y discussed in Section D2, the central y-region has shrunk to a small x-region around $x = 0$ whereas the fragmentation region appears expanded.

pp → p

Fig. 29 shows the lab rapidity distribution of protons for fixed transverse momenta $p_T = 0.2$, 0.4, 0.6, 0.8 and 1.0 GeV/c. The dashed and full curves give the data at 12 and 24 GeV/c of the BHM collaboration [57] (only a few of the experimental points are shown explicitly), the black points are ISR results [59] at equivalent lab momenta of 500, 1100 and 1500 GeV/c. Fig. 30 shows the proton rapidity distributions at 12 and 24 GeV/c

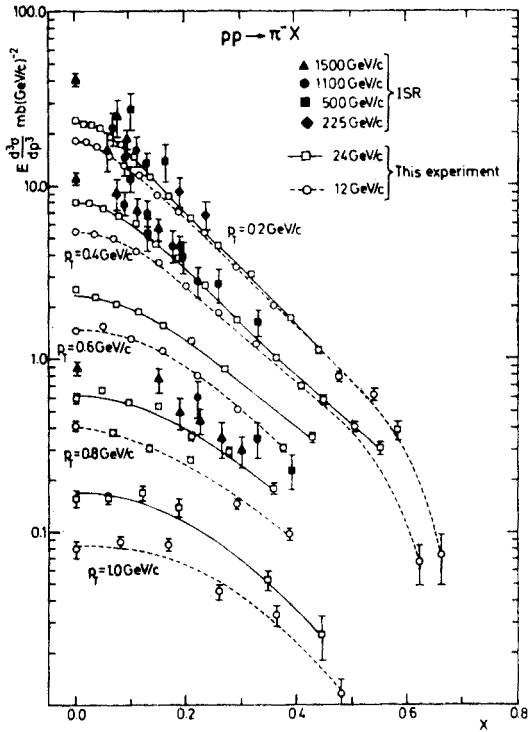

Fig. 28

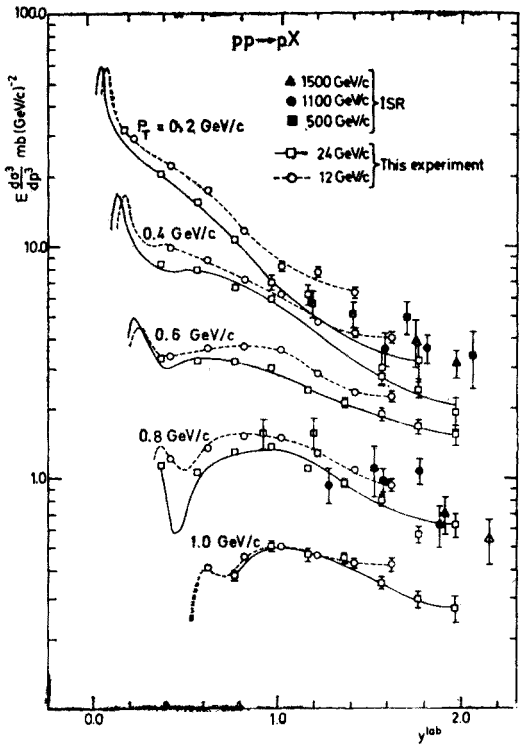

Fig. 29

Fig. 28. x-distributions of π^- for various transverse momenta at 12 and 24 GeV/c and at ISR energies [59] (from Ref. [57c])
Fig. 29. Lab rapidity-distributions of protons for various transverse momenta at 12 and 24 GeV/c and at ISR energies [59] (from Ref. [57c])

integrated over all transverse momenta. A compilation of ISR-results at $p_T = 0.4$ GeV/c is shown in Fig. 25 together with a dashed curve indicating the 24 GeV/c results of Allaby *et al.* [60].

Comments: The proton distributions show a marked difference when compared with the distributions of other particles (Figs. 24, 25, 30): When going from the fragmentation into the central region the proton distributions fall down, whereas the distributions

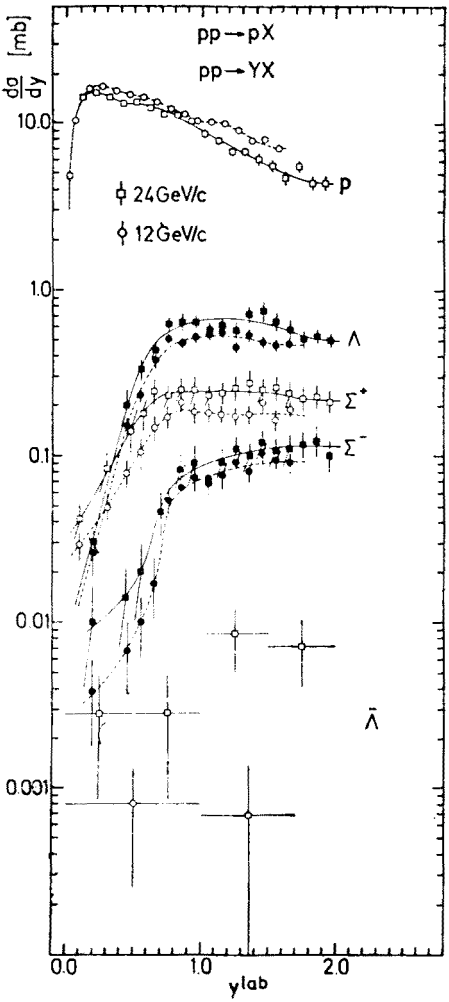

Fig. 30. Lab rapidity-distributions of p, Λ, Σ^+, Σ^-, $\bar{\Lambda}$, integrated over p_T, at 12 and 24 GeV/c (from Ref. [57c])

of the other particles rise. This means that the protons come mainly from fragmentation and that some of them tend to stay close to the incident protons in momentum space. This tendency is called the leading particle effect; it means that secondary particles with the same quantum numbers as the initial particles tend to keep the direction and a considerable part of the energy of the incident particles.

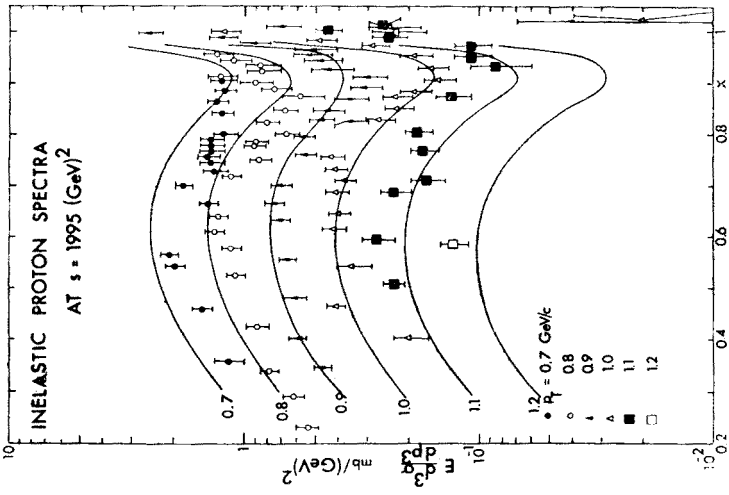

Fig. 32

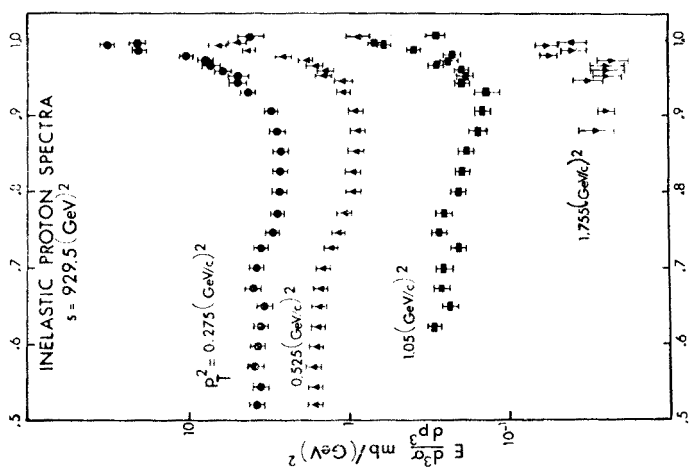

Fig. 31

Fig. 31. x-distributions of protons at $s = 929.5$ GeV^2 for various transverse momenta (from Ref. [61])
Fig. 32. x-distributions of protons at $s = 1995$ GeV^2 for various transverse momenta (from Ref. [61])

To study the proton behaviour further, we show in Figs 31 and 32 the x-distributions of the proton for various transverse momenta at two ISR energies ($s = 929.5$ GeV^2 and 1995 GeV^2 respectively) [61]. These figures (and also Fig. 25 near $y_{lab} = 0$) show a remarkable structure with a sharp peak towards $x = 1$ and a broad distribution between $x \sim 0.3$

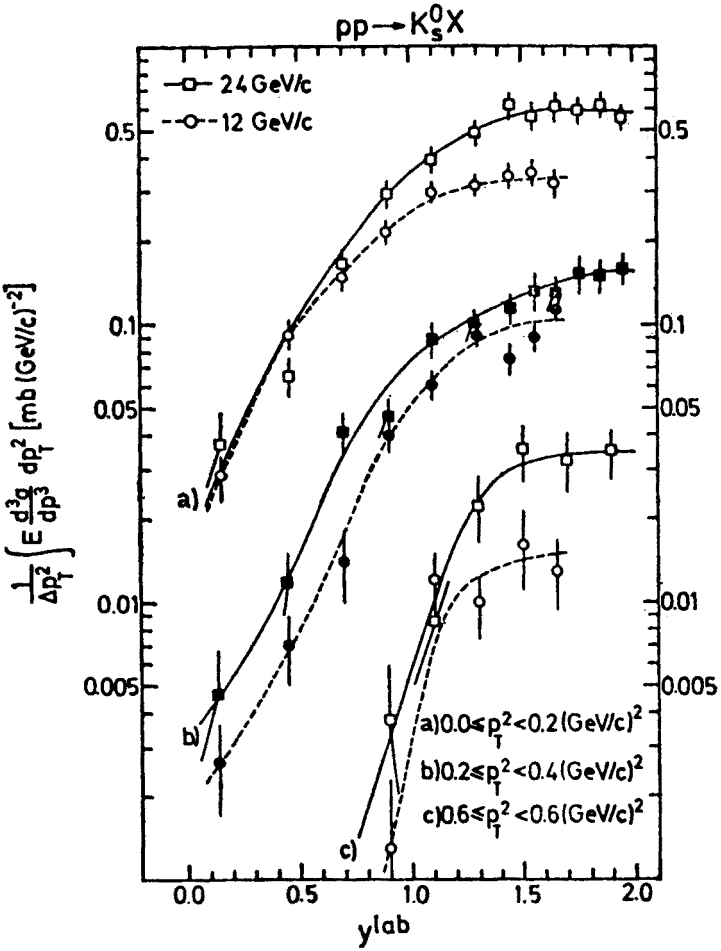

Fig. 33. Lab rapidity-distributions of K_s^0 for various intervals of transverse momentum at 12 and 24 GeV/c (from Ref. [57c])

and ~ 0.9. The peak is energy independent and corresponds to a cross section of about 7 mb [62]. The structure can be understood by single diffraction dissociation (see sketch):

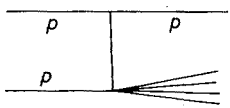

The protons near $x = 1$ are the single protons at the upper vertex, whereas the protons from proton fragmentation at the lower vertex contribute to the distribution between

~ 0.3 and ~ 0.9. A study of the multiplicities and missing masses connected with the protons in the forward peak shows [62], that with increasing energy also higher multiplicities contribute to single diffraction dissociation and that the missing mass distribution, apart from showing the low mass enhancement observed in diffraction dissociation at lower

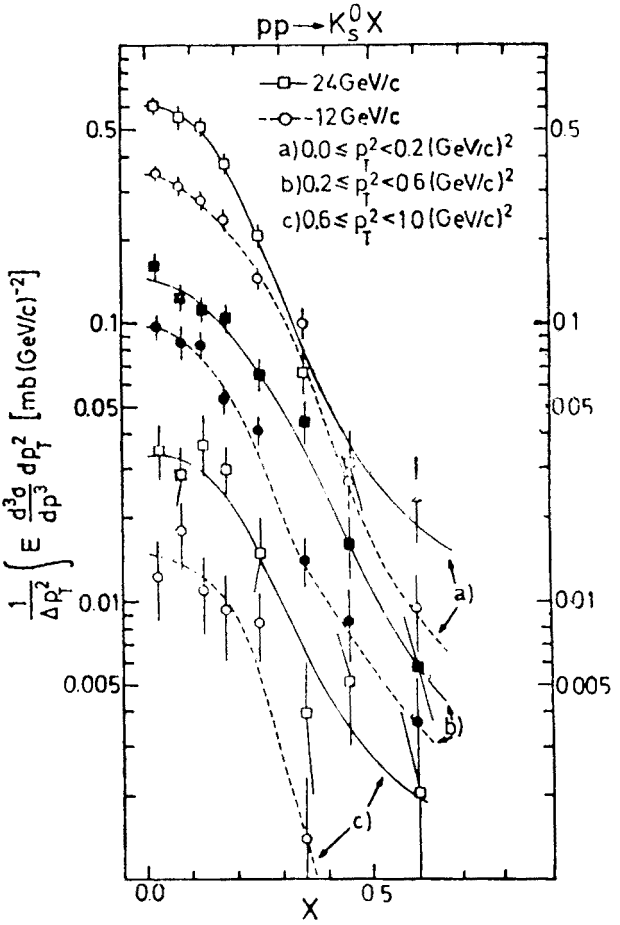

Fig. 34. x-distributions of K_s^0 for various intervals of transverse momentum at 12 and 24 GeV/c (from Ref. [57c])

energies, extends up to ~ 10 GeV. The average multiplicity increases with increasing missing mass.

Fig. 25 shows that protons are also found in the central region, although less frequently than in the fragmentation region, and that a plateau is seen to develop. At ISR energies this plateau seems to be roughly energy independent which may be understood [7] by two opposite effects according to two sources for the protons:

Some protons from fragmentation extend into the central region. As the fragmentation centers move away from each other with increasing energy, fragmentation tends to depopulate the central region.

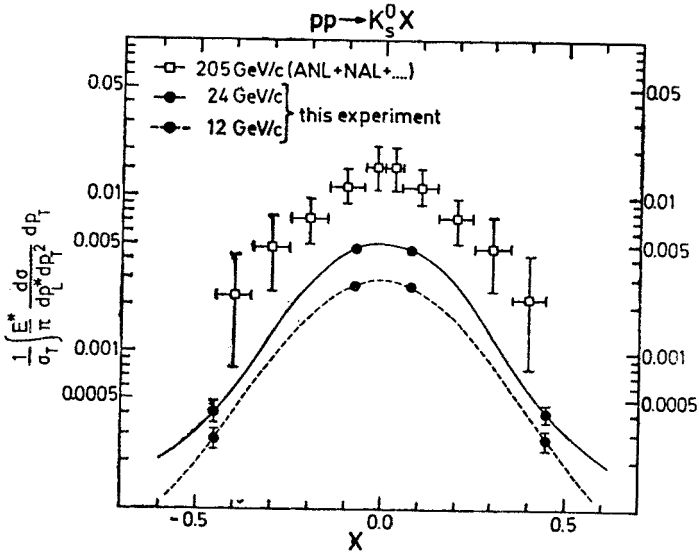

Fig. 35. Normalised x-distributions of K_s^0, integrated over p_T, at 12, 24 and 205 GeV/c [63]. In Figs 35–39 the curves are handdrawn through the experimental values, only a few of which are shown explicitly in the Figures (from Ref. [57c])

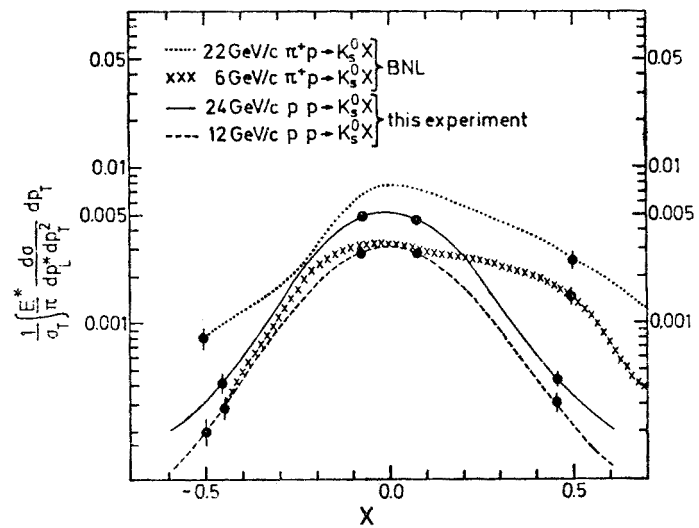

Fig. 36. Normalised x-distributions of K_s^0 from π^+p and pp-collisions at various lab momenta (from Ref. [57c])

The cross section for $p\bar{p}$ pair-production increases strongly with increasing energy, which leads to an increasing population of the central region.

In this picture the energy dependences of the two effects would roughly cancel each other at ISR energies leading to an energy independent cross section. Fig. 25 shows indeed

that in the central region the p and $\bar{p}$ distributions approach each other with increasing energy, however the p/$\bar{p}$ ratio is still ~ 2 at ISR energies in the central region whereas the π^+/π^- ratio is ~ 1.

From Fig. 29 it is seen that between 12 and 24 GeV/c the proton distribution decreases in contrast to other particles which show an increase (or constancy).

pp $\rightarrow \bar{p}$

The y-distribution for $\bar{p}$ at $p_T = 0.4$ GeV/c is shown in Fig. 25. A large increase of the cross section is observed between 24 GeV/c and ISR energies, in particular in the central region. So at accelerator energies one is far away from scaling. At ISR energies the distributions are still rising and a central plateau seems to develop in y.

pp $\rightarrow K^{\pm}$

The y-distributions for K^+ and K^- at $p_T = 0.4$ GeV/c are shown in Fig. 25. For K^- no scaling has been reached yet at accelerator energies, whereas for K^+ scaling seems to set in early. Energy independence and a central y plateau are observed at ISR energies.

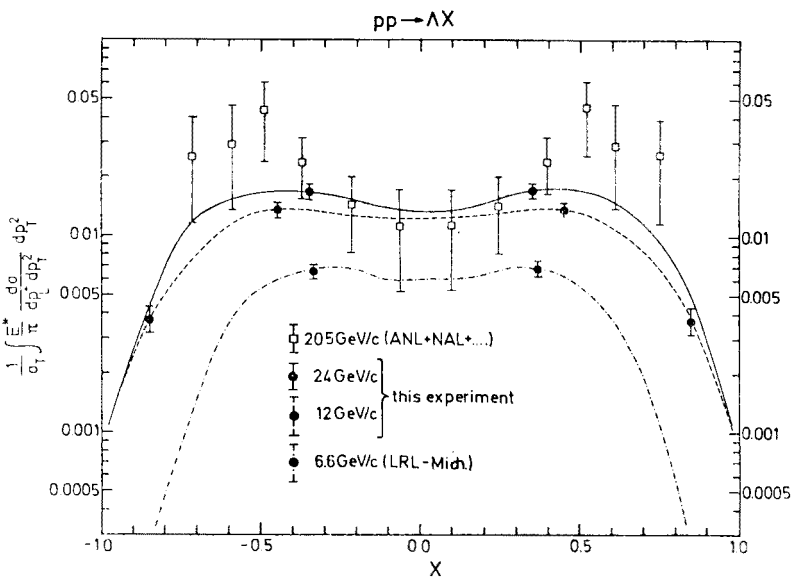

Fig. 37. Normalised x-distributions of Λ, integrated over p_T, at various lab momenta (from Ref. [57c])

pp $\rightarrow K_s^0$

y and x-distributions for K_s^0 at 12 and 24 GeV/c for various p_T-intervals are shown in Figs 33 and 34 respectively. Figs 24 and 35 show the y and x-distributions integrated over all p_T. The distributions show considerable increase with energy (by a factor of ~ 2) between 12 and 24 GeV/c, but also from 24 to 205 GeV/c [63].

Fig. 36 shows x-distributions of K_s^0 from pp and π^+p-collisions at various energies, normalised to the respective total cross sections. If factorisation holds, *i.e.* if the fragmen-

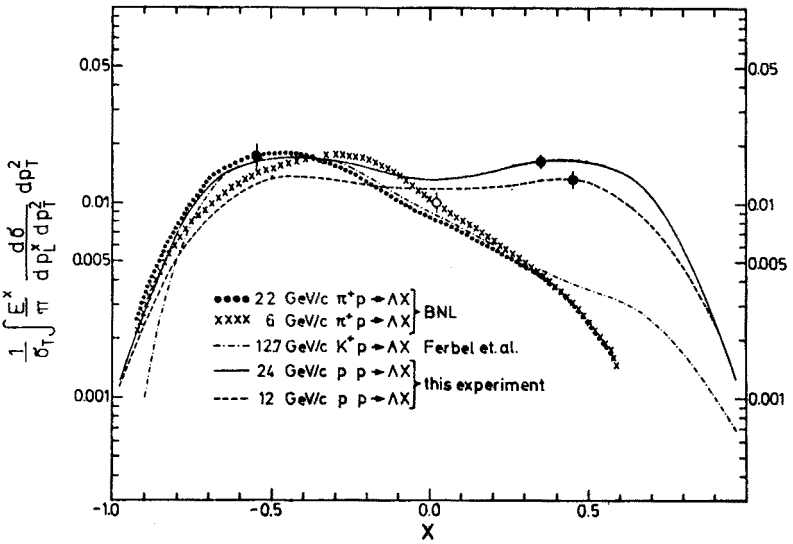

Fig. 38. Normalised x-distributions of Λ from π^+p, K^+p and pp-collisions at various lab momenta (from Ref. [57c])

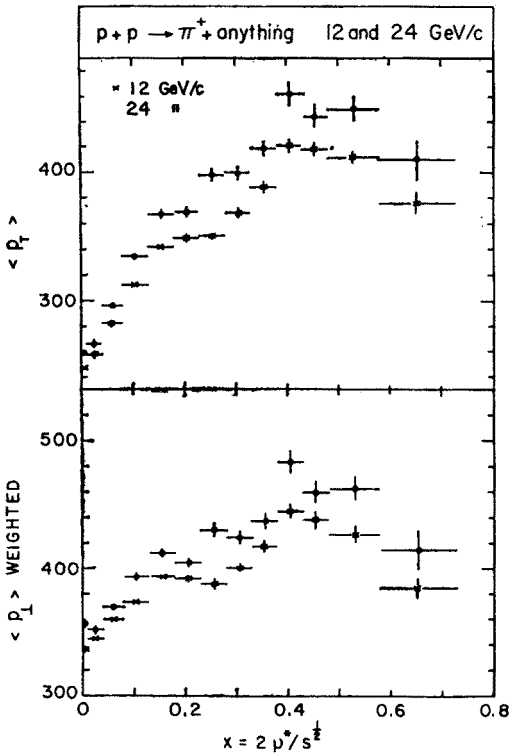

Fig. 39. Average transverse momentum and weighted average transverse momentum for π^+ *vs* x at 12 and 24 GeV/c (BHM collaboration, from Ref. [5])

tation of the primary proton into K_s^0 is independent of the second incident particle, the distributions for π^+p and pp reactions should coincide in the proton fragmentation region (negative x) at a given energy. It is seen that the data show considerable differences, although they are smaller in the proton fragmentation region than in the region of beam fragmentation.

$pp \rightarrow \Lambda, \Sigma^+, \Sigma^-$

y and x-distributions for Λ, integrated over p_T, at various energies are shown in Fig. 30 and Fig. 37 respectively. Also here scaling is not yet reached up to 200 GeV/c. The plateau

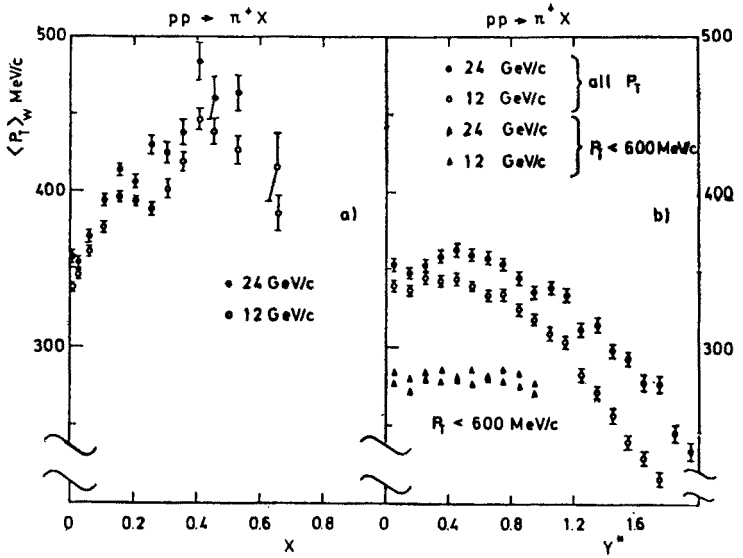

Fig. 40. Weighted average transverse momentum for π^+ at 12 and 24 GeV/c *vs* x (a) and y^* (b) (from Ref. [57b])

at lower energies seems to come merely from an overlap of the two fragmentation regions. They are more separated from each other at higher energies so that a valley develops, indicating that the Λ's come mainly from fragmentation.

Fig. 38 shows normalised x-distributions of Λ from pp, K^+p and π^+p collisions at various energies. In the proton fragmentation regions the distributions are not too different, which could indicate factorisation for the fragmentation of p into Λ at high energies. y-distributions of Σ^+ and Σ^- at 12 and 24 GeV/c are shown in Fig. 30.

c. Average transverse momenta and transverse momentum distributions

α. Average transverse momenta. The general properties of transverse momentum distributions are known since a long time [5]:

They fall off rather steeply leading to small values for the average transverse momentum $\langle p_T \rangle \sim 400$ MeV/c.

The $\langle p_T \rangle$-values, taken over all longitudinal momenta, are rather constant or only slowly rising with energy (from ~ 300 to ~ 500 MeV/c).

$\langle p_T \rangle$ increases slightly with the mass of the particle.

$\langle p_T \rangle$ is rather independent of the reaction, *i.e.* on the incident particles and on the multiplicity.

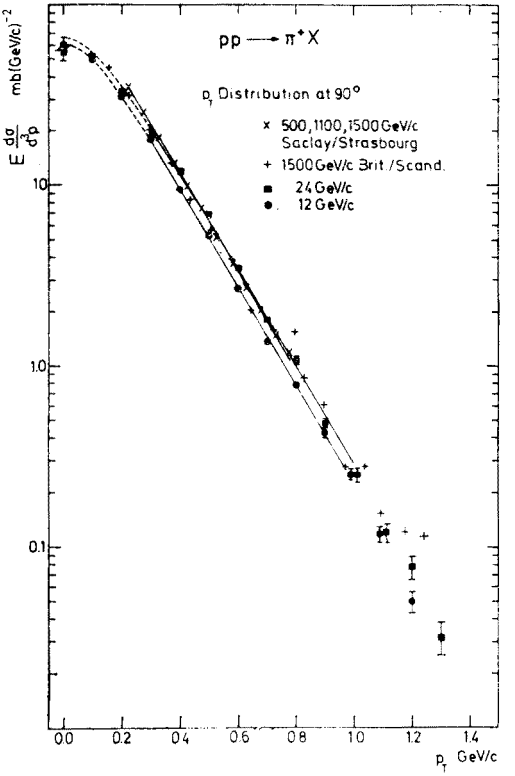

Fig. 41. Invariant cross section at $\Theta^* = 90°$ *vs* p_T for π^+ at 12 and 24 GeV/c and at ISR energies. The full straight lines are fits of the form e^{-Bp_T}, the dashed curves are fits of the form $e^{-C\mu}$ (see text) (from Ref. [57c])

β. Average transverse momenta of pions as a function of x and y.

If one plots the average transverse momentum $\langle p_T \rangle(x)$ defined by

$$\langle p_T \rangle (x) = \frac{\int p_T \frac{d\sigma}{d^3p} dp_T^2}{\int \frac{d\sigma}{d^3p} dp_T^2} \tag{95}$$

as a function of the scaled longitudinal momentum x, one observes a minimum at $x = 0$ (sea gull effect). The effect is partly due to the phase space factor $1/E$ in $d\sigma/d^3p = E^{-1}f(p)$. It becomes smaller, if one plots instead of (95) the weighted average transverse momentum

$\langle p_T \rangle_w$, which is calculated by using the invariant cross section $f(\boldsymbol{p})$ instead of $d\sigma/d^3p$

$$\langle p_T \rangle_w(x) = \frac{\int p_T E \frac{d\sigma}{d^3p} dp_T^2}{\int E \frac{d\sigma}{d^3p} dp_T^2}. \tag{96}$$

This is seen when comparing the unweighted and weighted average values in Fig. 39 of the BHM collaboration [57] at 12 and 24 GeV/c for pp → π^+. However the effect still appears in $\langle p_T \rangle_w$.

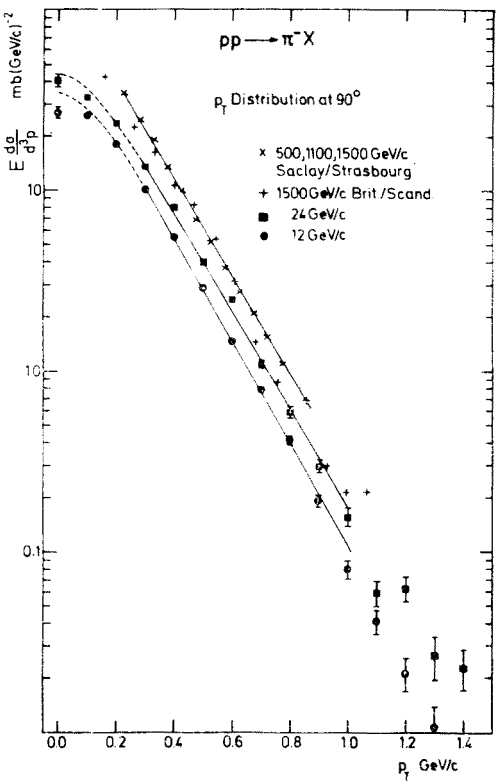

Fig. 42. The same as Fig. 41 for π^-

If one plots $\langle p_T \rangle_w$ *vs* the cms rapidity y^* rather than x (see Fig. 40b), the values are pretty constant in the central region of small $|y^*|$. For larger $|y^*|$, $\langle p_T \rangle_w$ decreases due to the kinematical boundary, since for large y^* only small p_T values can be reached (see Fig. 21). To reduce this kinematical effect, Fig. 40b shows also $\langle p_T \rangle_w$ *vs* y^* for the region $p_T <$ < 600 MeV/c. Now the weighted average is independent of y^*. The result that $\langle p_T \rangle_w$ is nearly independent of y^* in the central region indicates that the shape of the invariant

p_T-distribution is independent of y^*, *i. e.* that $f(p_T, y^*)$ factorises in the central region:

$$f(p_T, y^*) = g(p_T) \cdot h(y^*). \tag{97}$$

The sea gull effect in x would thus be a reflection of this factorisation in p_T and y^*.

γ. Transverse momentum distributions at accelerator energies. In the following we consider the invariant p_T-distributions

$$f(p) \equiv E\frac{d\sigma}{d^3p} = \frac{2E}{\pi\sqrt{s}}\frac{d\sigma}{dp_T^2 dx} = \frac{1}{\pi}\frac{d\sigma}{dp_T^2 dy} \tag{98}$$

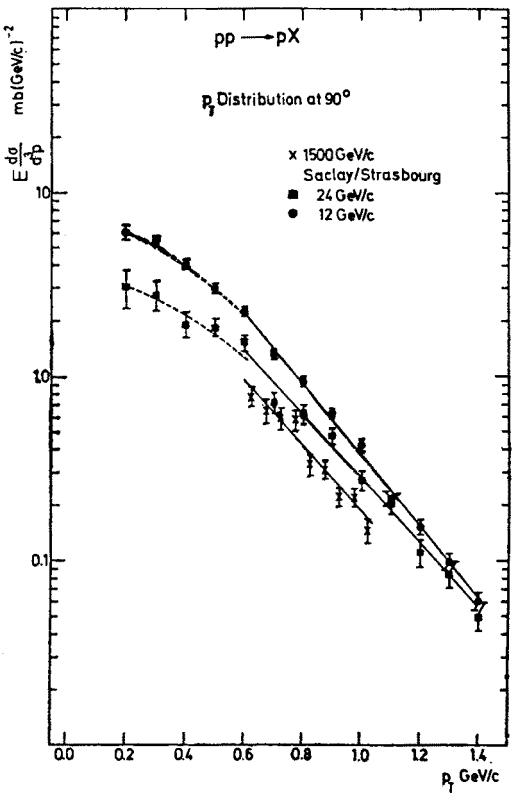

Fig. 43. The same as Fig. 41 for protons

(see (91)) for fixed x or y. We discuss mainly the data of the BHM collaboration [57] at 12 and 24 GeV/c and treat the central region and fragmentation region separately, although they are not yet well separated at these low energies.

Central region ($x \approx 0$)

Figs. 41 and 42 show for π^+ and π^- respectively the invariant distributions *vs* p_T at $x = 0$ ($\Theta^* = 90°$) at 12 and 24 GeV/c and at ISR energies. Above $p_T \approx 0.3$ GeV/c the distributions can well be fitted by an exponential e^{-Bp_T} in p_T (full curves), where $B \approx 6.2$ GeV^{-1}

independent of energy from 12 GeV/c to ISR energies. Thus the shape of the invariant distributions shows early scaling. For π^+ rough energy independence is observed also for the absolute magnitude of the distributions, whereas for π^- the distributions increase from

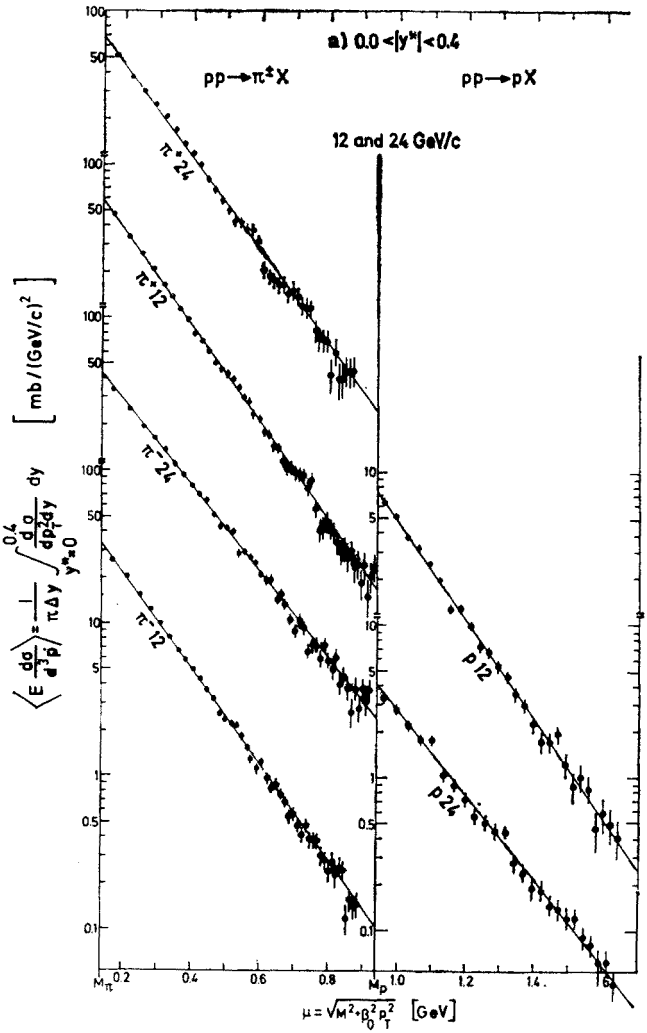

Fig. 44. Invariant cross section *vs* μ for π^+, π^- and protons for $0 < |y^*| < 0.4$ at 12 and 24 GeV/c. The straight lines are fits of the form $e^{-C\mu}$ (see text) (from Ref. [57c])

12 to 24 GeV/c and from there to ISR energies. Thus, in agreement with what was found already from the y-distributions in the central region (Figs 22 and 23), for π^+ scaling sets in already at accelerator energies whereas for π^- it is not yet reached there. For small $p_T \leqslant 0.2$ GeV/c the distributions at 12 and 24 GeV/c flatten off and do not follow an exponential anymore. The small-p_T behaviour at ISR energies is not yet known.

Fig. 43 shows the p_T-distributions for protons at $x = 0$ at 12, 24 GeV/c and ISR energies. An exponential fit works only above $p_T \approx 0.6$ GeV/c with $B \approx 4.5$ GeV^{-1} (*i. e.* not as steep as for $\pi^{\pm}$), whereas below ~ 0.5 GeV/c the distribution flattens off. Absolute scaling is not yet reached at accelerator energies.

The observation, that an exponential in p_T does not fit the distributions down to small p_T suggests that instead of p_T another variable may be more useful, which for large

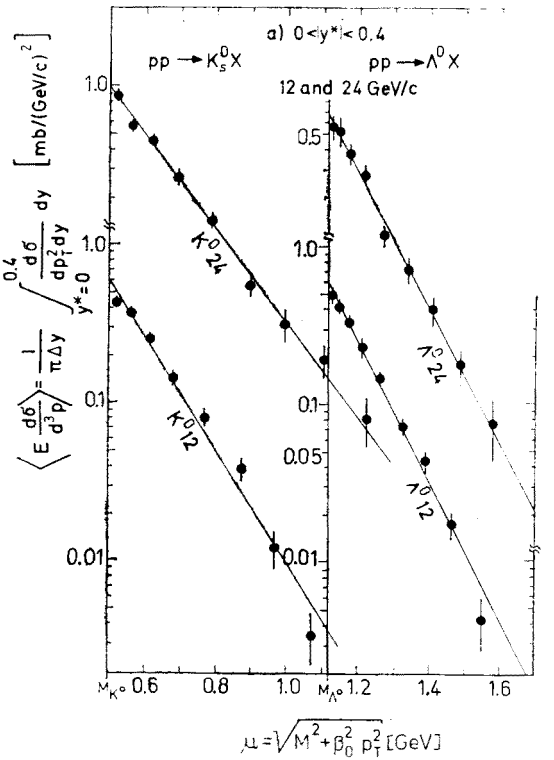

Fig. 45. The same as Fig. 44 for K_s^0 and Λ

p_T goes towards p_T. Such a variable has been proposed by Barshay and Chao [64]. They suggest that the invariant p_T-distribution should be an exponential function of μ rather than p_T, where for $a+b \to c+$ anything

$$\mu = \sqrt{m_c^2 + n^2}, \quad n^2 = (p_T^2)_c \frac{4(E_b p_a - E_a p_b)^2}{s^2} = -n_\alpha n^\alpha,$$

$$n_\alpha = \frac{2}{(p_a + p_b)^2} \varepsilon_{\alpha\beta\gamma\delta} p_a^\beta p_b^\gamma p_c^\delta. \tag{99}$$

For pp-collisions

$$n^2 = \beta_0^2 p_T^2, \tag{100}$$

where β_0 = cms velocity of the incoming proton. Therefore:

$$\mu = \sqrt{m^2+\beta_0^2 p_T^2} \xrightarrow[s\to\infty]{} \sqrt{m^2+p_T^2} = m_l \text{ (longitudinal mass)}$$

$$\approx p_T \quad \text{for} \quad p_T \gg m,$$

$$\approx m + \frac{1}{2}\frac{p_T^2}{m} \quad \text{for} \quad p_T \ll m. \tag{101}$$

Fig. 44 shows the invariant distributions for pions and protons at 12 and 24 GeV/c [57] in the central region $0 < |y^*| < 0.4$ as functions of μ. An exponential $e^{-C\mu}$ in μ rather than p_T is good for all p_T values, as is also seen from the dashed curves in Figs 41, 42, 43. In particular the deviation of the proton distributions from an exponential in p_T is reasonably well described (Fig. 43) by an exponential in μ. Values for the coefficient C at $x = 0$ are summarised in Table II. One sees that at a given energy the π and p-distributions have approximately the same slope in the central region.

TABLE II

Coefficients C (in GeV^{-1}) for the fit $E\frac{d\sigma}{d^3p} \propto e^{-C\mu}$ at $x = 0$

	12 GeV/c	24 GeV/c
π^+	7.11 ± 0.05	6.48 ± 0.05
π^-	7.26 ± 0.05	6.61 ± 0.05
p	7.43 ± 0.13	6.07 ± 0.2

Fig. 45 shows the invariant distributions for K_s^0 and Λ in the central region. Here again an exponential in μ gives good fits. The slopes, in particular for Λ, are steeper than for π and p.

Fragmentation region

Figs. 46 and 47 show the distributions for pions and protons *vs* μ in the regions $0.4 < |y^*| < 0.8$ and $0.8 < |y^*| < 1.2$ respectively. Fig. 48 shows the distributions for K_s^0 and Λ in the interval $0.4 < |y^*| < 0.8$. Apart from the points at very low μ, an exponential in μ gives also here a reasonable fit. For the heavy particles p and Λ the slope becomes steeper with increasing y^* and decreasing primary momentum. This can be explained by kinematics since with increasing y^* and decreasing s the upper p_T limit becomes smaller (see Fig. 21).

Fig. 49 shows for four y_{lab} intervals in the fragmentation region ($y_{lab} \lesssim 1$) the $\pi^\pm$ invariant cross-section as a function of p_T^2 at 12 and 24 GeV/c [57]. The distributions are curved concavely since they are plotted *vs* p_T^2 and not p_T, *i. e.* the slope decresaes with increasing p_T. Furthermore, the slope increases with decreasing y_{lab} (kinematical effect), *i. e.* the invariant function does not factorise into a y and a p_T dependent part in the frag-

mentation region, in contrast to the central region, see (97). Scaling at accelerator energies is observed for π^+, but not for π^- for $y_{lab} \gtrsim 0.5$, *i. e.* towards the central region.

The observation that the invariant distribution factorises in the central region but not in the fragmentation region is also seen from Fig. 50. The figure shows the slope of the

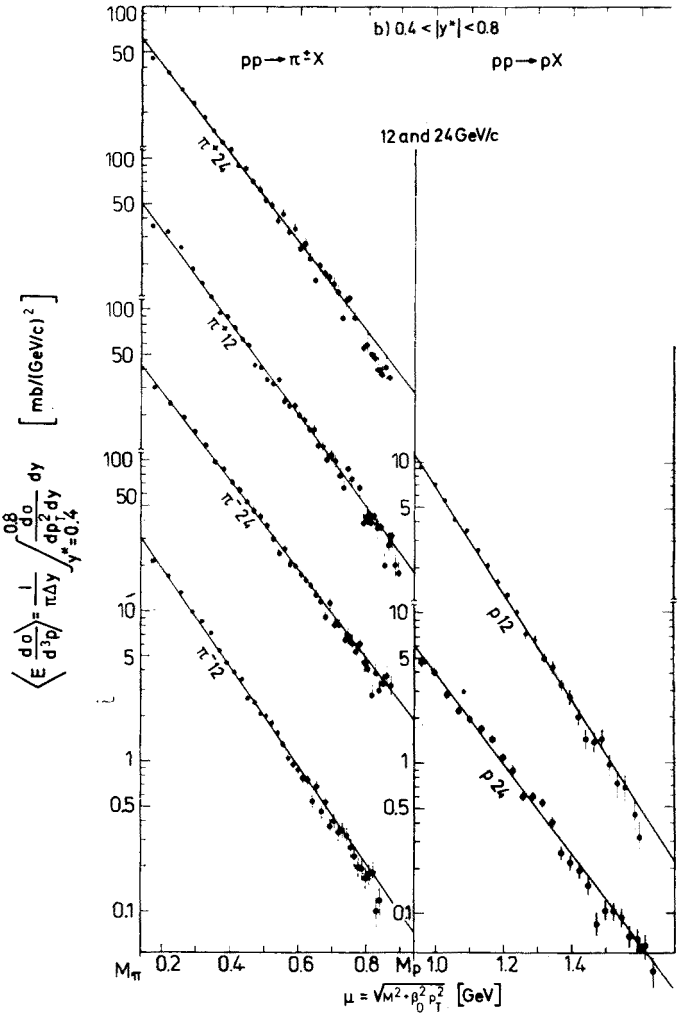

Fig. 46. The same as Fig. 44 for $0.4 < |y^*| < 0.8$

invariant distribution *vs* p_T^2 as a function of the rapidity for $p_T^2 = 0.1$ and 1.0 GeV² $\left[\text{slope} = -\frac{d}{dp_T^2}\left(\log\frac{d\sigma}{dp_T^2 dy}\right)\right]$ for the whole rapidity range. In the fragmentation region $y_{lab} \lesssim 1$ (*i. e.* $y^* \gtrsim 0.6$ at 12 GeV/*c*, $\gtrsim 1$ at 24 GeV/*c*) a y-dependence of the slope is observed, whereas in the central region the slope and therefore the shape of the distribution is independent of y. It should be noticed, that factorisation in y and p_T excludes

factorisation in x and p_T, since x depends on y and p_T. Furthermore it has been pointed out [5] that factorisation is difficult to understand theoretically for the following reason: The observed cross section is a product of a kinematical (phase space) and a dynamical

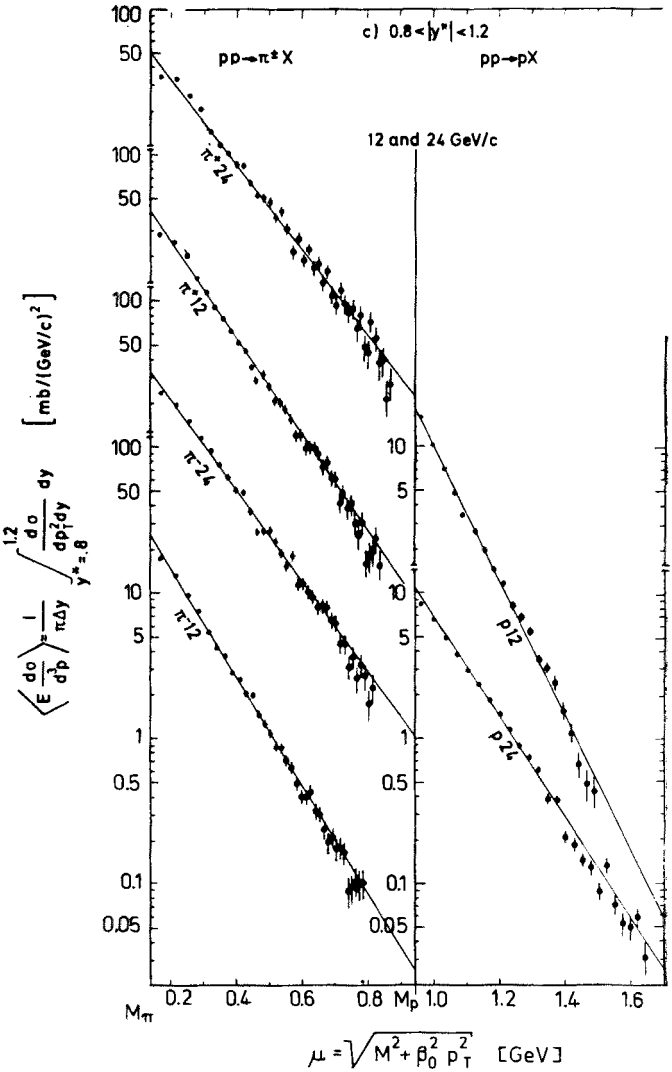

Fig. 47. The same as Fig. 44 for $0.8 < |y^*| < 1.2$

(physics) factor. Since the kinematical part does not factorise in y and p_T it is difficult to imagine a dynamical part such that factorisation is achieved for the product of kinematics and dynamics.

δ. Transverse momentum distributions at ISR energies. p_T-distributions have also been measured at ISR energies; they are treated in detail in the paper of Lillethun and will therefore not be discussed here. Some main results are:

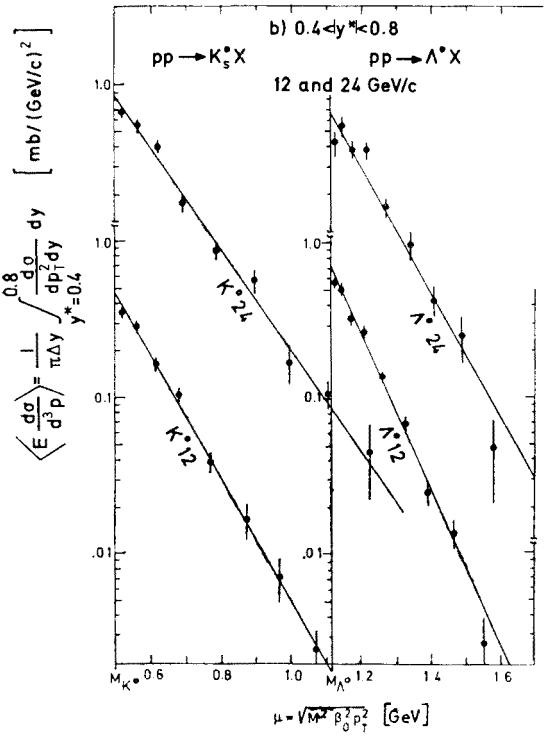

Fig. 48. The same as Fig. 44 for K_s^0 and Λ and for $0.4 < |y^*| < 0.8$

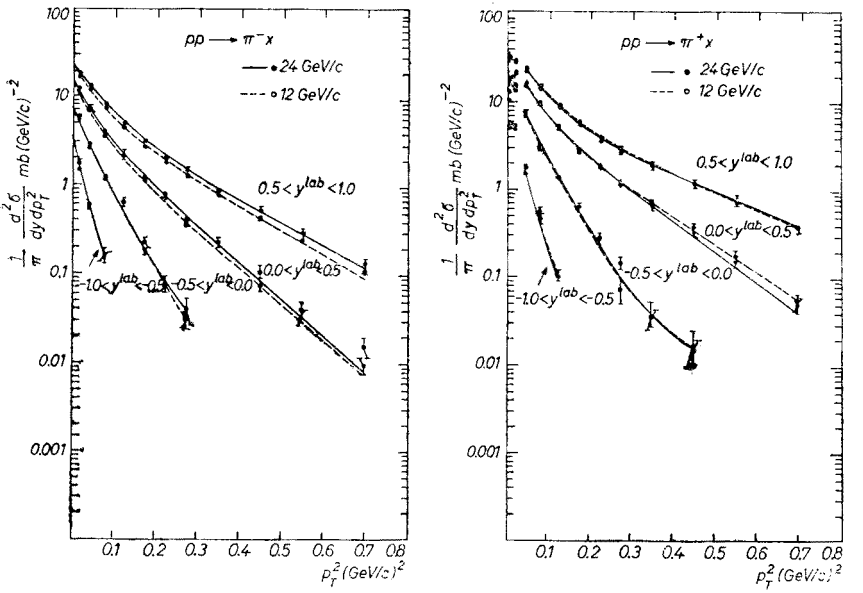

Fig. 49. Invariant cross sections *vs* p_T^2 for π^- and π^+ at 12 and 24 GeV/c for four intervals of the lab rapidity in the fragmentation region (from Ref. [57b])

The distributions for π^+ and π^- roughly coincide; they are energy independent (scaling) in the region of ISR energies. They can be fitted for $p_T \lesssim 1.5$ GeV by an exponential in p_T with a slope of $B \approx 6.2$ GeV/c^{-1}. Finally they are independent of y in the central region.

The distribution of π^0 at $x = 0$ has about the same slope as for π^+.

The distributions of p and $\bar{p}$ have roughly the same slope with $B \approx 4.2$ GeV^{-1}, *i. e.* smaller than the slope of the pion distributions.

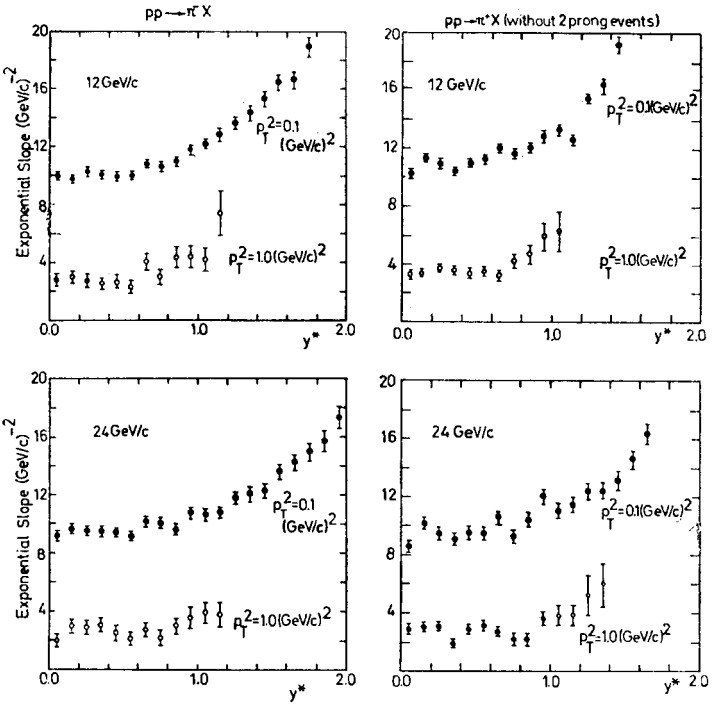

Fig. 50. Exponential slope of the p_T^2-distribution *vs* cms rapidity for π^+ and π^- at 12 and 24 GeV/c and at $p_T^2 = 0.1$ and 1.0 (GeV/c)^2 (see text for definition of slope) (from Ref. [57a])

One of the most surprising and most important discoveries made recently at the ISR is the observation, that the e^{-Bp_T} law obeyed at small $p_T \gtrsim 1.5$ GeV/c with $B \approx 6$ GeV^{-1} is not followed any longer by pions with large p_T. Instead pions with large p_T occur by several orders of magnitude more frequently than predicted by the extrapolation of e^{-6p_T} to high p_T values. This behaviour was observed for $\pi^\pm$ at 90° by the Saclay-Strasbourg collaboration, for π^0 by the CERN-Columbia-Rockefeller collaboration and for any charged particles by the Saclay-Strasbourg and British-Scandinavian collaborations. A compilation of some results up to $p_T \sim 9$ GeV/c is shown in Fig. 51.

The following observations were made [58, 62]:

The π^0-distributions at large p_T seem to be energy dependent in contrast to the scaling behaviour at small p_T.

The positive particles with high p_T occur more frequently than negative particles, the ratio being $n^+/n^- \approx 1.3$.

There are indications that the production rate for all charged particles is substantially higher than the rate for charged pions. Thus at high p_T the pions seem to loose the dominating rôle which they have at low p_T, and heavier particles become more important.

The associated and local multiplicity of a pp-reaction seems to increase with increasing transverse momentum of one particle (Pisa-Stony Brook collaboration).

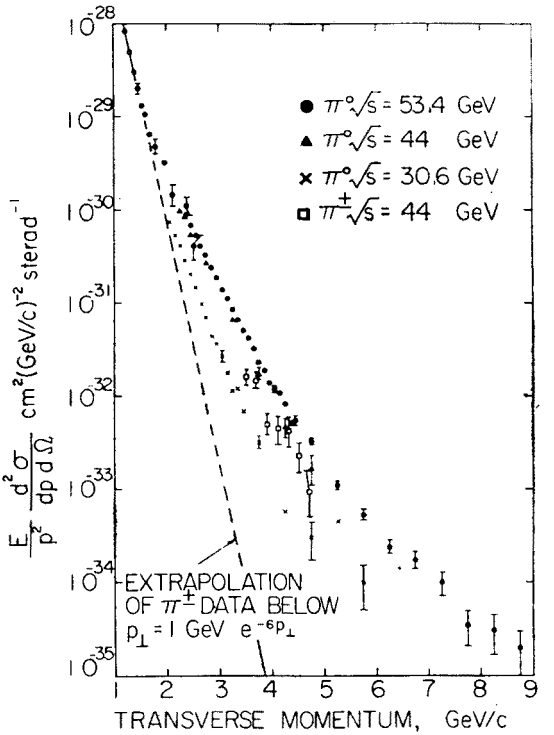

Fig. 51. Invariant cross section for π^+, π^-, π^0 *vs* p_T for large values of p_T at various ISR energies (π^0: CERN–Columbia–Rockefeller collaboration, $\pi^\pm$: Saclay–Strasbourg collaboration, from Ref. [62])

A number of interesting questions comes up with the unexpectedly frequent observation of events with a high-p_T particle, *e. g.*:

Are there several particles with high p_T in such events as one would expect in case that jets with high p_T are produced, decaying into several particles with high p_T? Or are the high-p_T particles single?

How is the high p_T balanced, by a high p_T particle or jet in roughly the opposite direction (local balance) or by particles with longer range correlations? This question of correlations is being studied by two arm spectrometer experiments.

What are exactly the correlations between high transverse momenta and multiplicities? Are high-p_T baryons produced in pairs or due to large angle scattering of the initial protons?

Some answers to such questions should come soon from further ISR experiments.

Two pictures have been adapted to explain the production of particles with high p_T, a multiperipheral picture [65] and a parton picture [66]. We mention briefly only the parton picture in a very descriptive way, since it seems to have good chances for explaining some of the observed features [58] ($n_+ > n_-$, no supremacy of pions, increase of multiplicity): Large transverse momenta probe small distances in hadronic matter and the flattening off of the p_T-distributions may indicate the existence of a granular structure (partons) of the proton. Two such partons inside the colliding protons can have head-on collisions, where the line of such a collision does not necessarily coincide with the direction of the two protons. Therefore such parton-parton collisions can lead to two narrow coplanar hadronic jets with large angle with respect to the proton direction, *i. e.* with large p_T. This would lead to two narrow cones, going in opposite direction, of several particles which share the available energy unevenly, the heavier particles getting in the average more energy than the lighter ones.

E. CORRELATIONS IN pp-COLLISIONS

1. Introduction

Single particle inclusive reactions have the practical advantage, that they are easy to obtain experimentally and that single particle distributions are easy to plot. On the other hand they reveal only a limited part of the underlying dynamics since one integrates over the variables of all other particles and sums over all possible exclusive reactions. A step further in learning more about the dynamics is the study of two-, three-*etc.* particle distributions and of correlations which might exist amongst several secondaries. Some of the questions which arise here are:

What correlations do exist between the multiplicity of the target fragments and the multiplicity of the beam fragments?
How does a single particle distribution depend on the multiplicity of the reaction? How does the multiplicity depend on the momentum of one particle (associated multiplicity)?
What correlations do exist between the momenta of several particles? Here the difficulty is encountered to separate purely kinematical correlations due to energy and momentum conservation from correlations caused by dynamics, *i. e.* by deviations from phase space.

The simplest case next to single particle distributions is the study of two-particle distributions and correlations. Here much experimental information has become available during the last year. We will discuss only briefly various types of correlation studies carried out for pp-collisions, giving only a few experimental examples and referring mainly to the reviews of Ref. [2], [5–7], [46], [47], [58], [67].

2. *Correlations between transverse momenta*

As an example we mention an early paper by Friedman, Risk and Smith [68] who have plotted for pp → pp$\pi^+\pi^+\pi^-\pi^-$ at 23 GeV/c the distribution of the angle φ between the transverse momenta $\boldsymbol{r}$ of two particles (transverse angle)

$$\cos\varphi = \frac{\boldsymbol{r}_1 \cdot \boldsymbol{r}_2}{|\boldsymbol{r}_1|\,|\boldsymbol{r}_2|}. \tag{102}$$

Fig. 52 shows the distributions of φ for various pairs of secondary particles. The experimental distributions are compared with the predictions of specific versions for two types of models:

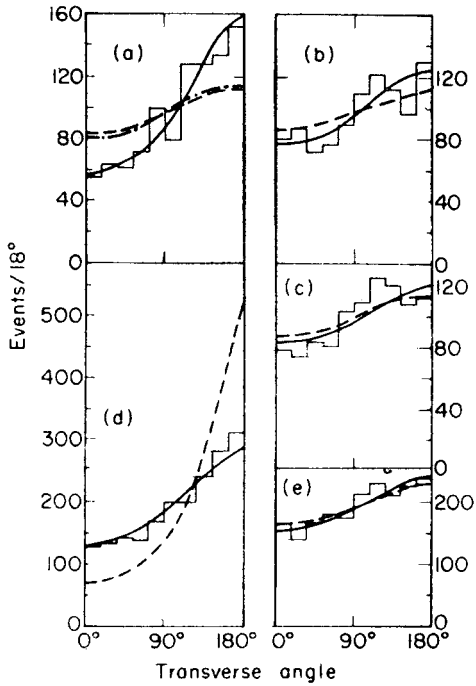

Fig. 52. Distribution of the transverse angle φ (see text) between pairs of secondary particles in pp → pp$\pi^+\pi^+\pi^-\pi^-$ at 23 GeV/c. (a): pp, (b): pions with largest positive and negative cms longitudinal momentum p^*_L,(c): pions with smallest p^*_L, (d): protons and pions with largest magnitude p^*_L, (e): pions with second and third largest p^*_L. The curves are predictions of a pionisation (full curves) and a multiperipheral (dashed curves) model (from Ref. [68])

dashed curves: "associated" model (the produced pions are associated with the leading protons), here: CLA multiperipheral model [9]; full curves: "unassociated" model, here: pionisation model.

As the curves show, the model predictions differ for combinations containing one or two protons; no difference is observed for the non-leading particles ($\pi\pi$). The pionisation model

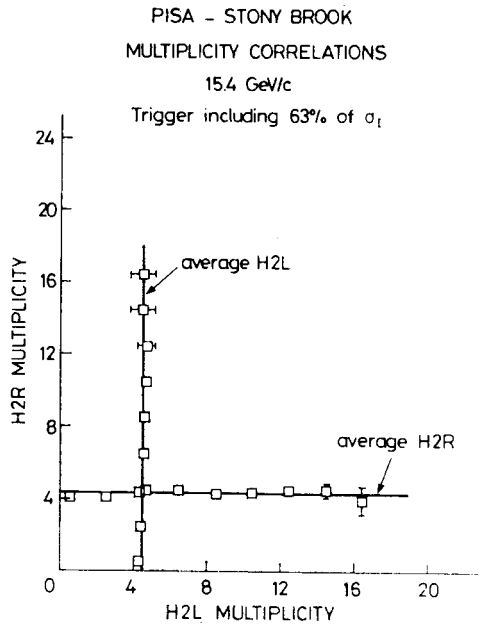

Fig. 53. Average multiplicity in the backward cms cone *vs* multiplicity in the forward cms cone and *vice versa* at $\sqrt{s} = 30$ GeV (Pisa-Stony Brook collaboration, from Ref. [7])

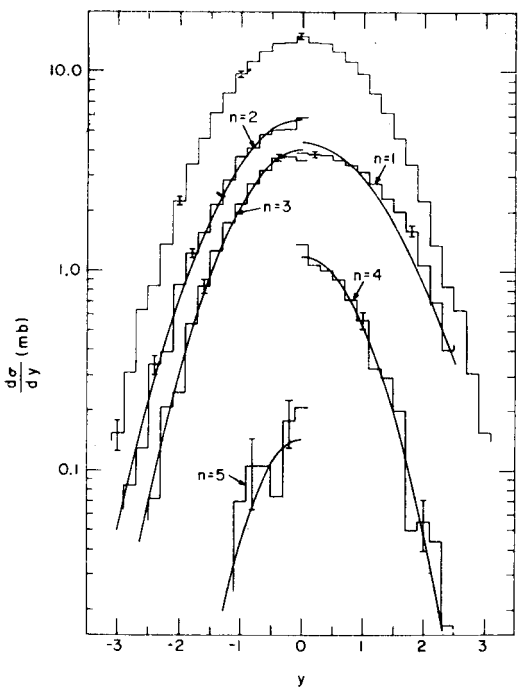

Fig. 54. cms rapidity-distribution of π^- in $pp \to \pi^- +$ anything at 28.5 GeV/c for all multiplicities and for $n_- = 1, \ldots, 5$ (*i.e.* 4 to 12 prongs). The curves are fits to Gaussians (see text) (from Ref. [70])

is favoured, however good agreement could also be obtained with the diffractive excitation model of Adair [69]. It should be mentioned that pure phase space predicts a peaking towards 180° because of transverse momentum balance.

3. *Multiplicity correlations*

Fig. 53 shows at ISR energies (Pisa-Stony Brook collaboration) the average multiplicity $\bar{n}_b(n_f)$ of particles in the backward cms hemisphere as a function of the multiplicity n_f in the forward hemisphere and *vice versa*. No mutual dependence of the multiplicities

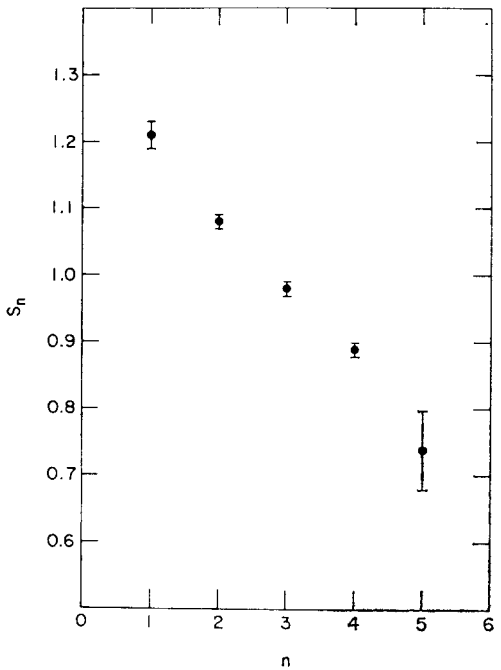

Fig. 55. Width S_{n_-} of the Gaussian fits in Fig. 54 *vs* n_- (from Ref. [70])

in the two hemispheres on each other is observed. In the DFP this would indicate, that the two incident protons fragment independently of each other at high energies.

Correlations between the average π^0 multiplicity and the charged multiplicity were already discussed in Section C1, see Figs 1–3.

4. *Rapidity distributions and multiplicity, clustering effect*

If one integrates the invariant distribution for π^- in pp $\rightarrow \pi^-$+anything over all p_T^2, the cms rapidity distribution $d\sigma/dy$ shown in Fig. 54 is obtained by Hanlon *et al.* [70] at 28.5 GeV/c (see also Fig. 24 at 12 and 24 GeV/c). It has a maximum at $y^* = 0$, a plateau

is not yet clearly developed at this energy. The interesting question arises, how this distribution is made up from the contributions of the various prong numbers. These contributions are also shown in Fig. 54 for $n = 4$ to 12 prongs, *i. e.* $n_- = 1, \ldots, 5$. These rapidity distributions for fixed n can be fitted reasonably well by Gaussians around $y^* = 0$, $d\sigma/dy \propto \exp(-y^{*2}/2S_{n_-}^2)$, where the width S_{n_-} becomes narrower with increasing n_-, see Fig. 55. Similar results were obtained at ISR energies by the Pisa-Stony Brook collaboration, see Fig. 56: The y-distribution is flat for small multiplicities and becomes

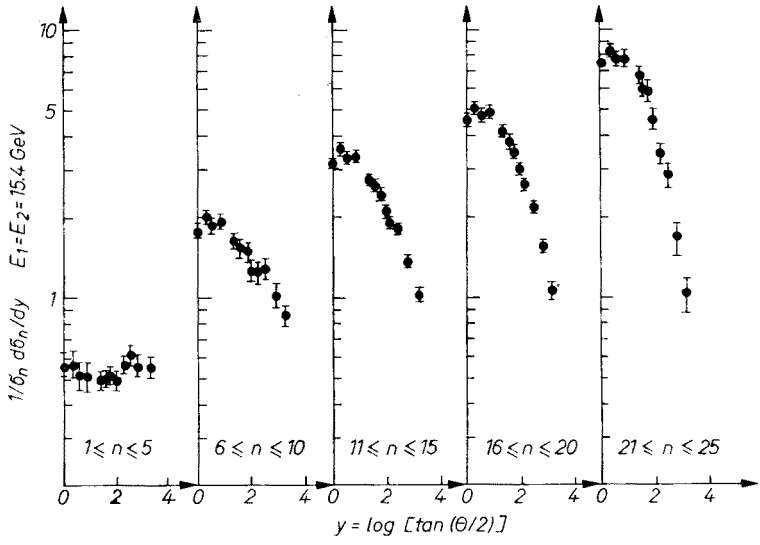

Fig. 56. η-distributions $\left(\eta = \log\left(\mathrm{tg}\frac{\Theta}{2}\right) \approx y\right)$ of charged particles at $\sqrt{s} = 30$ GeV for various intervals of the multiplicity (Pisa-Stony Brook collaboration, from Ref. [7])

narrower with increasing multiplicity. In the fragmentation picture this result can be understood qualitatively in the following way: The fragmentation of the two incident particles leads to two clusters with varying mass and correspondingly varying multiplicity. The light clusters, leading to low multiplicities, have relatively large longitudinal momenta; the corresponding secondaries contribute therefore to larger cms rapidities. Particles from heavier clusters on the other hand, connected with higher multiplicities, tend to have small cms rapidities. The separation of the two clusters is therefore the better, the higher the energy and the lower the multiplicity is. The observed effect is a long range correlation [58], since it means that selecting a certain rapidity of one particle leads to a bias towards certain values for the multiplicity of the whole event. Since furthermore the rapidity distribution of a second particle depends again on the multiplicity, the rapidities of the two particles are correlated over the whole y-range.

A somewhat different display of the observed effect is shown in Fig. 57 from pp and pn data of the Vanderbilt-BNL collaboration. The figure shows rapidity distributions for

protons and pions from four exclusive 4C-fit reactions at 28.5 GeV/c with the final state pp+$n\pi$ with $n = 1, \ldots, 4$ charged secondary pions. The proton with the highest absolute cms longitudinal momentum is defined as having positive rapidity; the rapidities of the other particles are then determined. For each reaction, the upper curves give the proton rapidities, the other curves give the rapidities for the fastest, second fastest *etc.* pion. The figure shows:

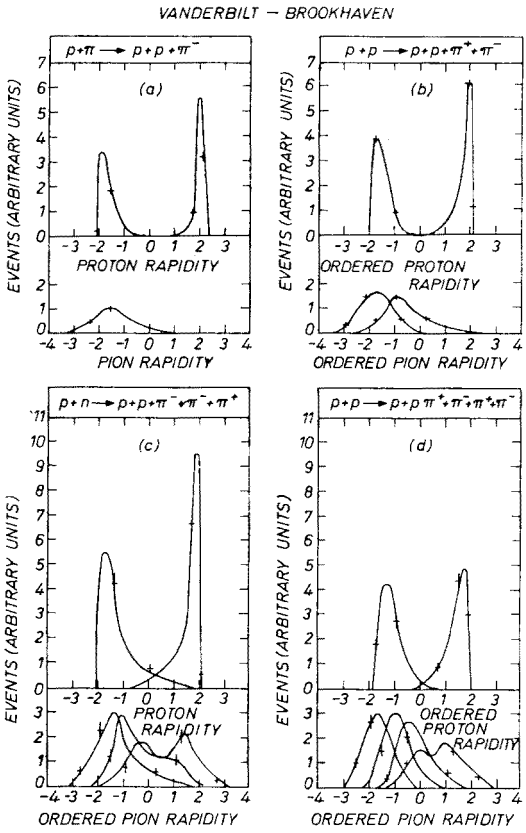

Fig. 57. cms rapidity-distributions for protons and pions from pp and pn-reactions at 28.5 GeV/c with the final states pp+$n\pi$ with $n = 1, \ldots, 4$ charged pions (see text for further explanations) (Vanderbilt-Brookhaven collaboration, from Ref. [67])

The leading particle effect of the proton

For low multiplicities the pions tend to have the same rapidity as the slower proton, *i. e.* to form a cluster with it (diffraction dissociation of one proton). A good separation of the two clusters (or cluster and single proton) is observed.

For higher multiplicities the overall pion rapidity distribution is much more smeared out and tends towards small cms rapidities.

5. *Two-particle inclusive distributions*

Information about the two particle inclusive reaction

$$a+b \to c_1+c_2+\text{anything} \tag{103}$$

is contained in the invariant distribution (see (62))

$$g_2(\boldsymbol{p}_1, \boldsymbol{p}_2, s) \equiv E_1E_2 \frac{d\sigma}{d^3p_1 d^3p_2} = \frac{4E_1E_2}{\pi^2 s} \frac{d\sigma}{dr_1^2 dx_1 dr_2^2 dx_2} = \frac{1}{\pi^2} \frac{d\sigma}{dr_1^2 dy_1 dr_2^2 dy_2}. \tag{104}$$

Since the interesting information lies in the longitudinal momenta, it is useful to study the distribution in x_1, x_2 or y_1, y_2, *e. g.* $d\sigma/dr_1^2 dy_1 dr_2^2 dy_2$ for fixed transverse momenta or $d\sigma/dy_1 dy_2$ after integration over the transverse momenta.

In two papers [70, 71] the distributions and correlations of $\pi^-\pi^-$ in the reaction $pp \to \pi^-\pi^-+$ anything have been studied at accelerator energies. As an example we show two figures from Ref. [70] at 28.5 GeV/c: Fig. 58 shows the rapidity (y_2) distributions for one π^- for fixed rapidity y_1 of the other π^-. The distributions can be approximated by Gaussians of the form

$$\frac{d\sigma}{dy_2} \propto \exp\left(-\frac{(y_2-\bar{y}_2)^2}{2S^2}\right), \tag{105}$$

where the central value $\bar{y}_2$ and the width S depend on y_1. Results for $\bar{y}_2(y_1)$ and $S(y_1)$ from the fits are shown in Fig. 59. The following observations are made:

For small y_1, $\bar{y}_2 = 0$ and S are independent of y_1, *i. e.* $d\sigma/dy_1 dy_2$ factorises into a y_1 and a y_2 dependent part.
For large positive y_1, $\bar{y}_2$ becomes negative, an effect which is expected from longitudinal momentum conservation: If one particle goes strongly forward, an other particle has a higher probability to go backward than to go forward.
For large $|y_1|$, the width S of the y_2-distribution becomes larger. This is an effect from the lower multiplicities mentioned above (Figs 54, 55): Since $d\sigma/dy$ is broader for lower multiplicities, low multiplicities are enriched in events with larger y_1, which then lead to a broader distribution also for y_2.

At ISR energies, with more particles being produced, kinematical effects between two particles should be less important and dynamical correlations should show up more clearly, if one restricts oneself to the central region. $1/\sigma_T\ d\sigma/d\eta_1 d\eta_2$[3] has been measured for charged particles at $\sqrt{s} = 30$ GeV in the central region, extending roughly from $\eta^* \approx -3$ to $+3$ by the Pisa-Stony Brook collaboration, see Fig. 60. The distributions

[3] The experiment measures $\eta = \log(\operatorname{tg} \Theta/2)$ which according to (76) is approximately the rapidity y for high energy particles in most kinematical regions.

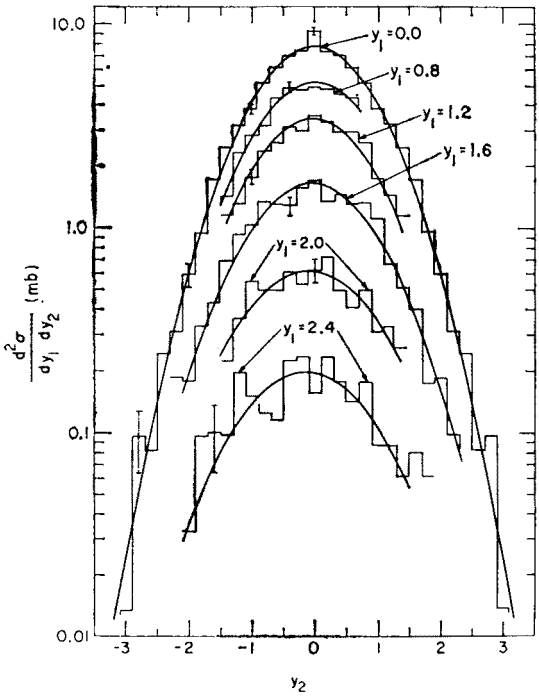

Fig. 58. cms rapidity (y_2) distributions of one π^- for various values of the rapidity y_1 of the other π^- in $pp \to \pi^-\pi^+$+anything at 28.5 GeV/c. The curves are fits to Gaussians (see text) (from Ref. [70])

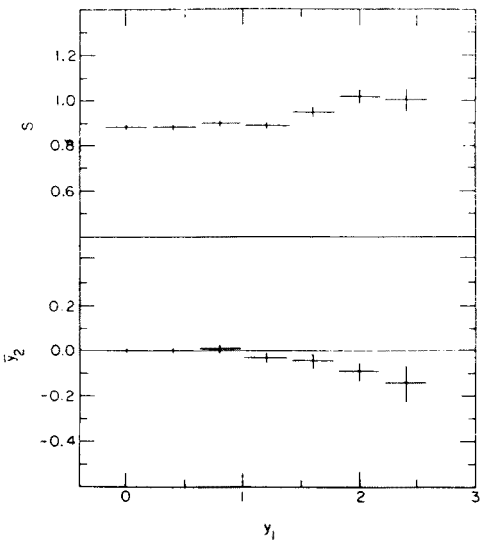

Fig. 59. Width S and position $\bar{y}_2$ of the maximum of the Gaussian fits in Fig. 58 *vs* y_1 (from Ref. [70])

have their maxima at $\eta_1 = \eta_2$, independent of η_1 (see arrows in Fig. 60). This indicates positive short range correlations (depending only on the difference $|\eta_1 - \eta_2|$ and not on the position η_1 in the central region). This is also seen from a comparison of the data points with the curves $1/\sigma_T^2 \, d\sigma/d\eta_1 d\sigma/d\eta_2$ expected for the case of no correlations.

Fig. 61 shows $1/\sigma_T d\sigma/d\eta_1 d\eta_2$ *vs* η_1 for $\eta_1 = \eta_2$ at various ISR energies (Pisa-Stony Brook collaboration). The figure shows:

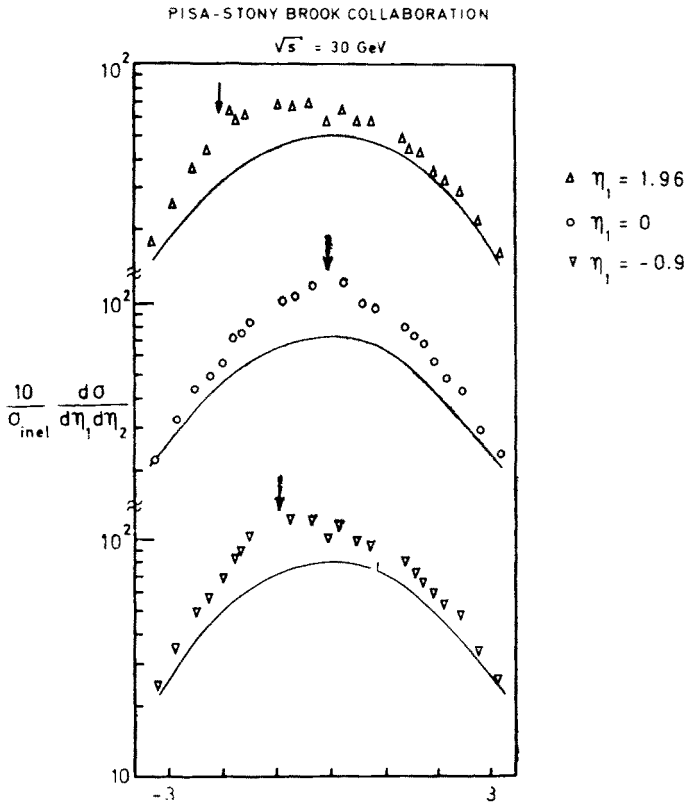

Fig. 60. Two particle distribution $\frac{1}{\sigma_T} \frac{d\sigma}{d\eta_1 d\eta_2}$ $\left(\text{where } \eta = \log\left(\text{tg}\,\frac{\Theta}{2}\right) \approx y\right)$ *vs* η_2 for three values of η_1 for charged particles in the central region at $\sqrt{s} = 30$ GeV. The arrows indicate the positions $\eta_1 = \eta_2$. The curves give $\frac{1}{\sigma_T^2} \cdot \frac{d\sigma}{d\eta_1} \cdot \frac{d\sigma}{d\eta_2}$ (no correlations) (Pisa-Stony Brook collaboration, from Ref. [58])

The two particle distribution increases with energy, the straight lines showing a fit proportionally to $\sqrt{s}$.

The central plateau (if there is any) is smaller than for single particle distributions (Fig. 25). This means that the probability for finding one particle is roughly constant over a wider y-region than the probability for finding simultaneously two particles with the same rapidity.

6. *Two-particle correlation function*

The correlation function $C(\boldsymbol{p}_1, \boldsymbol{p}_2, s)$ for the two particle inclusive reaction (103) is defined as

$$C(\boldsymbol{p}_1, \boldsymbol{p}_2, s) = \frac{1}{\sigma_T} \frac{d\sigma}{d^3p_1 d^3p_2} - \frac{1}{\sigma_T^2} \frac{d\sigma}{d^3p_1} \cdot \frac{d\sigma}{d^3p_2} . \tag{106}$$

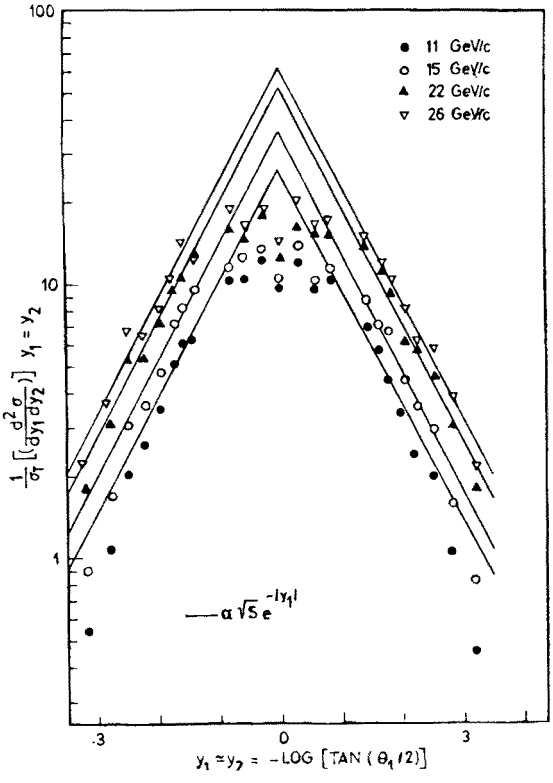

Fig. 61. Two particle distribution $\frac{1}{\sigma_T} \frac{d\sigma}{d\eta_1 d\eta_2}$ at $\eta_1 = \eta_2$ *vs* $\eta_1 \left(\eta = \log\left(\mathrm{tg}\frac{\Theta}{2}\right) \approx y\right)$ for charged particles at various ISR momenta. The straight lines are proportional to $\sqrt{s} \cdot e^{-|y_1|}$ (Pisa-Stony Brook collaboration, from Ref. [6])

$C(\boldsymbol{p}_1, \boldsymbol{p}_2) = 0$ if there are no correlations between the two particles c_1 and c_2, *i. e.* if the shape of the single particle distribution of one particle is independent of the momentum of the other particle.

The corresponding correlation function $C(y_1, y_2, s)$ for the two rapidities y_1 and y_2, after integration over the transverse momenta, is defined by:

$$C(y_1, y_2, s) = \frac{1}{\sigma_T} \frac{d\sigma}{dy_1 dy_2} - \frac{1}{\sigma_T^2} \frac{d\sigma}{dy_1} \cdot \frac{d\sigma}{dy_2} . \tag{107}$$

For several reasons [67] the correlation function as defined above may not be a very sensible quantity. We mention two of them:

The two terms of the correlation function C get contributions from different multiplicities. Consider *e. g.* the inclusive reaction pp → $\pi^-\pi^-+$ anything. The single particle distributions in C (for pp → π^-+ anything) get contributions from 4, 6, 8... prongs whereas only 6, 8... prongs contribute to the two-particle distribution. σ_T(for pp → anything) finally contains all prong numbers. Thus correlations are produced artificially by these

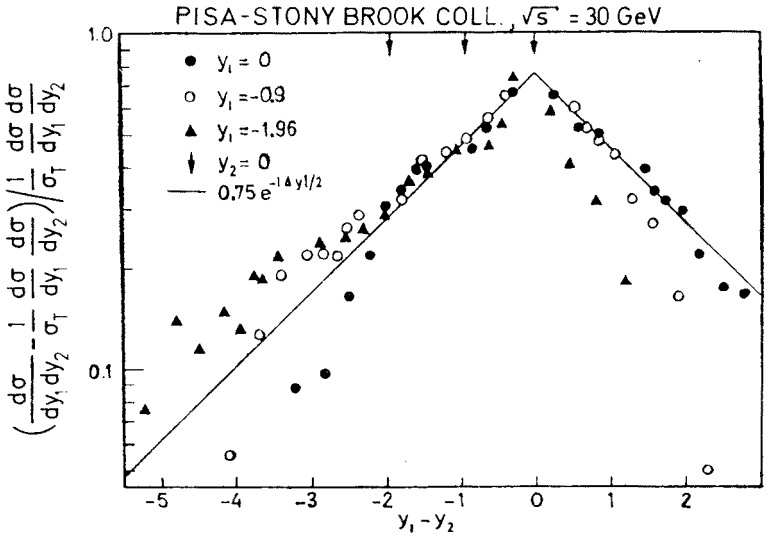

Fig. 62. Normalised two particle correlation function $\left(\eta = \log\left(\mathrm{tg}\frac{\Theta}{2}\right) \approx y\right)\left(\frac{d\sigma}{d\eta_2 d\eta_2} - \frac{1}{\sigma_T}\frac{d\sigma}{d\eta_1}\frac{d\sigma}{d\eta_2}\right)\Big/$ $\Big/\frac{1}{\sigma_T}\frac{d\sigma}{d\eta_1}\frac{d\sigma}{d\eta_2}$ *vs* $\eta_1 - \eta_2$ for three values of η_1 for charged particles at $\sqrt{s} = 30$ GeV. The straight lines show the expression $0.75 \exp\left(-\frac{|\eta_1 - \eta_2|}{2}\right)$ (Pisa-Stony Brook collaboration, from Ref. [6])

different multiplicities, in particular at low energies where the average multiplicity is small, *i. e* where the lowest multiplicities contribute substantially to the total cross section. This difficulty is avoided by defining a correlation function separately for each multiplicity and then taking the sum over all multiplicities to get the overall correlation function [70]. This latter correlation function is different from the definition (106) above.
The two particle distributions for the various multiplicities have different kinematical boundaries, which leads to kinematical correlations in the overall distribution.

The general difficulty to separate kinematical and dynamical effects from each other was already mentioned above.

Much work has been done recently to obtain experimental information on correlation functions [5–7], [58], [67], [72]. As an example we show Fig. 62 by the Pisa-Stony

Brook collaboration at $\sqrt{s} = 30$ GeV. Plotted is ($\eta = \log(\mathrm{tg}\,\Theta/2 \approx y$)

$$\frac{C(\eta_1, \eta_2)}{\frac{1}{\sigma_T^2}\frac{d\sigma}{d\eta_1}\cdot\frac{d\sigma}{d\eta_2}} = \left(\frac{d\sigma}{d\eta_1 d\eta_2} - \frac{1}{\sigma_T}\frac{d\sigma}{d\eta_1}\cdot\frac{d\sigma}{d\eta_2}\right)\Big/\frac{1}{\sigma_T}\frac{d\sigma}{d\eta_1}\cdot\frac{d\sigma}{d\eta_2} \tag{108}$$

vs $y_1 - y_2$ for $y_1 \approx 0, -1, -2$ (*i. e.* in the central region). Thus the points give the difference between the points and the curves in Fig. 60. The figure shows:

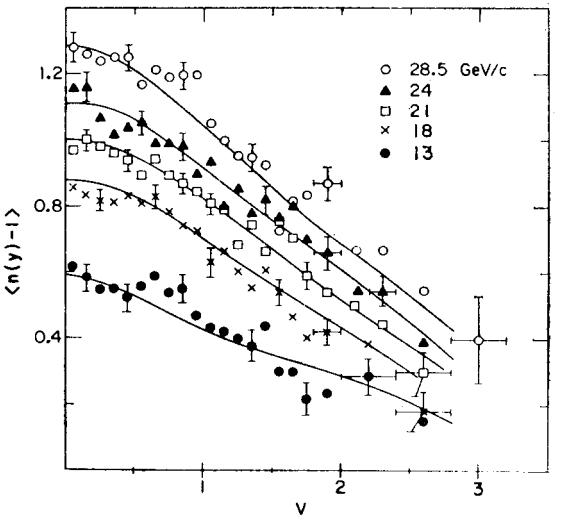

Fig. 63. Average associated multiplicity $\overline{n(y)-1}$ *vs* y for negative pions after removal of one π^- with cms rapidity y, for various lab momenta (from Ref. [71])

tf also $|y_2| \lesssim 2$ (*i. e.* in the central region)[4] and if furthermore $|y_1 - y_2|$ is small ($\lesssim 2$) Ihe points follow roughly an exponential of the form (see straight lines in Fig. 62)

$$C = 0.75 \cdot e^{-\frac{|y_1 - y_2|}{2}}$$

with a correlation length $\lambda \approx 2$, in agreement with the value predicted by the Mueller analysis (see below). Thus in the central region C seems to depend only on $|y_1 - y_2|$ and not any further on y_1 or y_2 alone. The decrease of C with increasing $|y_1 - y_2|$ and its independence on the position in rapidity space implies the existence of short range correlations in the central region.

If $|y_1|$ or $|y_2|$ becomes larger than ~ 2 or if $|y_1 - y_2|$ becomes larger than ~ 2 (fragmentation region), the correlation function starts to deviate from the simple form (109) and becomes y_1 dependent in addition to its $|y_1 - y_2|$ dependence. This implies the existence of long range correlations, which do not depend only on the rapidity difference.

[4] This means: $y_1 - y_2$ between -2 and 2; -3 and 1; -4 and 0 for $y_1 = 0, -1, -2$ respectively.

In conclusion one may say that both types of correlations (short range and long range) are observed, if the fragmentation region is included. For particles in the central region short range correlations show up rather purely [58].

What do the two pictures MPP and DFP predict qualitatively for the correlation function [6, 7, 58]?

In the multiperipheral picture MPP short range correlations are expected between particles which are close to each other in the multiperipheral chain, *i. e.* for which the rapidity distance $|y_1 - y_2|$ is small. With increasing distance $|y_1 - y_2|$ the correlation should become smaller.

In the fragmentation picture DFP short range correlations, depending on $|y_1 - y_2|$, are expected between particles in the same cluster. Correlations between particles in different clusters should disappear with increasing energy. In addition the rapidities of the particles within one cluster depend on the mass of the cluster (*i. e.* on the multiplicity). The correlation function therefore depends not only on $|y_1 - y_2|$, but also on the position of the particles in the total y-range. This is a long range effect.

A quantitative prediction for short range correlations is given by the Regge-analysis of Mueller. The prediction is

$$C \propto \exp\left(-\frac{|y_1 - y_2|}{\lambda}\right), \tag{110}$$

where the correlation length $\lambda \approx 2$. Furthermore for particles in the central region the correlation function should be independent of energy and only dependent on $|y_1 - y_2|$.

7. *Integrals over inclusive distributions, multiplicity moments*

In this and the following section we summarise for completeness some relations which exist between integrals over inclusive particle distributions and moments of multiplicities and correlated multiplicities [71, 73–76].

a. Single particle distributions

For the differential cross section $d\sigma/d^3p$ for the inclusive reaction $a+b \to c+$ anything the following relation holds:

$$\sigma_T \varrho_1(\boldsymbol{p}) \equiv \frac{d\sigma}{d^3p} = \sum_n n \frac{d\sigma_n}{d^3p}, \tag{111}$$

where:
$d\sigma_n/d^3p$ = cross section for the production of n particles c with one of them having momentum $\boldsymbol{p}$ (notice that each event with n particles c contributes n-times to $d\sigma/d^3p$); $\varrho_1(\boldsymbol{p})$ = = normalised inclusive single particle distribution.

Integrating $\varrho_1(\boldsymbol{p})$ yields:

$$F_1 \equiv \int \varrho_1(\boldsymbol{p}) d^3p = \frac{1}{\sigma_T} \sum_n n \int \frac{d\sigma_n}{d^3p} dp = \frac{1}{\sigma_T} \sum_n n\sigma_n, \tag{112}$$

where σ_n = cross section for the production of n particles c. Since

$$\bar{n} = \frac{\sum_n n\sigma_n}{\sum_n \sigma_n} = \frac{1}{\sigma_T} \sum_n n\sigma_n \tag{113}$$

is the average multiplicity of particles c, one obtains with (112):

$$F_1 = \int \varrho_1(\boldsymbol{p}) d^3p = \frac{1}{\sigma_T} \int \frac{d\sigma}{d^3p} d^3p = \bar{n} \tag{114}$$

i. e. the integral of the single particle distribution is the total cross section times the average multiplicity for particle c.

b. Two-particle distributions

Analogously for the differential cross section $d\sigma/d^3p_1 d^3p_2$ for the inclusive two particle reaction $a+b \to c_1+c_2+$ anything the following relation holds:

$$\sigma_T \varrho_2(\boldsymbol{p}_1, \boldsymbol{p}_2) \equiv \frac{d\sigma}{d^3p_1 d^3p_2} = \sum_{n_1 n_2} n_1 n_2 \frac{d\sigma_{n_1 n_2}}{d^3p_1 d^3p_2}, \tag{115}$$

where

$d\sigma_{n_1 n_2}/d^3p_1 d^3p_2$ = cross section for the production of n_1 particles c_1 and n_2 particles c_2 with one particle c_1 having momentum $\boldsymbol{p}_1$ and one particle c_2 having momentum $\boldsymbol{p}_2$. Notice that each event with n_1 particles c_1 and n_2 particles c_2 contributes $n_1 \cdot n_2$ times to the two particle distribution $d\sigma/d^3p_1 d^3p_2$. $d\sigma/d^3p_1 d^3p_2$ = inclusive two particle differential cross section.

Integrating (115) yields:

$$F_2 \equiv \int \varrho_2(\boldsymbol{p}_1, \boldsymbol{p}_2) d^3p_1 d^3p_2 = \frac{1}{\sigma_T} \sum_{n_1 n_2} n_1 n_2 \int \frac{d\sigma_{n_1 n_2}}{d^3p_1 d^3p_2} d^3p_1 d^3p_2 =$$

$$= \frac{1}{\sigma_T} \sum_{n_1 n_2} n_1 n_2 \sigma_{n_1 n_2} \tag{116}$$

where $\sigma_{n_1 n_2}$ = cross section for the production of n_1 particles c_1 and n_2 particles c_2.

Since

$$\overline{n_1 n_2} = \frac{\sum_{n_1 n_2} n_1 n_2 \sigma_{n_1 n_2}}{\sum_{n_1 n_2} \sigma_{n_1 n_2}} = \frac{1}{\sigma_T} \sum_{n_1 n_2} n_1 n_2 \sigma_{n_1 n_2} \tag{117}$$

one obtains with (116)

$$F_2 = \int \varrho_2(\boldsymbol{p}_1, \boldsymbol{p}_2) d^3p_1 d^3p_2 = \frac{1}{\sigma_T} \int \frac{d\sigma}{d^3p_1 d^3p_2} dp_1 dp_2 = \overline{n_1 n_2}. \tag{118}$$

Corresponding formulae hold for inclusive reactions of higher order.

If c_1 and c_2 are identical particles, it is easy to see that $n_1 \cdot n_2$ has to be replaced by $n(n-1)$, *i. e.*

$$\varrho_2(\boldsymbol{p}_1, \boldsymbol{p}_2) = \frac{1}{\sigma_T} \sum_n n(n-1) \frac{d\sigma_n}{d^3p_1 d^3p_2}, \tag{119}$$

$$F_2 = \int \varrho_2(\boldsymbol{p}_1, \boldsymbol{p}_2) d^3p_1 d^3p_2 = \frac{1}{\sigma_T} \int \frac{d\sigma}{d^3p_1 d^3p_2} d^3p_1 d^3p_2 = \overline{n(n-1)} = \overline{n^2} - \bar{n}. \tag{120}$$

For the integral of the correlation function $C(\boldsymbol{p}_1, \boldsymbol{p}_2)$ (defined by (106))

$$c(\boldsymbol{p}_1, \boldsymbol{p}_2) = \varrho_2(\boldsymbol{p}_1, \boldsymbol{p}_2) - \varrho_1(\boldsymbol{p}_1)\, \varrho_1'(\boldsymbol{p}_2) \tag{121}$$

one obtains from (114) and (118) the correlation parameter f_2:

$$f_2 \equiv \int c(\boldsymbol{p}_1, \boldsymbol{p}_2) d^3p_1 d^3p_2 = \overline{n_1 n_2} - \bar{n}_1 \cdot \bar{n}_2. \tag{122}$$

For identical particles

$$f_2 = \overline{n(n-1)} - \bar{n}^2 = \overline{n^2} - \bar{n} - \bar{n}^2 = D^2 - \bar{n} \text{ (see (5))}. \tag{123}$$

Thus, if the particles are produced without correlations ($C = 0$), the correlation parameter vanishes (*e. g.* Poisson distribution). The correlation parameter and the experimental results for it (Figs 10, 13) were discussed in Section C3.

8. *Partially integrated distributions* (Ref. [73–76])

If one does not integrate over the momenta of all particles, one obtains partially integrated distributions. We mention here briefly the case of two particle inclusive reactions. From (115) one obtains:

$$F_2(\boldsymbol{p}_1) \equiv \frac{1}{\sigma_T} \int \frac{d\sigma}{d^3p_1 d^3p_2} d^3p_2 = \frac{1}{\sigma_T} \sum_{n_1 n_2} n_1 n_2 \frac{d\sigma_{n_1 n_2}}{d^3p_1}, \tag{124}$$

where $d\sigma_{n_1 n_2}/d^3p_1 =$ single particle distribution of c_1 for fixed multiplicities n_1 for particles c_1 and n_2 for particles c_2. Correspondingly, the partially integrated correlation function yields

$$f_2(\boldsymbol{p}_1) \equiv \int C(\boldsymbol{p}_1, \boldsymbol{p}_2) d^3p_2 = F_2(\boldsymbol{p}_1) - \varrho_1(\boldsymbol{p}_1) \cdot \bar{n}_2 =$$

$$= \frac{1}{\sigma_T} \sum_{n_1 n_2} n_1 n_2 \frac{d\sigma_{n_1 n_2}}{d^3p_1} - \frac{\bar{n}_2}{\sigma_T} \sum_{n_1 n_2} n_1 \frac{d\sigma_{n_1 n_2}}{d^3p_1} = \frac{1}{\sigma_T} \sum_{n_1 n_2} n_1 \frac{d\sigma_{n_1 n_2}}{d^3p_1} (n_2 - \bar{n}_2). \tag{125}$$

Physical interpretation of $f_2(\boldsymbol{p}_1)$

The normalised probability $P(n_2, \boldsymbol{p}_1)$ to find n_2 particles c_2 when one particle c_1 has momentum $\boldsymbol{p}_1$ is given by

$$P(n_2, \boldsymbol{p}_1) = \frac{\sum_{n_1} n_1 \frac{d\sigma_{n_1 n_2}}{d^3 p_1}}{\sum_{n_1 n_2} n_1 \frac{d\sigma_{n_1 n_2}}{d^3 p_1}} = \frac{1}{\sigma_T \varrho_1(\boldsymbol{p}_1)} \sum_{n_1} n_1 \frac{d\sigma_{n_1 n_2}}{d^3 p_1} \tag{126}$$

with $\sum_{n_2} P(n_2, \boldsymbol{p}_1) = 1$.

Thus according to (125)

$$f_2(\boldsymbol{p}_1) = \varrho_1(\boldsymbol{p}_1) \cdot \sum_{n_2} P(n_2, \boldsymbol{p}_1)(n_2 - \bar{n}_2) = \varrho_1(\boldsymbol{p}_1)(\overline{n_2(\boldsymbol{p}_1)} - \bar{n}_2),$$

$$\frac{f_2(\boldsymbol{p}_1)}{\varrho_1(\boldsymbol{p}_1)} = \overline{n_2(\boldsymbol{p}_1)} - \bar{n}_2, \tag{127}$$

where $\overline{n_2(\boldsymbol{p}_1)}$ = average multiplicity of particles c_2 when one particle c_1 has momentum $\boldsymbol{p}_1$ (average associated multiplicity). If no correlations exist between c_1 and c_2, the average multiplicity of c_2 is independent of the momentum $\boldsymbol{p}_1$ of c_1, *i. e.* $\overline{n_2(\boldsymbol{p}_1)} = \bar{n}_2$ and $f_2(\boldsymbol{p}_1) = 0$. For identical particles c_1 and c_2 formulae (124), (125) and (127) have to be replaced by

$$F_2(\boldsymbol{p}) = \frac{1}{\sigma_T} \sum_n n(n-1) \frac{d\sigma_n}{d^3 p}, \tag{128}$$

$$f_2(\boldsymbol{p}) = \frac{1}{\sigma_T} \sum_n n \frac{d\sigma_n}{d^3 p} [(n-1) - \bar{n}], \tag{129}$$

$$\frac{f_2(\boldsymbol{p})}{\varrho_1(\boldsymbol{p})} = \overline{n(\boldsymbol{p}) - 1} - \bar{n}, \tag{130}$$

where $\overline{n(\boldsymbol{p}) - 1}$ is the average multiplicity of the remaining particles c after one particle c with momentum $\boldsymbol{p}$ has been removed.

Experimental results on partially integrated distributions and associated multiplicities can be found in Ref. [71], [73–76]. As an example we show in Fig. 63 for pp-collisions at various momenta between 13 and 28.5 GeV/c the average associated multiplicity $\overline{n(y) - 1}$ of the remaining π^-'s, after the removal of one π^- with rapidity y, *vs* y. $\overline{n(y) - 1}$ has been computed according to the formulae given above from the single and two particle distributions for pp $\to \pi^- +$ anything and pp $\to \pi^- \pi^- +$ anything respectively. The figure shows

a dependence of the average associated multiplicity on y: it decreases with increasing y. This correlation is a reflection of the fact discussed above (Figs 54–59) that large y-values are preferentially connected with small multiplicities whereas for large multiplicities the cms rapidity distribution becomes narrower.

REFERENCES

[1] G. Ranft, J. Ranft, *Fortschr. Phys.*, **19**, 393 (1971).
[2] W. R. Frazer *et al.*, *Rev. Mod. Phys.*, **44**, 284 (1972).
[3] L. Van Hove, *Phys. Reports*, **1C**, 347 (1971).
[4] D. Horn, *Proc. Intern. Conference on Duality and Symmetry in Hadron Physics*, Tel-Aviv 1971, p. 60; *Phys. Reports*, **4C**, 1 (1972).
[5] D. R. O. Morrison, *Proc. 4. Intern. Conference on High Energy Collisions*, Oxford 1972, Vol. I, p. 253.
[6] K. Gottfried, CERN-*preprint* TH 1615.
[7] M. Jacob, *Proceedings of the XVI Intern. Conf. on High Energy Physics*, Batavia 1972, Vol. 3, p. 373.
[8] D. Amati, S. Fubini, A. Stanghellini, *Nuovo Cimento*, **26**, 896 (1962).
[9] H. M. Chan, J. Łoskiewicz, W. W. M. Allison, *Nuovo Cimento*, **57A**, 93 (1968).
[10] G. F. Chew, A. Pignotti, *Phys. Rev.*, **176**, 2112 (1968).
[11] C. E. De Tar, *Phys. Rev.*, **D3**, 128 (1971).
[12] J. Benecke, T. T. Chou, C. N. Yang, E. Yen, *Phys. Rev.*, **188**, 2159 (1969).
[13] G. K. Wilson, Cornell *preprint* CLNS-134 (1970), unpublished.
[14] A. Białas, K. Fiałkowski, K. Zalewski, *Nuclear Phys.*, **B48**, 237 (1972).
[15] C. Quigg, J. D. Jackson, NAL-*Report* THY-93 (1972), unpublished.
[16] H. Harari, E. Rabinovici, *Phys. Letters*, **43B**, 49 (1973).
[17] K. Fiałkowski, *Phys. Letters*, **41B**, 379 (1972); *Acta Phys. Polon.*, **B5**, 535 (1973).
[18] K. Fiałkowski, H. I. Miettinen, *Phys. Letters*, **43B**, 61 (1973).
[19] L. Van Hove, *Phys. Letters*, **43B**, 65 (1973).
[20] W. R. Frazer *et al.*, *Phys. Rev.*, **D7**, 2647 (1973).
[21] G. Charlton *et al.*, *Phys. Rev. Letters*, **29**, 1759 (1972).
[22] G. Neuhofer *et al.*, *Phys. Letters*, **37B**, 438 (1971); **38B**, 51 (1972).
[23] J. C. Sens, *Proc. 4 Intern. Conf. on High Energy Collisions*, Oxford 1972, Vol. I, p. 177.
[24] A. K. Wróblewski, *Rapporteur's talk at the XV Intern. Conf. on High Energy Physics*, Kiev 1970.
[25] U. Amaldi *et al.*, *Phys. Letters*, **44B**, 112 (1973); S. R. Amendolia *et al.*, *Phys. Letters*, **44B**, 119 (1973).
[26] R. C. Hwa, *Phys. Rev. Letters*, **26**, 1143 (1971).
[27] *Proc. XVI Intern. Conf. on High Energy Physics*, Batavia 1972.
[28] J. W. Chapman *et al.*, *Phys. Rev. Letters*, **29**, 1686 (1972).
[29] G. Charlton *et al.*, *Phys. Rev. Letters*, **29**, 515 (1972).
[30] F. T. Dao *et al.*, *Phys. Rev. Letters*, **29**, 1627 (1972).
[31] Soviet-French collaboration, *Proc. 4 Intern. Conf. on High Energy Collisions*, Oxford 1972, Vol. II, p. 157.
[32] M. Antinucci *et al.*, CERN-*preprint*, January 1973.
[33] G. Giacomelli, *Proceedings of the XVI Intern. Conf. on High Energy Physics*, Batavia 1972, Vol. 3, p. 219.
[34] L. W. Jones *et al.*, *Nuclear Phys.*, **B43**, 477 (1972).
[35] T. Ferbel, *Phys. Rev. Letters*, **29**, 448 (1972); *Phys. Rev.*, **D7**, 925 (1973); *Proc. III Intern. Colloquium on Multiparticle Reactions*, Zakopane 1972, p. 100.
[36] E. L. Berger, *Phys. Rev. Letters*, **29**, 887 (1972).
[37] H. D. I. Abarbanel, G. L. Kane, *Phys. Rev. Letters*, **30**, 67 (1973).

[38] M. Le Bellac, J. L. Meunier, *Phys. Letters*, **53B**, 127 (1973).
[39] A. Wróblewski, *Proc. III Intern. Colloquium on Multiparticle Reactions*, Zakopane 1972, p. 140; Warsaw University *preprint* IFD No. 72/2 (1972); private communication; Zakopane lectures 1973.
[40] O. Czyżewski, K. Rybicki, Cracow *preprints* INP No. 703/PH (1970); No. 800/PH (1972).
[41] K. Rybicki, *Proc. III Intern. Colloquium on Multiparticle Reactions*, Zakopane 1972, p. 137.
[42] Z. Koba, H. B. Nielsen, P. Olesen, *Nuclear Phys.*, **B40**, 317 (1972).
[43] P. Slattery, *Phys. Rev. Letters*, **29**, 1624 (1972); *Phys. Rev.*, **D7**, 2073 (1973).
[44] K. Fiałkowski, H. I. Miettinen, *Phys. Letters*, **43B**, 493 (1973).
[45] R. P. Feynman, *Phys. Rev. Letters*, **23**, 1415 (1969); in *High Energy Collisions*, C. N. Yang ed., p. 237 (1969).
[46] E. L. Berger, *Proc. Colloquium on Multiparticle Dynamics*, Helsinki 1971, p. 326.
[47] E. L. Berger, Argonne *preprint* ANL/HEP 7148 (1971).
[48] C. Quigg, in *Particles and Fields*, Proc. of the Rochester Meeting of APS/DPF, p. 40 (1971).
[49] R. C. Arnold, Argonne *preprint* ANL/HEP 7139 (1971).
[50] W. Kittel, *Lectures at the Scandinavian Conf. on High Energy Physics*, Spatnid, *preprint* CERN/D. Ph.II/Phys. 72-11 (1972).
[51] R. G. Roberts, *Proc. 7 Finnish Summer School in Physics*, Loma-Koli 1972, p. 119.
[52] A. N. Diddens, K. Schlüpman, in *Landolt-Börnstein*, Group I, Vol. 6 (H. Schopper ed.), p. 53 (1972).
[53] A. H. Mueller, *Phys. Rev.*, **D2**, 2963 (1970).
[54] H. M. Chan, *Proc. 4 Intern. Conf. on High Energy Collisions*, Oxford 1972, Vol. I, p. 449.
[55] H. M. Chan, *Proc. 1972 CERN School of Physics*, Grado 1972, CERN 72-17, p. 1.
[56] P. Hoyer, *Proc. III Intern. Colloquium on Multiparticle Reactions*, Zakopane 1972, p. 182.
[57] Bonn-Hamburg-München collaboration, a) *Phys. Letters*, **39B**, 303 (1972); b) *Proc. 4 Intern. Conf. on High Energy Collisions*, Oxford 1972, Vol. 2, p. 117; c) to be published.
[58] M. Jacob, CERN-*preprint* TH. 1639 (1973).
[59] a) Argonne-Bologna-Michigan collaboration, L. G. Ratner *et al.*, *Phys. Rev. Letters*, **27**, 68 (1971); in *Particles and Fields*, Proc. of the Rochester Meeting of APS/DPF, p. 99 (1971); A. Bertin *et al.*, *Phys. Letters*, **38B**, 260 (1972); b) Saclay--Strasbourg collaboration, quoted in Ref. [23].
[60] J. V. Allaby *et al.*, *Proc. 4 Intern. Conf. on High Energy Collisions*, Oxford 1972, Vol. 2, p. 85.
[61] CERN-Holland-Lancester-Manchester collaboration, M. G. Albrow *et al.*, *Nuclear Phys.*, **B51**, 388 (1973); **B54**, 6 (1973).
[62] D. R. O. Morrison, CERN/D.PH.II/PHYS 73-11 (1973).
[63] G. R. Charlton *et al.*, *Contribution to the Batavia Conference* 1972.
[64] S. Barshay, Y. A. Chao, *Phys. Letters*, **38B**, 225 (1972).
[65] D. Amati, L. Caneschi, M. Testa, *Phys. Letters*, **43B**, 186 (1973).
[66] S. Berman, J. Bjorken, J. Kogut, *Phys, Rev.*, **D4**, 3388 (1971).
[67] D. R. O. Morrison, *Proc. III Intern. Colloquium on Multiparticle Reactions*, Zakopane 1972, p. 348.
[68] J. H. Friedman, C. Risk, D. B. Smith, *Phys. Rev. Letters*, **28**, 191 (1972).
[69] R. K. Adair, *Proc. 4 Intern. Conf. on High Energy Collisions*, Oxford 1972, Vol. 2, p. 327.
[70] J. Hanlon, R. S. Panvini, W. H. Sims, *Nuclear Phys.*, **B52**, 96 (1973).
[71] E. L. Berger, B. Y. Oh, G. A. Smith, *Phys. Rev. Letters*, **29**, 675 (1972).
[72] CERN-Hamburg-Vienna collaboration, H. Dibon *et al.*, submitted to *Phys. Letters*.
[73] A. Białas, K. Zalewski, *Nuclear Phys.*, **B42**, 325 (1972).
[74] A. Białas, K. Fiałkowski, R. Wit, *Nuclear Phys.*, **B43**, 413 (1972).
[75] K. Fiałkowski, K. Rybicki, R. Wit, *Nuclear Phys.*, **B44**, 509, (1972); **B51**, 645 (1973).
[76] Z. Koba, *Proc. III Intern. Colloquium on Multiparticle Reactions*, Zakopane 1972, p. 314.